Nuclear weak-interaction processes in stars

K. Langanke*

Institut for Fysik og Astronomi, Århus Universitet, DK-8000 Århus, Denmark

G. Martínez-Pinedo†

Department für Physik und Astronomie, Universität Basel, CH-4056 Basel, Switzerland

(Published 13 June 2003)

Recent experimental data and progress in nuclear structure modeling have led to improved descriptions of astrophysically important weak-interaction processes. This review discusses these advances and their applications to hydrostatic solar and stellar burning, to the slow and rapid neutron-capture processes, to neutrino nucleosynthesis, and to explosive hydrogen burning. Special emphasis is given to the weak-interaction processes associated with core-collapse supernovae. Despite significant progress, improvements in the modeling of these processes are still warranted and are expected to come from future radioactive ion-beam facilities.

CONTENTS

I. INTRODUCTION

The weak interaction is one of the four fundamental forces in nature. Like the other three—strong, electromagnetic, and gravitational—it plays a key role in many astrophysical processes. This can be nicely illustrated by the observation that new insights into the nature of the weak interaction usually have been closely followed by the recognition of their importance in some astrophysical context. Shortly after Pauli postulated the existence of the neutrino and Fermi developed the first theory of weak interaction (Fermi, 1934), Gamow and Schoenberg speculated about the possible role of neutrinos in stellar evolution and proposed their production in the star as an important source for stellar energy losses (Gamow and Schoenberg, 1940, 1941; Gamow, 1941). The development of the universal $V-A$ theory (Feynman and Gell-Mann, 1958) led Pontecorvo to realize that the bremsstrahlung radiation of neutrino pairs by electrons would be a very effective stellar energy-loss mechanism (Pontecorvo, 1959). Just after the discovery of the neutral weak current, Freedman (1974), Mazurek (1975), and Sato (1975) recognized that this interaction would result in a sizable elastic-scattering cross section between neutrinos and nucleons, leading to neutrino trapping during the core collapse of a massive star in a type-II supernova.

The unified model of electroweak interaction (Weinberg, 1967; Salam, 1968; Glashow *et al.*, 1970) allows derivation of accurate cross sections for weak processes among elementary particles (i.e., electrons, neutrinos, quarks), and also for neutrons and protons if proper form factors are taken into account which describe the composite nature of the nucleons. However, the situation is different for weak-interaction processes involving nuclei. Clearly, the smallness of the weak-interaction coupling parameter allows treatment of these processes in perturbation theory, basically reducing the calculation to a nuclear structure problem. However, the inability to adequately treat the nuclear many-body problem introduced—and in many cases still does introduce—a substantial uncertainty into some of the key weak-interaction rates used in astrophysical simulations. In recent years we have witnessed tremendous progress in nuclear many-body theory, made possible by new approaches and novel computer realizations of established models, as well as by the availability of large computational capabilities. This progress has allowed calculation of the rates for many of the stellar weak-interaction pro-

*Electronic address: langanke@phys.au.dk
†Present address: Institut d'Estudis Espacials de Catalunya, Edifici Nexus, Gran Capità 2, E-08034 Barcelona, Spain. Electronic address: martinez@ieec.fcr.es

cesses involving nuclei, either for the first time or with significantly improved accuracy. For a calculation to be more reliable, experimental data must be available which test, constrain, and guide the theoretical models. Thus the advances in modeling nuclear weak-interaction processes in stars also reflect the progress made by experimentalists in recent years. They have produced data that are relevant for the astrophysical applications discussed in this review either directly, e.g., half-lives for some short-lived nuclei on the r-process path (Pfeiffer *et al.*, 2001), or indirectly, like the Gamow-Teller distributions for nuclei in the iron mass range (Osterfeld, 1992), which decisively constrain the nuclear models. Another recent experimental first has been the measurement of charged- and neutral-current neutrino-nucleus cross sections.

This review will report on progress in modeling the nuclear weak-interaction processes and the possible implications for stellar evolution and nucleosynthesis. We shall restrict ourselves to advances achieved by improved nuclear models, treating the weak interaction within the standard model. Of course, it has long been recognized (e.g., Sato and Sato, 1975) that stars can be used as laboratories for fundamental physics (Raffelt, 1996), aiding in the search for new weakly interacting particles or constraining exotic components of the weak interaction outside the standard model. This field is rapidly growing (see, for example, Raffelt, 1996, 1999, 2000; Domínguez *et al.*, 1999; Corsico *et al.*, 2001).

Our review is structured as follows. Following a very brief discussion of the required ingredients of the weak interaction, we introduce the nuclear many-body models that have been used in the study of the weak-interaction processes (Sec. II). The remaining sections are devoted to the results of these calculations and their applications to astrophysics, which include the solar nuclear reaction network and neutrino problem, the core collapse of massive stars, s- and r-process nucleosynthesis, neutrino nucleosynthesis, explosive hydrogen burning, and type-Ia supernovae.

Although generally quite important, weak-interaction processes constitute only a part of the many nuclear reactions occurring in stars. For recent reviews about other stellar nuclear reaction networks and nucleosynthesis the reader is referred to the comprehensive and competent work of Wallerstein *et al.* (1997), Arnould and Takahashi (1999), Boyd (2000), and Smith and Rehm (2001).

II. THEORETICAL DESCRIPTION

A. Weak interactions in nuclei

Processes mediated by the weak interaction in stars can be classified as leptonic (all interacting particles are leptons) and semileptonic (leptons interact with hadrons via the weak interaction). Leptonic processes can be straightforwardly computed using the standard electroweak model (Grotz and Klapdor, 1990). The calculation of semileptonic processes (i.e., neutrino-nucleus reactions, charged-lepton capture, and β decay) is more complicated due to the description of the nuclear states involved. Fortunately the momenta of the particles turn out to be small compared with the masses of the Z,W bosons. Thus it is sufficient to consider the semileptonic processes of interest in the lowest-order approximation in the weak interaction. Then the interaction can be described by a current-current Hamiltonian density:

$$\mathcal{H}(\boldsymbol{x}) = -\frac{G}{\sqrt{2}} \mathcal{J}_\mu(\boldsymbol{x}) j_\mu(\boldsymbol{x}), \tag{1}$$

where $G = G_F V_{ud}$ for charged-current processes and $G = G_F$ for neutral-current processes, with G_F the Fermi coupling constant and V_{ud} the up-down entry of the Cabibbo-Kobayashi-Maskawa matrix (Groom *et al.*, 2000). $j_\mu(\boldsymbol{x})$ and $\mathcal{J}_\mu(\boldsymbol{x})$ are the weak leptonic and hadronic density operators (Walecka, 1975, 1995; Donnelly and Peccei, 1979). The structure of the leptonic current $j_\mu(\boldsymbol{x})$ for a particular process is given by the standard electroweak model (Weinberg, 1967; Salam, 1968; Glashow *et al.*, 1970) and contains both vector and axial-vector components. The standard model describes the hadronic current in terms of quark degrees of freedom. Since we are interested only in the matrix elements of $\mathcal{J}_\mu(\boldsymbol{x})$ in nuclei we need only retain the pieces which involve u and d quarks. (The contribution from strange quarks is normally neglected, but see the discussion in Sec. V.C.) As in nuclear physics, the nucleons are treated as elementary spin-1/2 fermions; the standard-model current is not immediately applicable. Moreover, nucleons in nuclei also interact via the strong interaction. It is then convenient to define an effective hadronic current using the arguments of Lorentz covariance and isospin invariance of the strong interaction. The effective hadronic current can be decomposed into strong isoscalar ($T=0$) and isovector ($T=1$) components and contains both vector (V) and axial-vector (A) pieces. The weak charge-changing current is isovector with $M_T = \pm 1$ and can be written in a general form as

$$\mathcal{J}_\mu = V_\mu^{1M_T} + A_\mu^{1M_T}. \tag{2}$$

This current governs processes (see Fig. 1) such as $\beta^\pm$ decay, e capture, neutrino (ν_l, l^-) and antineutrino $(\overline{\nu_l}, l^+)$ reactions ($l = e$, μ or τ). Under the conserved vector current hypothesis (Feynman and Gell-Mann, 1958) the current $V_\mu^{1M_T}$ has a structure identical to the isovector part of the electromagnetic current. As a consequence in this hypothesis the weak charge-changing vector current is a conserved quantity. For the weak neutral current one has $M_T = 0$ and, in general, both $T=0$ and $T=1$ pieces can occur. The general form of this current is

$$\mathcal{J}_\mu = \beta_V^{(0)} V_\mu^{00} + \beta_A^{(0)} A_\mu^{00} + \beta_V^{(1)} V_\mu^{10} + \beta_A^{(1)} A_\mu^{10}. \tag{3}$$

Assuming that the coupling constants are given by the standard model we have $\beta_V^{(0)} = -2\sin^2\theta_W$, $\beta_A^{(0)} = 0$, $\beta_V^{(1)} = 1 - 2\sin^2\theta_W$, $\beta_A^{(1)} = 1$ (Donnelly and Peccei, 1979, p. 25), where θ_W is the weak mixing angle. The neutral

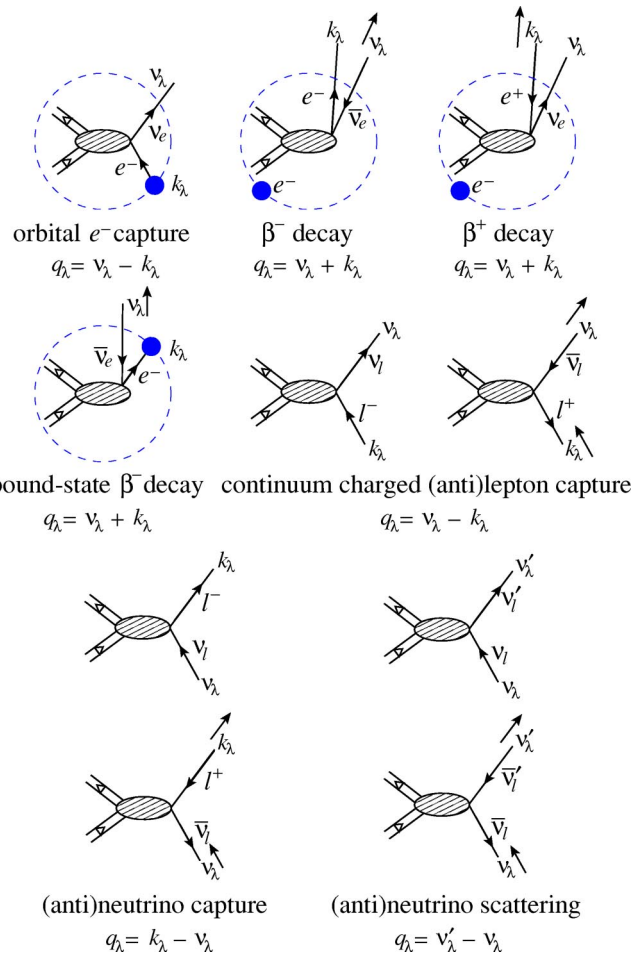

FIG. 1. (Color in online edition) Semileptonic weak processes that occur during the evolution of stars. For each process the hadronic current is on the left and the leptonic current to the right. The dashed circle indicates a bound electron in the initial or final state. The four-momentum transfer $q_\lambda=(-\omega,\boldsymbol{q})$ for each process is given in terms of the charged-lepton four-momentum $k_\lambda=(\epsilon,\boldsymbol{k})$ and the neutrino four-momentum $\nu_\lambda=(\nu,\boldsymbol{\nu})$. Here ω, ϵ, and ν represent the energy transfer, lepton energy, and neutrino energy, respectively. In the case of antiparticles the directions of the momenta are shown as an arrow close to the four-momentum label. The first row shows the usual decay modes in the laboratory. The second and third rows show processes that can occur under stellar conditions.

current describes weak interactions such as neutrino (ν,ν') and antineutrino $(\overline{\nu},\overline{\nu}')$ scattering.

The nuclear transitions that are induced by such weak currents (operators) involve initial and final states that are usually assumed to be eigenstates of angular momentum, parity, and isospin. It is then convenient to do a multipole expansion of the current operators. In that way one obtains the Coulomb, longitudinal, transverse electric, and transverse magnetic multipoles defined by Walecka (1975, p. 136). The expressions necessary for the calculation of the processes shown in Fig. 1 can be obtained from Walecka (1975) and Donnelly and Peccei (1979) in terms of the multipole operators. In general the multipole operators are A-body nuclear operators (with A the nucleon number). In practice, at the energy scales we are interested in, weak interactions perturb the nucleus only slightly, so that to a good approximation one-body components dominate most of the transitions. Two-body meson exchange currents and other many-body effects are neglected (see Marcucci *et al.*, 2001; Schiavilla and Wiringa, 2002, for a description of the nuclear current including two-body operators). It is further assumed that a nucleon in a nucleus undergoing a weak interaction can be treated as a free nucleon, which for the purpose of constructing interaction operators satisfies the Dirac equation. This latter approximation is known as the impulse approximation. For a single free nucleon, we have—using Lorentz covariance, conservation of parity, time-reversal invariance, and isospin invariance—the following general form for the vector and axial-vector currents:

$$\langle \boldsymbol{k}'\lambda';1/2m_{t'}|V_\mu^{TM_T}|\boldsymbol{k}\lambda;1/2m_t\rangle = i\overline{u}(\boldsymbol{k}'\lambda')[F_1^{(T)}\gamma_\mu + F_2^{(T)}\sigma_{\mu\nu}q_\nu]u(\boldsymbol{k}\lambda) \times\langle 1/2m_{t'}|I_T^{M_T}|1/2m_t\rangle, \tag{4a}$$

$$\langle \boldsymbol{k}'\lambda';1/2m_{t'}|A_\mu^{TM_T}|\boldsymbol{k}\lambda;1/2m_t\rangle = i\overline{u}(\boldsymbol{k}'\lambda')[F_A^{(T)}\gamma_5\gamma_\mu - iF_P^{(T)}\gamma_5 q_\mu]u(\boldsymbol{k}\lambda) \times\langle 1/2m_{t'}|I_T^{M_T}|1/2m_t\rangle. \tag{4b}$$

Here, the plane-wave single-nucleon states are labeled with the three-momenta $\boldsymbol{k}$ $(\boldsymbol{k}')$, helicities λ (λ'), isospin 1/2 and isospin projections m_t $(m_{t'})$. The momentum transfer, $q_\mu^2=q^2-\omega^2$, with $q=|\boldsymbol{q}|$, is defined in Fig. 1. Bold letters denote the three-momentum. The single-nucleon form factors $F_X^{(T)}=F_X^{(T)}(q_\mu^2)$, $T=0,1$, $X=1,2,A,P$ (vector Dirac, vector Pauli, axial, and pseudoscalar) are all functions of q_μ^2 (Donnelly and Peccei, 1979; Kuramoto *et al.*, 1990; Beise and McKeown, 1991; Musolf and Donnelly, 1992). Second-class currents are not included in Eq. (4). The isospin dependence in Eqs. (4) is contained in

$$I_T^{M_T}\equiv\frac{1}{2}\times\begin{cases}1, & T=0,M_T=0\\ \tau_0, & T=1,M_T=0\\ \tau_{\pm1}=\mp\dfrac{1}{\sqrt{2}}(\tau_1\pm i\tau_2), & T=1,M_T=\pm1.\end{cases} \tag{5}$$

To evaluate weak-interaction processes in nuclei, one needs matrix elements of the multipole operators between nuclear many-body states, labeled $|J_iM_{J_i};T_iM_{T_i}\rangle$, which are complicated nuclear configurations of protons and neutrons. Using the Wigner-Eckart theorem we can write the matrix element of an arbitrary multipole operator $\hat{T}_{JM_J;TM_T}$ as (Edmonds, 1960)

$$\langle J_1 M_{J_1}; T_1 M_{T_1} | \hat{T}_{JM_J;TM_T}(q) | J_2 M_{J_2}; T_2 M_{T_2} \rangle$$
$$= (-1)^{J_1 - M_{J_1}} \begin{pmatrix} J_1 & J & J_2 \\ -M_{J_1} & M_J & M_{J_2} \end{pmatrix} \times (-1)^{T_1 - M_{T_1}} \begin{pmatrix} T_1 & T & T_2 \\ -M_{T_1} & M_T & M_{T_2} \end{pmatrix} \times \langle J_1; T_1 ||| \hat{T}_{J;T}(q) ||| J_2; T_2 \rangle, \quad (6)$$

where the symbol ||| denotes that the matrix element is reduced in both angular momentum and isospin. If we assume that the multipole operators are one-body operators, we can write (Heyde, 1994)

$$\langle J_1; T_1 ||| \hat{T}_{J;T}(q) ||| J_2; T_2 \rangle = \sum_{\alpha\alpha'} \frac{\langle J_1; T_1 ||| [a^\dagger_{\alpha'} \otimes \tilde{a}_\alpha]_{J;T} ||| J_2; T_2 \rangle}{\sqrt{(2J+1)(2T+1)}} \times \langle \alpha' ||| T_{J;T}(q) ||| \alpha \rangle \quad (7)$$

with the sums extending over complete sets of single-particle wave functions $\alpha = n,l,j$. The tensor product involves the single-particle creation operator $a^\dagger_\alpha \equiv a^\dagger_{\alpha;m_{j_\alpha} m_{t_\alpha}}$ and $\tilde{a}_\alpha \equiv (-1)^{j_\alpha - m_\alpha}(-1)^{1/2 - m_{t_\alpha}} a_{\alpha;-m_{j_\alpha}-m_{t_\alpha}}$, with a the destruction operator. The phase factor is introduced so that the operator $\tilde{a}$ transforms as a spherical tensor (Edmonds, 1960).

In practice the infinite sums in Eq. (7) are approximated to include a finite number of (hopefully) dominant terms. The number of terms to include depends both on the computed observable and the model used (shell model, random-phase approximation, . . .). Typical nuclear models are nonrelativistic, requiring a nonrelativistic reduction of the single-particle operators; the respective expressions are given, for example, by Walecka (1975) and Donnelly and Peccei (1979). Donnelly and Haxton (1979) give the expressions for the single-particle matrix elements of these operators with harmonic-oscillator wave functions. Donnelly and Haxton (1980) provide expressions for general wave functions.

The above discussion presents the general theory of semileptonic processes. However, in many applications the momentum transfers involved are small compared with the typical nuclear momentum $Q \approx R^{-1}$, where R is the nuclear radius. In that case, the above formulas can be expanded in powers of (qR), the long-wavelength limit, and one obtains the standard approximations to allowed (Gamow-Teller and Fermi) and forbidden transitions (Behrens and Bühring, 1971, 1982; Bambynek *et al.*, 1977). In these limits the effect of the electromagnetic interaction on the initial or final charged lepton, which has been neglected in the above expressions, can be included (Schopper, 1966).

B. Nuclear models

As discussed in the previous section, one of the basic ingredients for the evaluation of weak-interaction processes involving nuclei is the description of the nuclear many-body states. Moreover, the calculation of weak processes in stars has to account for the peculiarities of the medium (high temperatures and densities) and the presence of an electron plasma. When the temperatures and densities are small (for example, during the r and s processes), weak transitions could be determined using the experimentally measured half-lives (in some cases one has to account for the presence of low-lying isomeric states). However, as many of the very neutron-rich nuclei that participate in the r process are not currently accessible experimentally (see Pfeiffer *et al.*, 2001, for recent experimental advances in the study of r-process nuclei), the necessary nuclear properties have to be extracted from theoretical models.

As the degrees of freedom increase drastically with the number of nucleons, models of varying sophistication have to be chosen for the various regions in the nuclear charts. Exact calculations using realistic nucleon-nucleon interactions, e.g., by Green's-function Monte Carlo techniques, are restricted to light nuclei with mass $A \leqslant 10$ (Carlson and Schiavilla, 1998; Wiringa *et al.*, 2000; Pieper, 2002). As an alternative, methods based on effective-field theory (van Kolck, 1999; Beane *et al.*, 2001) have recently been developed for very light nuclei ($A \leqslant 3$; Marcucci *et al.*, 2000, 2001; Park *et al.*, 2001a, 2001b). For heavier nuclei different approximations are required. In particular, restricted model spaces are used so that effective interactions and operators are necessary (Hjorth-Jensen *et al.*, 1995). For medium-mass nuclei ($A \leqslant 70$) the shell model is the method of choice (Talmi, 1993). This model explicitly treats all two-body correlations among a set of valance particles by a residual interaction. By diagonalizing the respective Hamiltonian matrix in the model space spanned by the independent-particle states of the valence particles, one can obtain a quite satisfactory description of the ground state, the spectrum at moderate excitation energies, and the electromagnetic and weak transitions among these states (Caurier *et al.*, 1994; Martínez-Pinedo *et al.*, 1997). Today, due to progress in both computer technology and programming techniques, shell-model calculations are now possible in model spaces which seemed impossible only a few years ago; i.e., the diagonalization codes ANTOINE or NATHAN developed by Etienne Caurier allow for complete calculations in the pf shell, where the maximum dimension currently attained is 2.3×10^9, $M = 0$ Slater determinants for a complete diagonalization of ^{60}Zn (Mazzocchi *et al.*, 2001; Caurier, 2002). To treat even larger model spaces in the diagonalization shell model, different schemes are required. One method is to expand the nuclear many-body wave functions in terms of a few quasiparticle determinants of the symmetry-projected Hartree-Fock-Bogoliubov (HFB) –type (Schmid *et al.*, 1987, 1989; Schmid, 2001). A novel approach, introduced by Honma *et al.* (1995; see also Otsuka *et al.*, 2001), employs stochastical methods to determine the most important Slater determinants in the chosen model space. As an alternative to the diagonalization method, the shell-model Monte Carlo (SMMC;

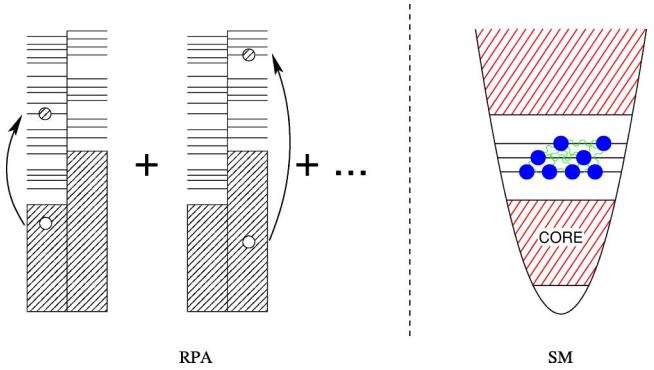

FIG. 2. (Color in online edition) The most commonly used nuclear models for the calculation of weak processes in stars are the random-phase aproximation (RPA) and the shell model (SM). In the RPA, the basis states are characterized by particle-hole excitations around a given configuration (typically a closed-shell nucleus). In the shell model, all the possible two-body correlations in a given valence space are considered. Excitations from the core or outside the model space are neglected, but this effect can be included perturbatively using effective interactions and operators.

Johnson, Koonin, *et al.*, 1992; Koonin *et al.*, 1997) allows calculation of nuclear properties as thermal averages, employing the Hubbard-Stratonovich transformation to rewrite the two-body parts of the residual interaction by integrals over fluctuating auxiliary fields. The integrations are performed by Monte Carlo techniques, making the SMMC method available for basically unrestricted model spaces. While the strength of the SMMC method is the study of nuclear properties at finite temperature, it does not allow for detailed nuclear spectroscopy.

The evaluation of nuclear matrix elements for the Fermi operator is straightforward. The Gamow-Teller operator connects Slater determinants within a model space spanned by a single harmonic-oscillator shell ($0\hbar\omega$ space). The shell model is then the method of choice for calculating the nuclear states involved in weak-interaction processes dominated by allowed transitions, as complete or sufficiently converged truncated calculations are now possible for such $0\hbar\omega$ model spaces. The practical calculation of the Gamow-Teller distribution is achieved by adopting the Lanczos method (Wilkinson, 1965), as proposed by Whitehead (1980; see also Langanke and Poves, 2000; Poves and Nowacki, 2001).

The calculation of forbidden transitions, however, involves nuclear transitions between different harmonic-oscillator shells and thus requires multi-$\hbar\omega$ model spaces. These are currently feasible only for light nuclei where *ab initio* shell-model calculations are possible (Navrátil *et al.*, 2000; Caurier *et al.*, 2001). Such multi-$\hbar\omega$ calculations have been used for the calculation of neutrino scattering from ^{12}C (Hayes and Towner, 2000; Volpe *et al.*, 2000). However, for heavier nuclei one has to rely on more strongly truncated nuclear models. As the kinematics of stellar weak-interaction processes are often such that forbidden transitions are dominated by the collective response of the nucleus, the random-phase approximation (RPA; Rowe, 1968) is usually the method of choice (Fig. 2). Another advantage of this method is that, in contrast to the shell model, it allows for global calculations of these processes for the many nuclei often involved in nuclear networks. An illustrative example is the evaluation of nuclear half-lives based on the calculation of the Gamow-Teller strength function within the quasiparticle RPA model (Krumlinde and Möller, 1984; Möller and Randrup, 1990). The RPA method considers the residual correlations among nucleons via one-particle/one-hole ($1p$-$1h$) excitations in large multi-$\hbar\omega$ model spaces. The neglect of higher-order correlations renders the RPA method inferior to the shell model, for matrix elements between individual, noncollective states. A prominent example is the Gamow-Teller transition from the ^{12}C ground state to the $T=1$ triad in the $A=12$ nuclei (see, for example, Engel *et al.*, 1996). While the shell model is able to reproduce the Gamow-Teller matrix element between these states (Cohen and Kurath, 1965; Warburton and Brown, 1992), RPA calculations miss an important part of the nucleon correlations and overestimate these matrix elements by about a factor of 2 (Kolbe *et al.*, 1994; Engel *et al.*, 1996). Recent developments have extended the RPA method to include the complete set of $2p$-$2h$ excitations in a given model space (Drożdż *et al.*, 1990). Such $2p$-$2h$ RPA models have, however, not yet been applied to semileptonic weak processes in stars. Moreover, the RPA allows for the proper treatment of the momentum dependence in the different multipole operators, as it can be important in certain stellar neutrino-nucleus processes (see below), and for the inclusion of the continuum (Buballa *et al.*, 1991). Detailed studies indicate that standard and continuum RPA calculations yield nearly the same results for total semileptonic cross sections (Kolbe *et al.*, 2000). This is related to the fact that both RPA versions obey the same sum rules. The RPA has also been extended to deal with partial occupation of the orbits so that configuration mixing in the same shell is included schematically (Rowe, 1968; Kolbe, Langanke, and Vogel, 1999).

III. HYDROGEN BURNING AND SOLAR NEUTRINOS

The tale of the solar neutrinos and their "famous" problem took an exciting turn from its original goal of measuring the central temperature of the sun to providing convincing evidence for neutrino oscillations, thus opening the door to physics beyond the standard model of the weak interaction. In 1946, Pontecorvo suggested (Pontecorvo, 1946, 1991; later independently proposed by Álvarez, 1949) that chlorine would be a good detector material for neutrinos. Subsequently, in the 1950s, Davis built a radiochemical neutrino detector which observed reactor neutrinos via the $^{37}\mathrm{Cl}(\nu_e,e^-)^{37}\mathrm{Ar}$ reaction (Davis, 1955). After the $^3\mathrm{He}(\alpha,\gamma)^7\mathrm{Be}$ cross section at low energies had been found to be significantly larger than expected (Holmgren and Johnston, 1958) and, slightly later, the $^7\mathrm{Be}(p,\gamma)^8\mathrm{B}$ cross section at low energies had been measured (Kavanagh, 1960), it became clear that the Sun should also operate by what are now

TABLE I. The solar pp chains. The neutrino terminations are from the BP2000 solar model (Bahcall *et al.*, 2001). The neutrino energies include the solar corrections (Bahcall, 1997).

Reaction	Term (%)	ν Energy (MeV)
$p+p\rightarrow{}^2\mathrm{H}+e^+ +\nu_e$	99.96	$\leqslant 0.423$
or		
$p+e^-+p\rightarrow{}^2\mathrm{H}+\nu_e$	0.44	1.445
${}^2\mathrm{H}+p\rightarrow{}^3\mathrm{H}+\gamma$	100	
${}^3\mathrm{He}+{}^3\mathrm{He}\rightarrow\alpha+2p$	85	
or		
${}^3\mathrm{He}+{}^4\mathrm{He}\rightarrow{}^7\mathrm{Be}+\gamma$	15	
${}^7\mathrm{Be}+e^-\rightarrow{}^7\mathrm{Li}+\nu_e$	15	0.863 90% 0.385 10%
${}^7\mathrm{Li}+p\rightarrow 2\alpha$		
or		
${}^7\mathrm{Be}+p\rightarrow{}^8\mathrm{B}+\gamma$	0.02	
${}^8\mathrm{B}\rightarrow{}^8\mathrm{Be}^*+e^+ +\nu_e$		<15
${}^8\mathrm{Be}^*\rightarrow 2\alpha$		
or		
${}^3\mathrm{He}+p\rightarrow{}^4\mathrm{He}+e^+ +\nu_e$	0.00003	<18.8

known as the ppII and ppIII chains and in that way generate neutrinos with energies high enough to be detectable by a chlorine detector (Cameron, 1958; Fowler, 1958). This idea was then seriously pursued by Davis, in close collaboration with Bahcall. The observed solar neutrino flux turned out to be lower than predicted by the solar models (the original solar neutrino problem; Bahcall *et al.*, 1968; Davis *et al.*, 1968), triggering the development of further solar neutrino detectors. Thus the field of neutrino-oscillation experiments was initiated and, after precision helioseismology data (Christensen-Dalsgaard, 2002), boosted the confidence in the solar models, finally culminating in conclusive evidence for neutrino oscillations in the solar flux. A detailed recent review of the solar hydrogen burning and neutrino problem is given by Kirsten (1999).

The Sun generates its energy from nuclear fusion reactions in the pp chain (see Table I), with a small contribution by the CNO cycle. Several of these reactions are mediated by the weak interaction and hence create (electron) neutrinos, which in the standard solar model can leave the Sun unhindered. The predicted flux of solar neutrinos on the surface of the earth is shown in Fig. 3. These predictions depend on the knowledge of the relevant nuclear cross sections at solar energies (a few keV) which, with the notable exception of the ${}^3\mathrm{He}({}^3\mathrm{He},2p){}^4\mathrm{He}$ reaction (Bonetti *et al.*, 1999), which has been measured directly in the underground laboratory in the Gran Sasso, relies on the extrapolation of data taken at higher energies. As these reactions are all nonresonant, the extrapolations are quite mild and appear to be under control (Adelberger *et al.*, 1998). The cross section for the initial $p+p$ fusion reaction is so low that no data exist, and the respective solar reaction rate relies completely on theoretical modeling. Nevertheless the underlying theory is thought to be sound and the

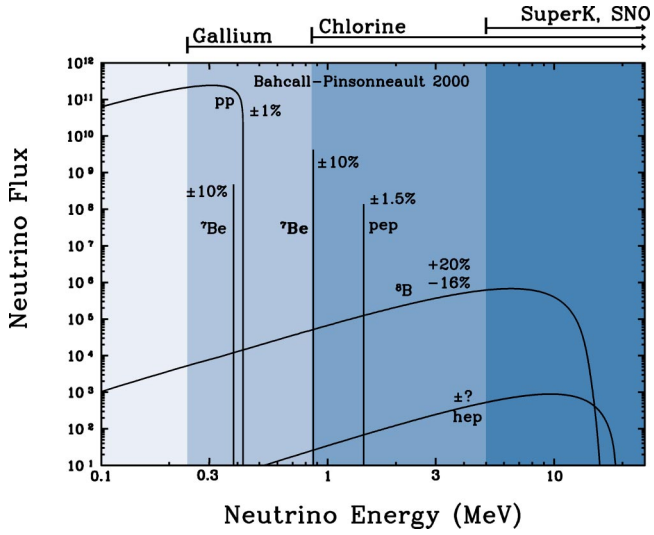

FIG. 3. (Color in online edition) The energy spectrum of neutrinos predicted by the standard solar model (Bahcall *et al.*, 2001). The neutrino fluxes from continuum sources (like pp and ${}^8\mathrm{B}$) are given in units of number per cm^2 per second per MeV, while the line fluxes (e.g., ${}^7\mathrm{Be}$) are given in number per cm^2 per second. The ranges of neutrino energies observable in the various detectors are indicated by arrows at the top. The uncertainties in the various fluxes are given in percent. Courtesy of J. N. Bahcall.

uncertainty in this important rate is estimated to be about 1% (Kamionkowski and Bahcall, 1994), based on potential model calculations. It is probably even smaller if effective-field theory is applied (Park *et al.*, 1998, 2001a; Kong and Ravndal, 2001). In the solar plasma the reaction rates are slightly enhanced due to screening effects (Dzitko *et al.*, 1995; Gruzinov and Bahcall, 1998). The most significant plasma modification is found for the lifetime of ${}^7\mathrm{Be}$ with respect to electron capture, where capture of continuum and bound electrons with the relevant screening corrections have to be accounted for (Johnson, Kolbe, *et al.*, 1992; Gruzinov and Bahcall, 1998). It is generally believed that the ${}^7\mathrm{Be}(p,\gamma){}^8\mathrm{B}$ reaction is the least known nuclear input in nuclear models. Although this reaction occurs in the weak ppIII chain, the decay of ${}^8\mathrm{B}$ is the source of the high-energy neutrinos observed by the solar neutrino detectors. Recent direct and indirect experimental methods have improved the knowledge of the ${}^7\mathrm{Be}(p,\gamma){}^8\mathrm{B}$ rate considerably (Davids *et al.*, 2001, and references therein). While these data point to an astrophysical S factor in the range of 18–20 eV b, a very recent direct measurement with special emphasis on the control and determination of the potential errors yielded a slightly larger value (Junghans *et al.*, 2001; Junghans and Snover, 2002). The neutrino energy distribution arising from the subsequent ${}^8\mathrm{B}$ decay has been measured precisely by Ortiz *et al.* (2000). In principle, high-energy neutrinos are also produced in the ${}^3\mathrm{He}+p$ fusion reaction which, however, occurs only in a weak branch in the solar pp cycles. Although the calculation of this cross section represents a severe theoretical challenge, it appears to be determined now with the required accuracy using state-of-the-art few-body

methods (Marcucci *et al.*, 2000, 2001; Kong and Ravndal, 2001; Park *et al.*, 2001a, 2001b).

The solar nuclear cross sections have been reviewed by Adelberger *et al.* (1998), including the reactions occurring in the CNO cycle. Except for some discrepancies in the $^{14}N(p,\gamma)^{15}O$ cross section at low energies (Adelberger *et al.*, 1998; Angulo and Descouvemont, 2001), all relevant solar rates are sufficiently well known.

There are currently five solar neutrino detectors operating. Three of them, the Homestake chlorine detector (Bahcall, 1989, p. 487), GALLEX[1] (Anselmann *et al.*, 1992), and SAGE (Abdurashitov *et al.*, 1994), can only observe charged-current (electron) neutrino reactions, while the two water Čerenkov detectors, Super-Kamiokande (Fukuda *et al.*, 1998b) and SNO (Boger *et al.*, 2000), also observe neutral-current events, which can be triggered by all neutrino flavors. All neutrino detectors have characteristic energy thresholds for neutrino detection, dictated by the various observation schemes; i.e., the detectors are blind to neutrinos with energies less than the threshold energy E_{th}. The pioneering chlorine experiment of Davis uses the $^{37}Cl(\nu_e,e^-)^{37}Ar$ reaction as the detector, with $E_{th}=814$ keV. GALLEX and SAGE detect neutrinos via $^{71}Ga(\nu_e,e^-)^{71}Ge$ with the threshold energy $E_{th}=233.2$ keV. In Super-Kamiokande (SK) solar neutrinos are identified by the observation of relativistic electrons produced from inelastic $\nu+e^-$ scattering. Due to high background at low energies, the observational threshold is set to ~ 7 MeV. SNO has an inner vessel of heavy water, surrounded by normal water. Like SK, this detector can also observe neutrinos via inelastic scattering off electrons. Additionally, and more importantly, SNO can also detect neutrinos by the dissociation of the deuteron in heavy water, with the threshold energy of order 6 MeV.

The threshold energies and the predicted solar neutrino fluxes are shown in Fig. 3. One notes that SK and SNO are sensitive only to ^{8}B neutrinos (neglecting the weak *hep* flux), the chlorine experiment detects mainly ^{8}B (76% of the flux predicted by Bahcall *et al.*, 2001) and ^{7}Be neutrinos, while GALLEX and SAGE can also observe neutrinos generated in the main solar energy source, the $p+p$ fusion reaction (54% of the predicted flux). It is important to note that the solar neutrino detectors have been calibrated, using known neutrino sources.

The original solar neutrino problem was simply that the earthbound detectors observed fewer neutrinos than predicted by the solar model. The current comparison is depicted in Fig. 4. Importantly, SAGE and GALLEX, in close agreement with each other, have observed a neutrino flux that is consistent with the fact that the current solar luminosity is powered by the $p+p$ fusion reaction (Abdurashitov *et al.*, 1999; Hampel *et al.*, 1999). With improved input (nuclear reaction rates, opacities, etc.)

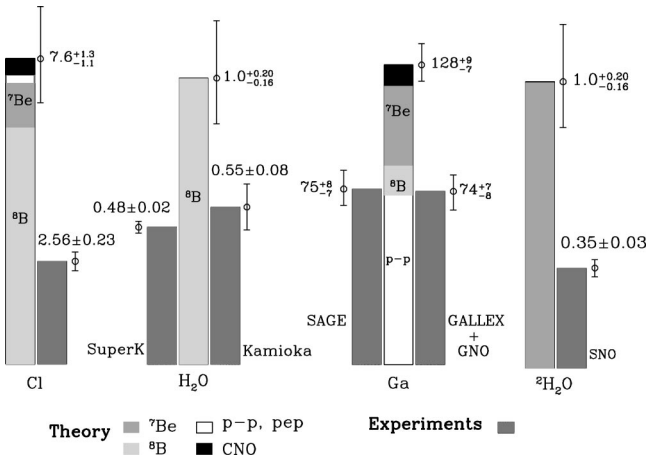

FIG. 4. Comparison of the predicted solar neutrino fluxes (Bahcall *et al.*, 2001) for the various neutrino detectors with the observed fluxes. The unit for the chlorine detector (Cl) and the gallium detectors (Ga) are Solar Neutrino Units (SNU; see Bahcall, 1989), while for SNO and SK the comparison is in percentage of the predicted flux. Courtesy of John N. Bahcall.

the solar models evolved and passed the stringent test of detailed comparison to the sound-speed distribution derived from helioseismology (Christensen-Dalsgaard *et al.*, 1996). It became clear that the solution to the solar neutrino problem pointed to weak-interaction physics beyond the standard model. This line of reasoning was supported by the observation (Heeger and Robertson, 1996) that any solar model assuming standard weak-interaction physics leads to contradictions between the observed fluxes in the various detectors.

It has been speculated for a long time (Pontecorvo, 1968) that the solution to the observed neutrino flux deficiency lies in the possibility that neutrinos change their flavor on their way from the center of the Sun to the earthbound detectors. Neutrino oscillations can occur if the flavor eigenstates (the physical ν_e,ν_μ,ν_τ neutrinos) are not identical with the mass eigenstates (ν_1,ν_2,ν_3) of the weak Hamiltonian, but rather are given by a unitary transformation of these states defined by a set of mixing angles. Importantly, oscillations between two flavor states can only occur if at least one of these states does not propagate with the speed of light, implying that this neutrino has a mass different from zero; more precisely, $\Delta m^2=m_1^2-m_2^2\neq 0$, where $m_{1,2}$ are the masses of the oscillating neutrinos. As all neutrino masses are assumed to be zero in the Weinberg-Salam model, the observation of neutrino oscillations opens the door to new physics beyond the standard model of weak interaction. Neutrino oscillations can occur for free-propagating neutrinos (vacuum oscillations). However, their occurrence can also be influenced by the environment. In particular, it has been pointed out that the high-energy (ν_e) solar neutrinos can, for a certain range of mixing angles and mass differences, transform resonantly into other flavors, mediated by the interaction of the ν_e neutrinos with the electrons in the solar plasma, and resulting in matter-enhanced oscillations (the so-called MSW effect, Wolfenstein, 1978; Mikheyev and Smirnov, 1986).

[1]The GALLEX detector has been recently upgraded and has changed its name to GNO (Altmann *et al.*, 2000).

The first clear evidence for neutrino oscillations was reported by the SK Collaboration, which observed a deficit of ν_μ-induced events from atmospheric neutrinos and could link this deficit to $\nu_\mu \rightleftarrows \nu_\tau$ oscillations (Fukuda *et al.*, 1998a, 1999). Further evidence for neutrino oscillations has been given by the LSND Collaboration (Athanassopoulos *et al.*, 1996, 1998). This result, however, was for most of the allowed parameter space not confirmed by the KARMEN experiment (Armbruster *et al.*, 1998a, 1998b). The complete LSND result will be tested by the MiniBoone experiment, which is currently under construction.[2] A clear link between neutrino oscillations and the solar neutrino problem has been presented recently by a combined analysis (Ahmad *et al.*, 2001) of the first SNO data with the precise SK data (Fukuda *et al.*, 2001). SNO measured the integrated event rate above the kinetic-energy threshold $T_{\rm eff}$ $=6.75$ MeV (the electron-energy threshold then is $E_{\rm th}$ $=T_{\rm eff}+0.511$ MeV) for charged-current reactions on the deuteron and inelastic electron scattering. As no evidence for a deviation of the spectral shape from the predicted shape under the no-oscillation hypothesis has been observed, the integrated rate could be converted into the measured ^{8}B neutrino flux, resulting in $\Phi^{\rm CC}_{\rm SNO}(\nu_e)=1.75\pm0.07({\rm stat})\pm0.12({\rm syst})\pm0.05({\rm theor})$ $\times10^6$ cm^{-2} s^{-1}, $\Phi^{\rm ES}_{\rm SNO}(\nu)=2.39\pm0.34({\rm stat})\pm0.15({\rm syst})$ $\times10^6$ cm^{-2} s^{-1}. The SNO electron-scattering flux result agrees with the more precise measurement from SK, which yields $\Phi^{\rm ES}_{\rm SK}(\nu)=2.32\pm0.03({\rm stat})\pm0.08({\rm syst})$ $\times10^6$ cm^{-2} s^{-1}. We note that the charged-current reaction can only be triggered by ν_e neutrinos at the energies of the solar neutrinos. Thus, from the measurement of the ν_e+D event rate, SNO has determined the solar ν_e flux arriving on earth stemming from the decay of ^{8}B. On the other hand, neutrino-electron scattering can occur for all neutrino types, whereby the ν_e+e^- cross section is about seven times larger than the $\nu_{\mu,\tau}+e^-$ cross section. If no oscillations involving solar ν_e neutrinos occur, the SNO charged-current flux $\Phi^{\rm CC}_{\rm SNO}$ and the SK inelastic electron-scattering flux $\Phi^{\rm ES}_{\rm SK}$ should be the same; that is excluded by 3.3 σ. [The exclusion is even slightly more severe if the recent revision of the ν_e+D cross section including radiative corrections is considered (Kurylov *et al.*, 2002).] If $\nu_e \rightleftarrows \nu_{\mu,\tau}$ oscillations occur, $\Phi^{\rm ES}_{\rm SK}$ should be larger than $\Phi^{\rm CC}_{\rm SNO}$ as it then contains additional neutral-current contributions from $\nu_{\mu,\tau}$ neutrinos. From a best fit to the SNO and SK data (see Fig. 5), this contribution has been determined as (with 1σ uncertainty) $\Phi_{\mu,\tau}=3.69\pm1.13\times10^6$ cm^{-2} s^{-1} (Ahmad *et al.*, 2001), implying that the total solar flux is $\Phi^{\rm CC}_{\rm SNO}(\nu_e)+\Phi(\nu_{\mu,\tau})=5.44\pm0.99\times10^6$ cm^{-2} s^{-1}. This result agrees very nicely with the ^{8}B neutrino flux predicted by the solar model (Bahcall *et al.*, 2001; 5.05 $\times10^6$ cm^{-2} s^{-1}).

For years the measurement of the neutral-current $\nu+D$ reaction at SNO has been anticipated as the "smoking gun" for solar neutrino oscillations. While the authors were finishing this review, the first results of this milestone experiment were published (Ahmad *et al.*, 2002a). They lead to the same conclusions as the earlier SNO results (Ahmad *et al.*, 2001), showing a clear excess of neutral-current over charged-current events, as expected if neutrino oscillations are the origin of the solar neutrino problem. Furthermore, the observed neutral-current event rate is again consistent with the prediction of the solar model (Bahcall *et al.*, 2001).

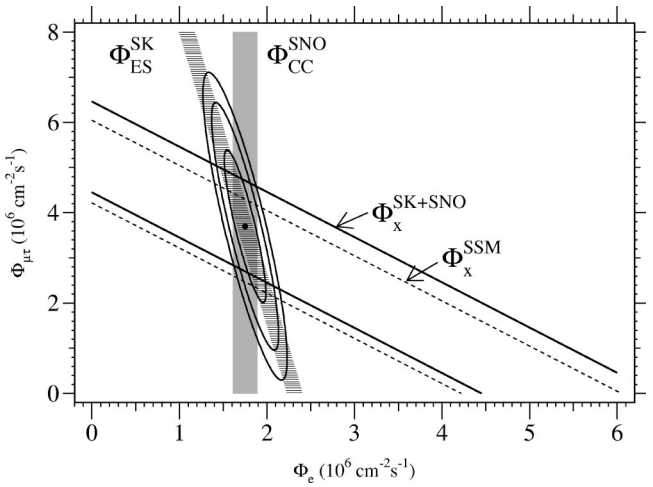

FIG. 5. Flux of $\nu_{\mu,\tau}$ neutrinos vs electron neutrinos as deduced from the SNO and SK ^{8}B neutrino data. The diagonal bands show the total ^{8}B flux: dashed lines, as predicted by the standard solar model (SSM, Bahcall *et al.*, 2001); solid lines, as derived from the SNO and SK measurements. The intercepts with the axis represent 1σ errors. From Ahmad *et al.*, 2001.

A global analysis of the latest solar neutrino data, including the SNO charged-current rate, favors matter-enhanced neutrino oscillations with large mixing angles (Krastev and Smirnoy, 2002). Considering the recent constraints on the $^7{\rm Be}(p,\gamma)^8{\rm B}$ cross section and the accordingly predicted ^{8}B solar neutrino flux, vacuum oscillations are essentially excluded. A similar result is obtained by Bahcall *et al.* (2002) including the recent day-night asymmetry measured at SNO (Ahmad *et al.*, 2002b)

For more than 30 years the solar neutrino problem has posed a challenge for experimentalists and theorists, for nuclear, particle, and astrophysicists alike. The challenge appears to have been met, leading to new physics without the need of the many desperate solution attempts put forward over the years.

IV. LATE-STAGE STELLAR EVOLUTION

A. General remarks

Weak interactions play an essential role during hydrostatic burning; the neutrinos generated by these processes can leave the star unhindered, thus carrying away energy and cooling the star. While the consideration of energy losses by neutrinos is required during hydrogen burning, the heat flux in the early stages of stellar burn-

[2]http://www-boone.fnal.gov/

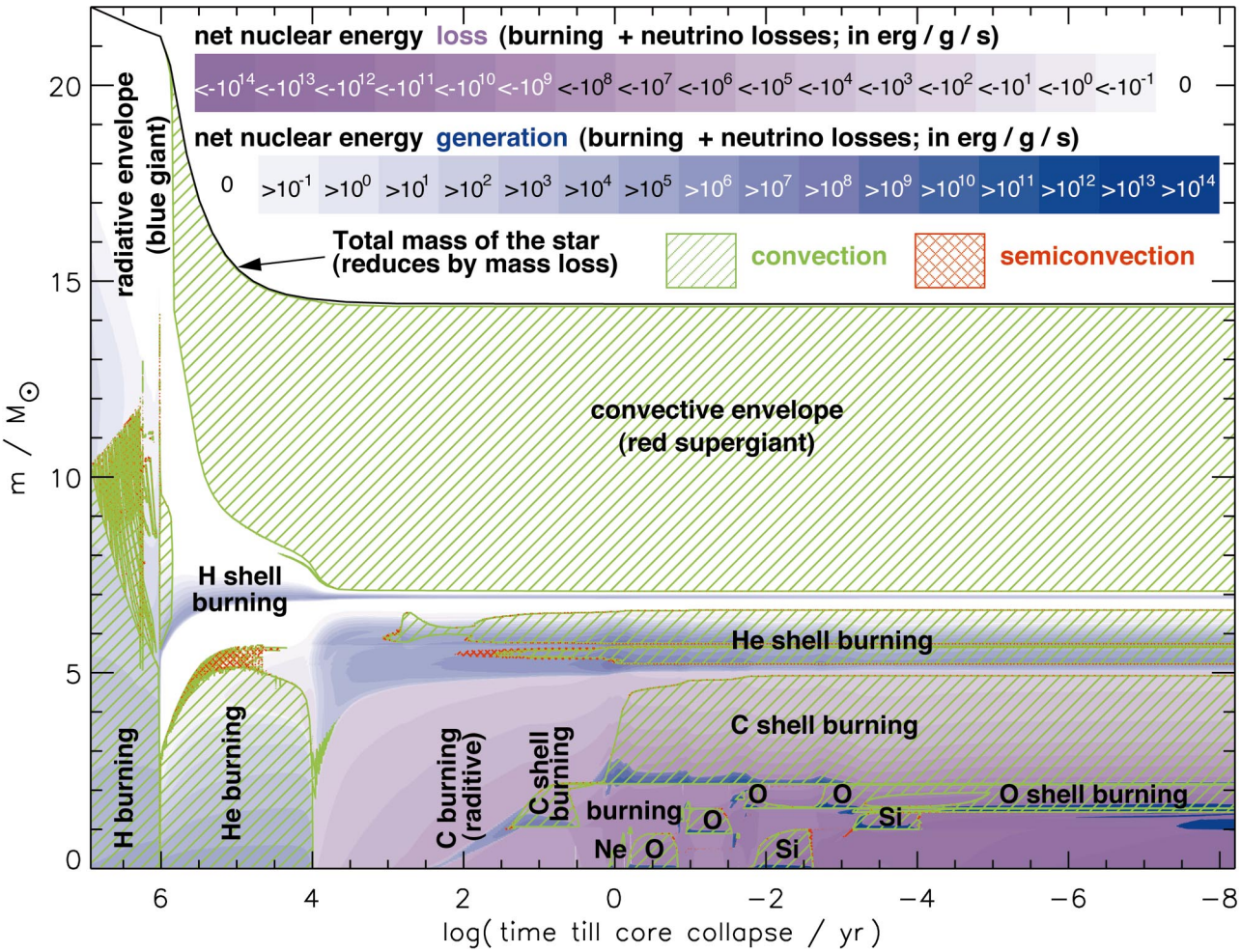

FIG. 6. (Color) Energy history of a $22M_{\odot}$ star as a function of time until core collapse. The y axis defines the included mass from the center. Hydrogen and helium core and shell burning are major energy sources. In the later burning stages, following oxygen core burning, neutrino losses related to weak processes in the stellar interior become increasingly important and can dominate over the nuclear energy production. Convection plays an important role in the envelope outside the helium burning shell, but also in shells during oxygen and silicon burning. From Heger and Woosley, 2001.

ing is predominantly by radiation. This changes, following helium burning, when the stellar temperatures reach $\sim 5\times 10^8$ K and neutrino-antineutrino pair production and emission becomes the leading energy-loss mechanism. The resulting cooling rate is a local property of the star depending on density ρ and, very sensitively, on temperature T; i.e., the energy-loss rate for $\nu\overline{\nu}$ emission scales approximately as T^{11}, implying that the hot inner regions of the star cool most efficiently. However, the dominant nuclear reactions, occurring after helium burning, have even stronger temperature dependences. For example, the heat production ϵ in the $^{12}C+^{12}C$ or $^{16}O+^{16}O$ fusion reactions, which dominate hydrostatic carbon and oxygen burning, scales as $\epsilon \approx T^{22}$ and $\approx T^{35}$ around $T=10^9$ K. As a consequence of the temperature gradient in the stellar interior and the vast difference in the temperature sensitivity, nuclear reaction heating overcomes the neutrino energy loss in the center. However, in the cooler mantle region surrounding the core, neutrino cooling dominates. The resulting entropy difference leads to convective instabilities (see Arnett, 1996). First attempts at modeling late-stage stellar burning and nucleosynthesis, including a two-dimensional treatment of convection, are reported by Baleisis and Arnett (2001).

The importance of convection has, of course, already been noticed and is accounted for in one-dimensional models within the so-called mixing-length theory (Clayton, 1968). It has been found that this convective transport is far more efficient at carrying energy and mixing the matter composition than radiative transport. For example, convection dominates the envelope region in massive stars during helium shell burning, as can be seen in Fig. 6, which shows the energy history of a $22M_{\odot}$ star (Heger and Woosley, 2001). The figure also identifies the various subsequent energy reservoirs of the star: hydrogen, helium, carbon, neon, oxygen, and silicon core and shell burning. However, the figure also demonstrates the importance of neutrino losses, which, following oxygen core burning, can overcome the nuclear energy generation, except at the high temperatures in the very inner core. Obviously weak-interaction processes are crucial in this late epoch of massive stars. Not only is this true for the star's energy budget, but these processes can also

alter the matter composition and entropy, which in turn can affect the location and extension of convective shells, e.g., during oxygen and silicon burning, with subsequent changes in the stellar structure. Such effects have recently been observed after the improved shell-model weak-interaction rates (Sec. IV.C) were incorporated into stellar models (Fig. 6 is based on these rates).

B. Shell-model electron capture and β decay rates

The late evolution stages of massive stars are strongly influenced by weak interactions, which act to determine the core entropy and electron-to-baryon ratio Y_e of the presupernova star, hence its Chandrasekhar mass which is proportional to Y_e^2. Electron capture reduces the number of electrons available for pressure support, while beta decay acts in the opposite direction. Both processes generate neutrinos, which for densities $\rho \lesssim 10^{11}$ g cm^{-3} escape the star, carrying away energy and entropy from the core.

Electron capture and beta decay during the final evolution of a massive star are dominated by Fermi and Gamow-Teller (GT) transitions. While the treatment of Fermi transitions (important only in beta decays) is straightforward, a correct description of the GT transitions is a difficult problem in nuclear structure. In the astrophysical environment nuclei are fully ionized, so one has continuum electron capture from the degenerate electron plasma. The energies of the electrons are high enough to induce transitions to the Gamow-Teller resonance. Shortly after the discovery of this collective excitation Bethe *et al.* (1979) recognized its importance for stellar electron capture. The presence of the degenerate electron gas blocks the phase space for the produced electron in beta decay. Then the decay rate of a given nuclear state is greatly reduced or even completely blocked at high densities. However, due to the finite temperature, excited states in the decaying nucleus can be thermally populated. Some of these states are connected by strong GT transitions to low-lying states in the daughter nucleus, which with increased phase space can significantly contribute to the stellar beta decay rates. The importance of these states in the parent nucleus for beta decay was first recognized by Fuller, Fowler, and Newman (1980, 1982a, 1982b, 1985, commonly abbreviated as FFN), who coined the term "backresonances" (see Fig. 7).

Over the years, many calculations of weak interaction rates for astrophysical applications have become available (Hansen, 1966, 1968; Mazurek, 1973; Takahashi *et al.*, 1973; Mazurek *et al.*, 1974; Aufderheide, Fushiki, Woosley, *et al.*, 1994). For approximately 15 years, though, the standard in the field was the tabulations of Fuller, Fowler, and Newman (1980, 1982a, 1982b, 1985). These authors calculated rates for electron capture, positron capture, beta decay, and positron emission plus the associated neutrino losses for all the astrophysically relevant nuclei ranging in mass number from 21 to 60. Their calculations were based upon an examination of all available experimental information in the mid 1980s

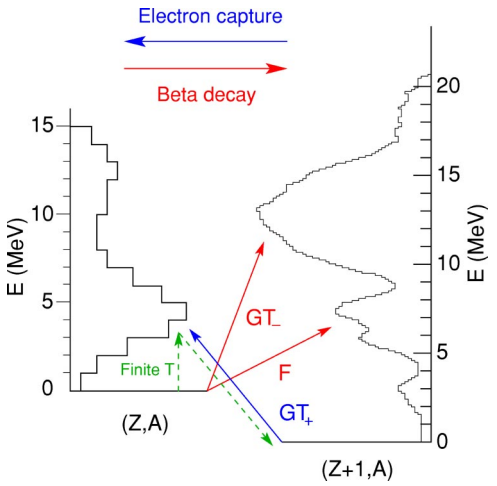

FIG. 7. (Color in online edition) The figure shows schematically the electron-capture and beta-decay processes in the stellar environment. Electron capture proceeds by Gamow-Teller transitions to the GT_+ resonance. In the case of beta decay both the Fermi and Gamow-Teller resonances are typically outside of the Q_β window and hence are not populated in laboratory decays. Due to the finite temperature in stars, excited states in the decaying nucleus can be thermally populated. Some of these states have strong GT transitions to low-lying states in the daughter nucleus. These states in the decaying nucleus are called "backresonances."

for individual transitions between ground states and low-lying excited states in the nuclei of interest. Recognizing that this only saturated a small part of the Gamow-Teller distribution, they added the collective strength via a single-state representation. Both excitation energy and strength collected in this single state were determined using an independent-particle model.

Recent experimental data on GT distributions in iron group nuclei (Rapaport *et al.*, 1983; Anderson *et al.*, 1985, 1990; Alford *et al.*, 1990, 1993; Vetterli *et al.*, 1990; Rönnqvist *et al.*, 1993; El-Kateb *et al.*, 1994; Williams *et al.*, 1995), measured in charge-exchange reactions (Goodman *et al.*, 1980; Osterfeld, 1992), show that the GT strength is strongly quenched, compared with the independent-particle-model value, and fragmented over many states in the daughter nucleus. Both effects are caused by the residual interaction among the valence nucleons. An accurate description of these correlations is essential for a reliable evaluation of the stellar weak-interaction rates due to the strong phase-space energy dependence, particularly of the stellar electron-capture rates. The shell model is the only known tool to reliably describe GT distributions in nuclei (Brown and Wildenthal, 1988). Indeed, Caurier *et al.* (1999) demonstrated that the shell model reproduces very well all measured GT_+ distributions (in this direction a proton is changed into a neutron, as in electron capture) for nuclei in the iron mass range and gives a very reasonable account of the experimentally known GT_- distributions (in this direction, a neutron is changed into a proton, as in β decay). Further, the lifetimes of the p-f-shell nuclei

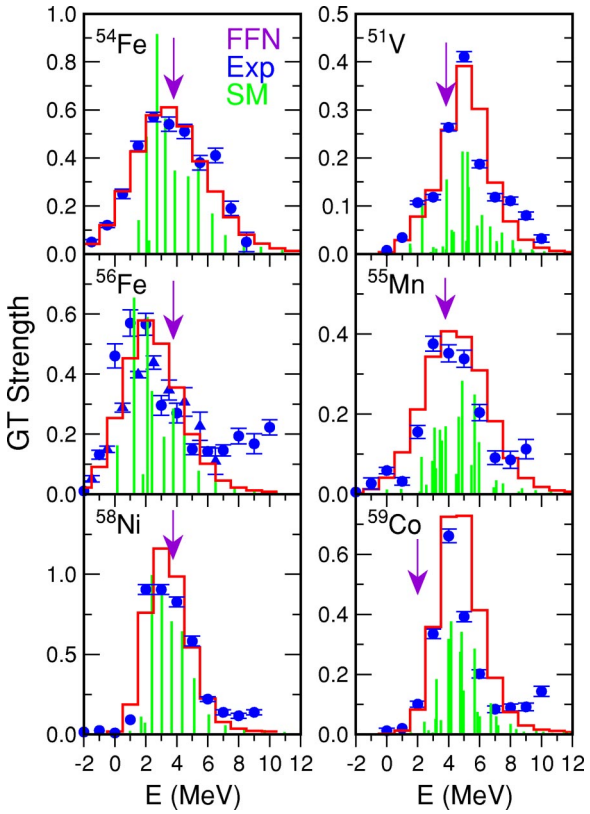

FIG. 8. (Color in online edition) Comparison of shell-model GT_+ distributions with experimental data (Alford *et al.*, 1993; Rönnqvist *et al.*, 1993; El-Kateb *et al.*, 1994) for selected nuclei. The shell-model results (discrete lines) have been folded with the experimental resolution (histograms). The arrows indicate the positions where Fuller *et al.* (1982b) placed the GT resonance in their calculations of the stellar weak-interaction rates. Adapted from Caurier *et al.*, 1999.

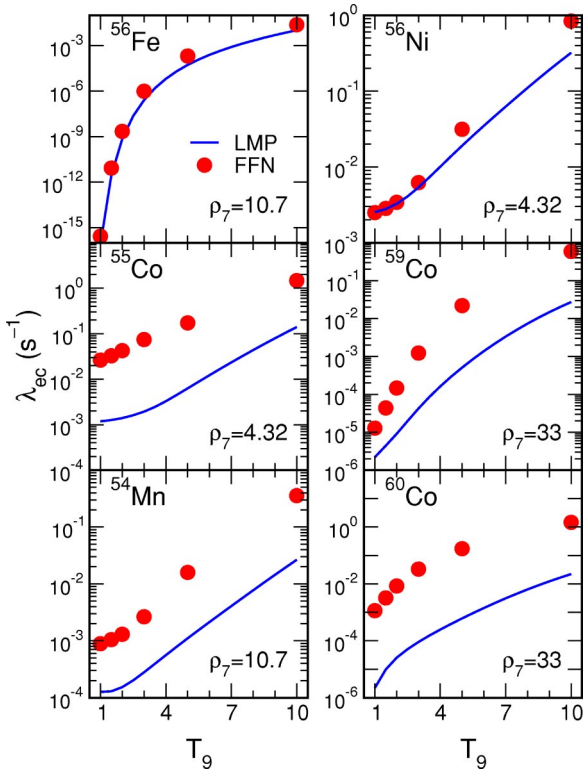

FIG. 9. (Color in online edition) Shell-model electron-capture rates as a function of temperature (T_9 measures the temperature in 10^9 K) and for selected densities (ρ_7 defines the density in 10^7 g cm^{-3}) and nuclei. For comparison, the FFN rates are given by the full points.

and their spectroscopy at low energies are likewise described well. Figure 8 compares the shell-model GT_+ distributions to the pioneering measurement performed at TRIUMF. These measurements had a typical energy resolution of ~1 MeV. Recently developed techniques, involving, for example, (^{3}He,t) charge-exchange reactions (Fujita *et al.*, 1996) and (d,^{2}He) charge-exchange reactions (Wörtche, 2001) at intermediate energies, demonstrated in pilot experiments an improvement in the energy resolution by an order of magnitude or more. Again, the shell-model calculations agree quite favorably with the improved data.

Several years ago, Aufderheide (1991), Aufderheide *et al.* (1993a, 1993b, 1996), and Aufderheide, Fushiki, Woosley, *et al.* (1994) pointed out that the interacting shell model is the method of choice for the calculation of stellar weak-interaction rates. Following the work by Brown and Wildenthal (1988), Oda *et al.* (1994) calculated shell-model rates for all the relevant weak processes for s-d-shell nuclei ($A=17-39$). This work was then extended to heavier nuclei ($A=45-65$) by Langanke and Martínez-Pinedo (2001) based on shell-model calculations in the complete p-f shell. Following the spirit of FFN, the shell-model results were replaced by experimental data (excitation energy, transition strengths) wherever available.

Weak-interaction rates have also been computed using the proton-neutron quasiparticle RPA model (Nabi and Klapdor-Kleingrothaus, 1999a, 1999b) and the spectral distribution theory (Kar *et al.*, 1994; Sutaria and Ray, 1995).

After oxygen burning, the important weak processes are electron captures and beta decays on nuclei in the iron mass range ($A\sim45-65$). Conventional stellar models described these weak processes using the rates estimated by Fuller, Fowler, and Newman (1982b). These rates are compared to the shell-model electron-capture rates in Fig. 9 at relevant temperatures and densities. Importantly, the shell-model rates are nearly always lower than the FFN rates. Thus this difference represents a systematic trend, which is not expected to be washed out if the many nuclei in the stellar composition are considered. The difference is caused, for example, by the reduction of the Gamow-Teller strength (quenching) compared to the independent-particle-model value and a systematic misplacement of the Gamow-Teller centroid in nuclei with certain pairing structure (Langanke and Martínez-Pinedo, 2000). In some cases, experimental data that were not available to Fuller, Fowler, and Newman, but could be used by Langanke and Martínez-Pinedo (2001), led to significant changes. The FFN and

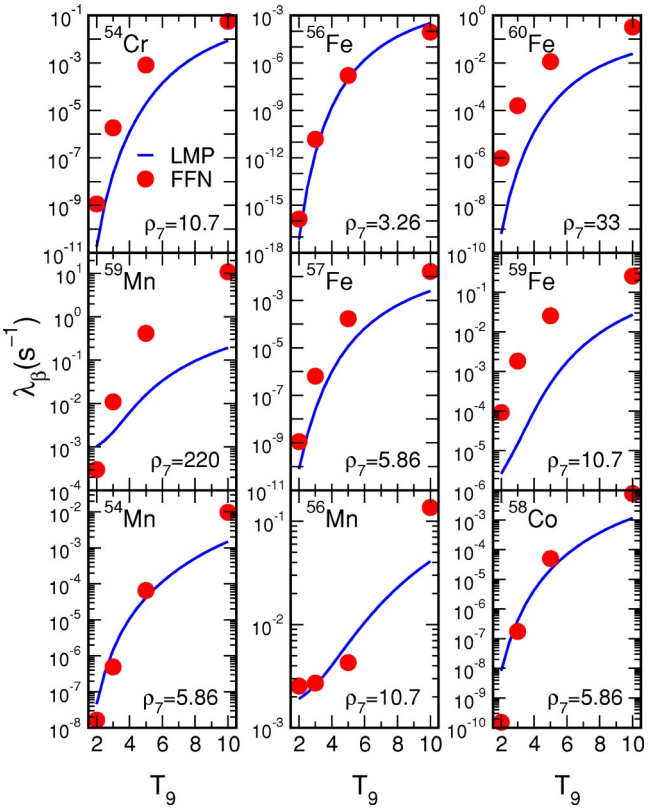

FIG. 10. (Color in online edition) Shell-model beta decay rates as a function of temperature (T_9 measures the temperature in 10^9 K) and for selected densities (ρ_7 defines the density in 10^7 g cm^{-3}) and nuclei. For comparison, the FFN rates are given by the full points. From Martínez-Pinedo *et al.*, 2000.

shell-model beta decay rates are compared in Fig. 10. Martínez-Pinedo *et al.* (2000) discuss the differences between the two rate sets.

C. Consequences of the shell-model rates in stellar models

Heger, Langanke, *et al.* (2001) and Heger, Woosley, *et al.* (2001) have investigated the influence of the shell-model rates on the late-stage evolution of massive stars by repeating the calculations of Woosley and Weaver (1995), keeping the stellar physics, except for the weak rates, as close to the original studies as possible. The new calculations incorporated the shell-model weak-interaction rates for nuclei with mass numbers $A=45-65$, supplemented by rates from Oda *et al.* (1994) for lighter nuclei. The earlier calculations of Weaver and Woosley used the FFN rates for electron capture and an older set of beta decay rates (Mazurek, 1973; Mazurek *et al.*, 1974). As an aside we note that late-stage evolution of massive stars is quite sensitive to the $^{12}C(\alpha,\gamma)^{16}O$ rate, which is still not sufficiently well known. The value adopted in the standard Weaver and Woosley and Heger *et al.* models [$S(E=300\text{ keV})=170$ keV b] agrees, however, rather nicely with the recent data analysis [$S(300)=165\pm50$ keV b (Kunz *et al.*, 2001)] and the value derived from nucleosynthesis arguments by Weaver and Woosley (1993) [$S(300)=170\pm20$ keV b].

Figure 11 illustrates the consequences of the shell-model weak-interaction rates for presupernova models in terms of the three decisive quantities: the central electron-to-baryon ratio Y_e, the entropy, and the iron-core mass. The central values of Y_e at the onset of core collapse increased by 0.01–0.015 for the new rates. This is a significant effect. For example, a change from $Y_e=0.43$ in the Weaver and Woosley model for a $20M_\odot$ star to $Y_e=0.445$ in the new models increases the respective Chandrasekhar mass by about $0.075M_\odot$. We note that the new models also result in lower core en-

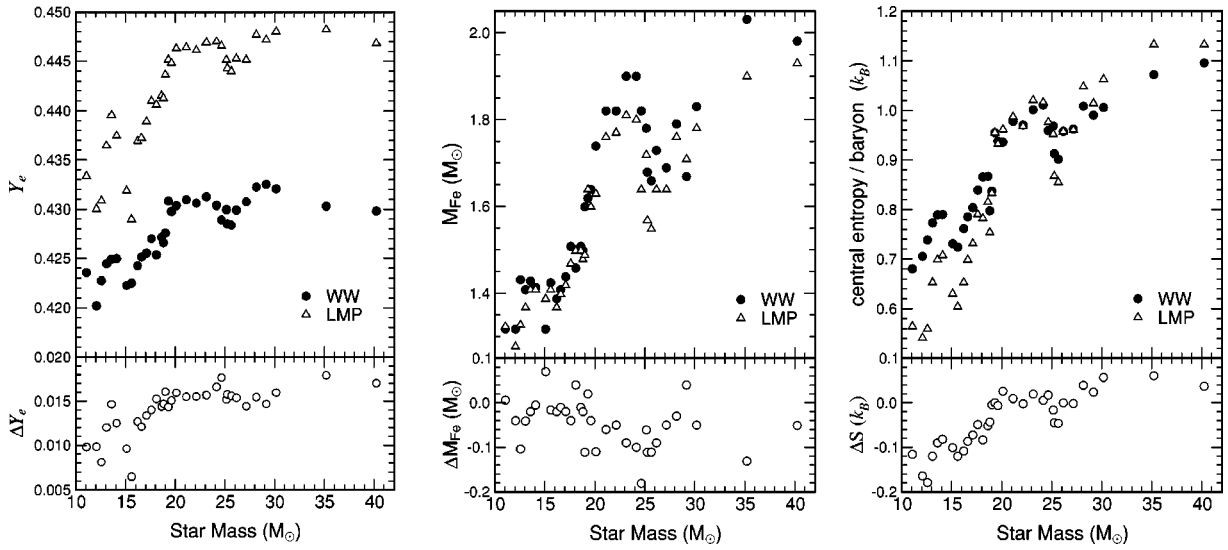

FIG. 11. Comparison of the center values of Y_e (left), the iron-core sizes (middle), and the central entropy (right) for $11-40M_\odot$ stars between the Weaver and Woosley (WW) models and the ones using the shell-model weak-interaction rates of Langanke and Martínez Pinedo (LMP) from Heger, Langanke, *et al.*, 2001. The lower parts define the changes in the three quantities between the LMP and WW models.

tropies for stars with $M \leqslant 20M_\odot$, while for $M \geqslant 20M_\odot$, the new models actually have a slightly larger entropy. The iron-core masses are generally smaller in the new models where the effect is larger for more massive stars ($M \geqslant 20M_\odot$), while for the most common supernovae ($M \leqslant 20M_\odot$) the reduction is by about $0.05M_\odot$. [We define the iron core as the mass interior to the point where the composition becomes at least 50% of iron-group elements ($A \geqslant 48$).] This reduction of the iron-core mass appears to be counterintuitive at first glance with respect to the slower electron-capture rates in the new models. It is, however, related to changes in the entropy profile during silicon shell burning, which reduces the growth of the iron core just prior to collapse (Heger, Langanke, *et al.*, 2001).

It is intriguing to speculate what effects these changes might have for the subsequent core collapse and supernova explosion. At first we note that in the current supernova picture (Bethe, 1990; Burrows, 2000; Langanke and Wiescher, 2001; Woosley *et al.*, 2002) gravitation overcomes the resisting electron-degeneracy pressure in the core, leading to increasing densities and temperatures. Shortly after neutrino trapping at densities of a few 10^{11} g cm^{-3}, a homologous core, which stays in sonic communication, forms in the center. Once the core reaches densities somewhat in excess of nuclear matter density (a few 10^{14} g cm^{-3}) the nuclear equation of state stiffens and a springlike bounce is created, triggering the formation of a shock wave at the surface of the homologous core (Bethe, 1990). This shock wave tries to traverse the rest of the infalling matter in the iron core. However, the shock loses its energy by dissociation of the infalling matter and by neutrino emission, and it is generally believed now that supernovae do not explode promptly due to the bounce shock. Probably this happens in the "delayed mechanism" (Wilson, 1985), where the shock is revived by energy deposition from the neutrinos generated by the cooling of the protoneutron star, the remnant in the center of the explosion.

With the larger Y_e values obtained in the calculations with the improved weak rates, the core contains more electrons, whose pressure acts against the collapse. It is also expected that the size of the homologous core, which scales like $\sim Y_e^2$ with the Y_e value at neutrino trapping, should be larger. This, combined with the smaller iron cores, yields less material that the shock has to traverse. Furthermore, the change in entropy will affect the mass fraction of free protons, which in the later stage of the collapse contribute significantly to electron capture. For presupernova models with masses $M < 20M_\odot$, however, the number fraction of protons is very low ($\lesssim 10^{-6}$, Heger, Langanke, *et al.*, 2001) so that for these stars electron capture should still be dominated by nuclei, even at densities in excess of 10^{10} g cm^{-3}. We shall return to this problem below.

To understand the origin of these differences it is illustrative to investigate the role of the weak-interaction rates in greater detail. The evolution of Y_e during the collapse phase is plotted in Fig. 12. Weak processes become particularly important in reducing Y_e below 0.5

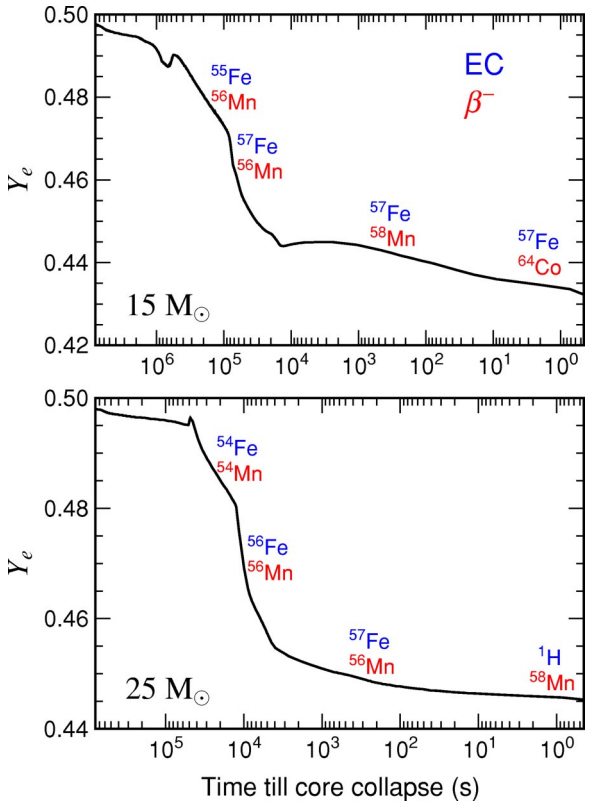

FIG. 12. (Color in online edition) Evolution of the Y_e value in the center of a $15M_\odot$ star (upper part) and $25M_\odot$ star (lower part) as a function of time until bounce. The most important Y_e-changing nuclei for the calculations adopting the shell-model rates are indicated at different times, where the upper nucleus refers to electron capture and the lower to β decay.

after oxygen depletion ($\sim 10^7$ s and 10^6 s before core collapse for the $15M_\odot$ and $25M_\odot$ stars, respectively) and Y_e begins a decline which becomes precipitous during silicon burning. Initially electron capture occurs much

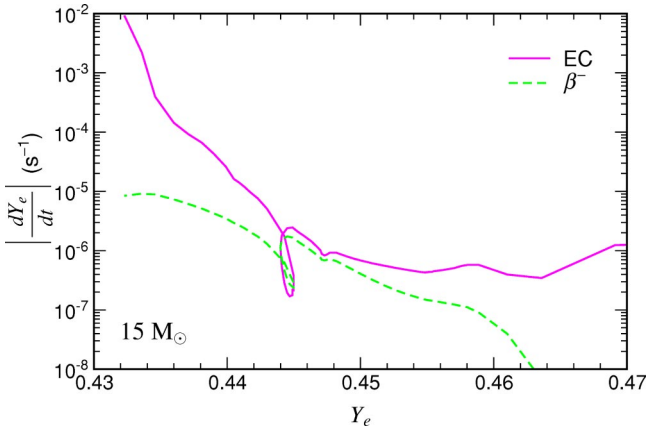

FIG. 13. (Color in online edition) Comparison of the change of the Y_e value with time, $|dY_e/dt|$ due to electron capture and beta decay in a $15M_\odot$ star. In general, the Y_e value decreases with time during the collapse, caused by electron captures. The loops indicate that during this period beta decay, which increases Y_e, dominates over electron capture.

more rapidly than beta decay. As the shell-model rates are generally smaller than the FFN electron-capture rates, the initial reduction of Y_e is smaller in the new models; the temperature in these models is correspondingly larger as less energy is radiated away by neutrino emission.

An important feature of the new models is demonstrated in Fig. 13. Beta decay becomes temporarily competitive with electron capture after silicon depletion in the core and during silicon shell burning (this had been foreseen by Aufderheide, Fushiki, Fuller, *et al.*, 1994). The presence of an important beta-decay contribution has two effects. Obviously it counteracts the reduction of Y_e in the core, but equally important, beta decays are an additional neutrino source and thus they add to the cooling of the core and a reduction in entropy. This cooling can be quite efficient, as often the average neutrino energy in the involved beta decays is larger than for the competing electron captures. As a consequence the new models have significantly lower core temperatures than the Weaver and Woosley models after silicon burning. At later stages of the collapse, beta decay becomes unimportant again as an increased electron chemical potential drastically reduces the phase space.

We note that the shell-model weak-interaction rates predict that the presupernova evolution will proceed along a temperature-density-Y_e trajectory in which the weak processes are dominated by nuclei rather close to stability. Thus it will be possible, after next-generation radioactive ion-beam facilities become operational, to further constrain the shell-model calculations by measuring relevant GT distributions for unstable nuclei by charge-exchange reaction. Here again the GT_+ distribution is also crucial for stellar β decays. Figure 12 identifies those nuclei which dominate (defined by the product of abundance times rate) electron capture and beta decay during various stages of the final evolution of $15M_\odot$ and $25M_\odot$ stars. Heger, Woosley, *et al.* (2001) give an exhaustive list of the most important nuclei for both electron capture and beta decay during the final stages of stellar evolution for stars of different masses.

In total, the weak-interaction processes shift the matter composition to smaller Y_e values (see Fig. 12) and hence more neutron-rich nuclei, subsequently affecting nucleosynthesis. Its importance for the elemental abundance distribution, however, strongly depends on the location of the mass cut in the supernova explosion. It is currently assumed that the remnant will have a baryonic mass between the iron core and oxygen shell masses (Woosley, Heger, and Weaver, 2002). As the reduction in Y_e occurs mainly during silicon burning, it is essential to determine how much of this material will be ejected. Another important issue is the possible long-term mixing of material during the explosion (see, for example, Kifonidis *et al.*, 2000). Changes of the elemental abundances due to the improved weak-interaction rates are rather small, as the differences from the FFN model occur in regions of the star that are probably not ejected (however, for type-Ia supernovae, see below). The weak interaction also determines the decay of the newly synthesized nuclei in supernova explosions. Some of these are proton-rich nuclei that decay by orbital electron capture, leaving atomic K-shell electron vacancies. The x rays emitted can escape the supernova ejecta for sufficiently long-lived isotopes and can possibly be detected by the current generation of x-ray telescopes (Leising, 2001).

In a dense stellar environment the electron-capture rates have to be corrected for screening effects caused by the relativistically degenerate electron liquid. Studies in which this has been done within the linear-response theory have recently been performed (Itoh *et al.*, 2002). Itoh *et al.* find typical screening corrections of order a few percent.

V. COLLAPSE AND POST-BOUNCE STAGE

The models we have described above constitute the so-called presupernova models. They follow late-stage stellar evolution until core densities just below $10^{10}\,\mathrm{g\,cm^{-3}}$ and temperatures between 5 and 10 GK. More precisely, Woosley and Weaver (1995) define the final stage of presupernova models as the time when the collapse velocity near the edge of the iron core first reaches $1000\,\mathrm{km\,s^{-1}}$. As we have stressed above, stellar evolution up to this time requires the consideration of an extensive nuclear network, but is simplified by the fact that neutrinos need only be treated as a source for energy losses. This is no longer valid at later stages of the collapse. As neutrinos will eventually be trapped in the collapsing core and their interaction with the surrounding matter is believed to be crucial for the supernova explosion, computer simulations of the collapse, bounce, and explosion necessitate a detailed time- and space-dependent bookkeeping of the various neutrino (ν_e, ν_μ, ν_τ neutrinos and their antiparticles) distributions in the core. Building on the pioneering work of Bruenn (1985), this is done in terms of multigroup (neutrinos of different flavor and energy) Boltzmann neutrino transport (Rampp and Janka, 2000; Liebendörfer *et al.*, 2001; Mezzacappa *et al.*, 2001). Advantageously, the temperature during the collapse and explosion is high enough that the matter composition is given by nuclear statistical equilibrium without the need of reaction networks for the strong and electromagnetic interactions. The transition from a rather complex global nuclear network involving many neutron, proton, and α fusion reactions and their inverses, through a quasistatistical equilibrium in which reactions within mini-cycles are fast enough to bring constrained regions of the nuclear chart into equilibrium, and finally to global nuclear statistical equilibrium is extensively discussed by Woosley (1986).

Presupernova models are the input for collapse and explosion simulations. Currently one-dimensional models with sophisticated neutrino transport do not explode (Rampp and Janka, 2000; Liebendörfer *et al.*, 2001; Mezzacappa *et al.*, 2001). This includes the first attempts at presupernova models derived with the improved weak-interaction rates discussed above (Messer *et al.*, 2002).

Explosions can, however, be achieved if the shock revival in the delayed mechanism is modeled by two-dimensional hydrodynamics allowing for more efficient neutrino energy transfer (Herant *et al.*, 1994; Burrows *et al.*, 1995; Janka and Müller, 1996). Thus the intriguing question arises: Are supernova explosions three-dimensional phenomena requiring convective motion and perhaps rotation and magnetic fields? Or do one-dimensional models fail due to incorrect or insufficient nuclear physics input? Although first steps have been taken in modeling the multidimensional effects (for reviews and references see Janka *et al.*, 2001; Woosley *et al.*, 2002), these require extremely demanding and computationally challenging simulations. In the following we shall briefly discuss some nuclear physics ingredients in the collapse models and their possible improvements.

The crucial weak processes during the collapse are (Bruenn, 1985; Burrows, 2001; Rampp and Janka, 2002)

$$p+e^- \rightleftarrows n+\nu_e, \tag{8a}$$

$$n+e^+ \rightleftarrows p+\overline{\nu}_e, \tag{8b}$$

$$(A,Z)+e^- \rightleftarrows (A,Z-1)+\nu_e, \tag{8c}$$

$$(A,Z)+e^+ \rightleftarrows (A,Z+1)+\overline{\nu}_e, \tag{8d}$$

$$\nu+N \rightleftarrows \nu+N, \tag{8e}$$

$$N+N \rightleftarrows N+N+\nu+\overline{\nu}, \tag{8f}$$

$$\nu+(A,Z) \rightleftarrows \nu+(A,Z), \tag{8g}$$

$$\nu+e^{\pm} \rightleftarrows \nu+e^{\pm}, \tag{8h}$$

$$\nu+(A,Z) \rightleftarrows \nu+(A,Z)^*, \tag{8i}$$

$$e^+ + e^- \rightleftarrows \nu+\overline{\nu}, \tag{8j}$$

$$(A,Z)^* \rightleftarrows (A,Z)+\nu+\overline{\nu}. \tag{8k}$$

Here, a nucleus is symbolized by its mass number A and charge Z, N denotes either a neutron or a proton, and ν represents any neutrino or antineutrino. In the early collapse stage, before trapping, these reactions proceed dominantly to the right. We note that, due to the generally accepted collapse picture (e.g., that of Bethe, 1990), elastic scattering of neutrinos on nuclei [Eq. (8g)] is mainly responsible for the trapping, as it determines the diffusion time scale of the outwards-streaming neutrinos. Shortly after trapping, the neutrinos are thermalized by the energy downscattering, experienced mainly in inelastic scattering off electrons [Eq. (8h)]. The relevant cross sections for these processes are readily derived (Bruenn, 1985). For elastic neutrino-nucleus scattering one usually makes the simplifying assumption that the nucleus has a $J=0^+$ spin/parity assignment, as appropriate for the ground state of even-even nuclei. The scattering process is then restricted to the Fermi part of the neutral current (pure vector coupling; Freedman, 1974; Tubbs and Schramm, 1975) and gives rise to coherent scattering; i.e., the cross section scales with A^2, except from a correction $\sim(N-Z)/A$ arising from the neutron excess. This assumption is, in principle, not correct for the ground states of odd-A and odd-odd nuclei and for all nuclei at finite temperature, as then $J \geqslant 0$ and the cross section will also have an axial-vector Gamow-Teller contribution. However, the relevant GT_0 strength is not concentrated in one state, but rather fragmented over many nuclear levels. Thus one can expect that GT contributions to the elastic neutrino-nucleus cross sections will in general be small enough to be neglected.

Reactions (8a) and (8c) are equally important, as they control the neutronization of the matter and, in a large portion, also the star's energy losses. Due to their strong phase-space sensitivity ($\sim E_e^5$), electron-capture cross sections increase rapidly during the collapse as the density (the electron chemical potential scales like $\sim\rho^{1/3}$) and the temperature increase. We have already observed above that beta decay is rather unimportant during collapse due to Pauli blocking of the electron phase space in the final state. We also noted how sensitively the electron-capture rate for nuclei depends on a proper description of nuclear structure. As we shall discuss now, this is also expected for this stage of the collapse, although the relevant nuclear structure issues are somewhat different.

A. Electron capture on nuclei

The new presupernova models indicate that electron capture on nuclei will still be important, at least in the early stage of the collapse. Although capture on free protons, compared to nuclei, is favored by a significantly lower Q value, or difference between the nuclear mass of the initial and final state, the number fraction of free protons Y_p, i.e., the number of free protons divided by the total number of nucleons, is quite low ($Y_p \sim 10^{-6}$ in the $15M_\odot$ presupernova model of Heger, Woosley, *et al.*, 2001). This tendency had already been observed before, but has been strengthened in the new presupernova models, where the Y_e values are significantly larger and thus the nuclei present in the matter composition are less neutron rich, implying lower Q values for electron capture. Furthermore, the entropy is smaller in stars with $\lesssim 20M_\odot$, yielding a smaller fraction of free protons.

As the entropy is rather low (Bethe *et al.*, 1979), most of the collapsing matter survives in heavy nuclei. However, Y_e decreases during the collapse, making the matter composition more neutron rich and hence energetically favoring increasingly heavy nuclei. In computer studies of collapse, the ensemble of heavy nuclei is described by one representative, which is generally chosen to be the most abundant in the nuclear statistical equilibrium composition. Due to a simulation of the infall phase (Mezzacappa and Bruenn, 1993a, 1993b), such representative nuclei are ^{70}Zn and ^{88}Kr at different stages of the collapse (Mezzacappa, 2001).

In current collapse simulations the treatment of electron capture on nuclei is schematic and rather simplistic. The nuclear structure required to derive the capture rate is then described solely on the basis of an independent-

particle model for iron-range nuclei, i.e., considering only Gamow-Teller transitions from $f_{7/2}$ protons to $f_{5/2}$ neutrons (Bethe *et al.*, 1979; Bruenn, 1985; Mezzacappa and Bruenn, 1993a, 1993b). In particular, this model predicts that electron capture vanishes for nuclei with charge number $Z<40$ and neutron number $N\geqslant 40$, arguing that Gamow-Teller transitions are blocked by the Pauli principle, as all possible final neutron orbitals are already occupied in nuclei with $N\geqslant 40$ (closed p-f shell; Fuller, 1982). Such a situation would, for example, occur for the two nuclei ^{70}Zn and ^{88}Kr with $Z=30$, $N=40$ and $Z=36$, $N=52$, respectively. It has been pointed out (Cooperstein and Wambach, 1984) that this picture is too simple and that the blocking of the GT transitions will be overcome by thermal excitation which either moves protons into $g_{9/2}$ orbitals or removes neutrons from the p-f shell, in both ways reallowing GT transitions. In fact, due to this "thermal unblocking," GT transitions again dominate the electron capture on nuclei for temperatures of order 1.5 MeV (Cooperstein and Wambach, 1984). An even more important unblocking effect, which is already relevant at lower temperatures, is, however, expected from the residual interaction, which will mix the $g_{9/2}$ (and higher) orbitals with those in the p-f shell.

A consistent calculation of the electron-capture rates for nuclei with neutron numbers $N>40$ and proton numbers $20<Z<40$, including configuration mixing and finite temperature, is not yet feasible by direct shell-model diagonalization due to the large model spaces and many states involved. It can, however, be performed in a reasonable way adopting a hybrid model: The capture rates are calculated within the RPA approach with a partial occupation formalism, including allowed and forbidden transitions. The partial occupation numbers represent an "average" state of the parent nucleus and depend on temperature. They are calculated within the shell-model Monte Carlo approach at finite temperature (Koonin *et al.*, 1997) and include an appropriate residual interaction. Exploratory studies, performed for a chain of germanium isotopes ($Z=32$), confirm that the GT transition is not blocked for $N\geqslant 40$ and still dominates the electron-capture process for such nuclei at stellar conditions (Langanke, Kolbe, and Dean, 2001). This is demonstrated in Fig. 14, which compares electron-capture rates for ^{78}Ge calculated within the hybrid model with the results in the independent-particle model (IPM). For this nucleus ($N=46$) the rate in the independent-particle model is given solely by forbidden transitions (mainly induced by 1^- and 2^- multipoles). However, correlations and finite temperature unblock the GT transitions in the hybrid model, which increases the rate significantly. The differences are particularly important at lower densities (a few 10^{10} g cm^{-3}), where the electron chemical potential does not suffice to induce forbidden transitions.

We note again that many nuclei are present with similar mass abundances during the supernova collapse phase and that their relative abundances are approximately described by nuclear statistical equilibrium. Fig-

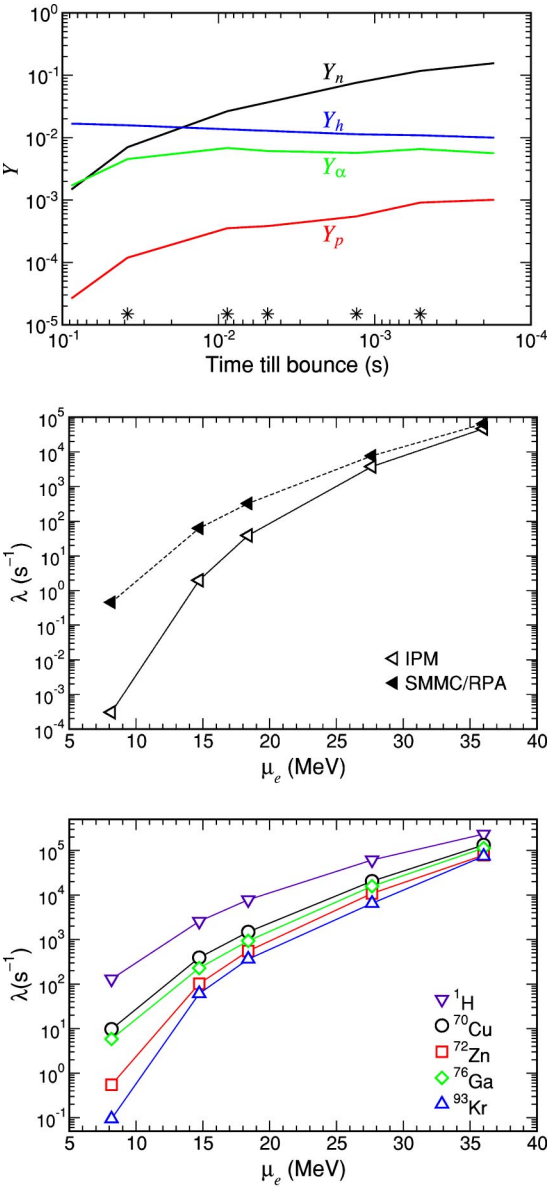

FIG. 14. (Color in online edition) Electron-capture rates on free protons and several representative nuclei as a function of electron chemical potential μ_e (lower panel). The rates have been determined for conditions during the infall phase (Liebendörfer, 2002): $(T, Y_e, \rho_{11}) = (0.846, 0.429, 0.102)$, $(1.133, 0.410, 0.601)$, $(1.259, 0.400, 1.186)$, $(1.617, 0.372, 4.287)$, $(2.000, 0.349, 10.063)$, where the temperature T is given in MeV and ρ_{11} measures the density in 10^{11} g cm^{-3}. The electron chemical potential increases during the infall, $\mu_e \sim \rho^{1/3}$. The middle panel compares the capture rates on ^{78}Ge in the independent-particle model (IPM), in which Gamow-Teller transitions are Pauli blocked, with the results obtained in the hybrid model (SMMC/RPA), which unblocks these transitions due to correlations and finite-temperature effects. The rates have been calculated without neutrino final-state Pauli blocking, which will become important at trapping densities. The upper panel shows the time evolution of the number abundances for neutrons Y_n, protons Y_p, α particles Y_α, and heavy nuclei Y_h, calculated along the same stellar trajectory for which the rates have been calculated at selected points. These points are marked by asterisks. From Sampaio, Langanke, Martínez-Pinedo, Dean, and Kolbe, 2002.

ure 14 shows the capture rates for several representative nuclei during the collapse phase, identified by the average charge and mass number of the matter composition following the time evolution of a certain ($M=0.6M_\odot$) mass trajectory (Liebendörfer *et al.*, 2001). (For the conditions shown in Fig. 14, ^{93}Kr and ^{72}Zn are examples of representative nuclei at $\rho_{11}=10.063$ and 0.601, respectively.) The general trend of the rates reflects the competition of the two main energy scales of the capture process: the electron chemical potential μ_e, which grows like $\rho^{1/3}$ during infall, and the reaction Q value. As the Q value is smaller for free protons ($Q=1.29$ MeV) than for neutron-rich nuclei ($Q\sim$a few MeV), the capture rate on free protons is larger than for the heavy nuclei. However, this difference diminishes with increasing density. This is expected because the electron energies involved are then significantly higher (for example, the electron chemical potential is $\mu_e\sim 18$ MeV at $\rho=10^{11}$ g cm^{-3}) than the Q values for the capture reactions on the abundant nuclei (i.e., ^{93}Kr has a Q value of about 11 MeV). As nuclear structure effects at the relatively high temperatures involved are rather unimportant, the capture rates on the abundant nuclei at the later stage of the collapse are rather similar. However, the capture rate is quite sensitive to the reaction Q value for the lower electron chemical potentials. To quantify this argument we take the point of the stellar trajectory from Fig. 14 with the lowest electron chemical potential ($\mu_e\sim 8$ MeV) as an example. Under these conditions the capture rates on ^{70}Cu and ^{76}Ga (both nuclei have Q values around 4 MeV) are noticeably larger than for ^{78}Ge and ^{72}Zn with Q values around 8 MeV. However, in nuclear statistical equilibrium the relative mass fraction of ^{72}Zn (about 1.2×10^{-2}) is larger than for ^{70}Cu (4.0×10^{-3}) or ^{76}Ga (1.8×10^{-3}). The most abundant nucleus, ^{66}Ni, has a mass fraction of 4.3×10^{-2} and a capture rate comparable to ^{72}Zn. ^{93}Kr is too neutron rich to have a significant abundance at this stage of the collapse. This discussion indicates that the most abundant nuclei are not necessarily the nuclei which dominate electron capture in the infall phase. Thus a single-nucleus approximation can be quite inaccurate and should be replaced by an ensemble average.

What matters for the comparison of capture on nuclei to that on free protons is the product of number abundance times capture rate. Figure 14 shows the time evolution of the number abundances for free neutrons, protons, α particles, and heavy nuclei, calculated for the same stellar trajectory (obtained from Liebendörfer, 2002) for which the capture rates have been evaluated under the assumption of nuclear statistical equilibrium. [We note that the commonly adopted equations of state (Lattimer and Swesty, 1991; Shen *et al.*, 1998a) yield somewhat larger Y_p fractions than are obtained in nuclear statistical equilibrium.] Importantly, the number abundance of heavy nuclei is significantly larger than that of free protons (by more than two orders of magnitude at the example point discussed above) to compensate for the smaller capture rates on heavy nuclei. It appears thus that electron capture on nuclei cannot be neglected during the collapse. We note that the average energies of the neutrinos produced by capture on nuclei are significantly smaller than for capture on free protons, making this process a potentially important source for low-energy neutrinos.

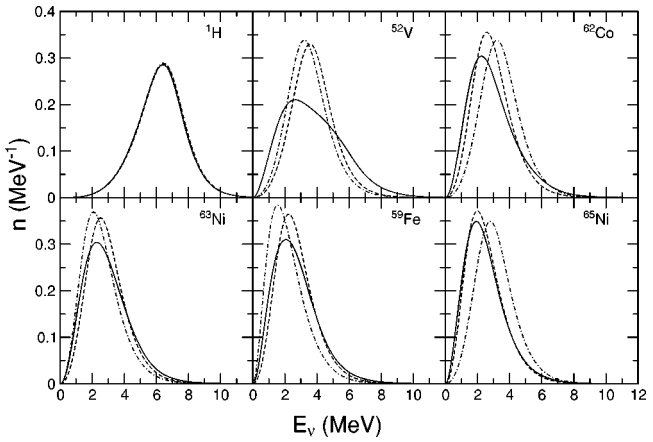

FIG. 15. Normalized neutrino spectra for stellar electron capture on the six most important "electron-capturing nuclei" in the presupernova model of a $15M_\odot$ star, as identified by Heger, Langanke, *et al.*, 2001. The stellar parameters are $T=7.2\times10^9$ K, $\rho=9.1\times10^9$ g cm^{-3}, and $Y_e=0.43$. The solid lines represent the spectra derived from the shell-model electron-capture rates. The dashed and dashed-dotted lines correspond to parametrizations recommended by Langanke, Martínez-Pinedo, and Sampaio (2001) and Bruenn (1985), respectively.

The neutron number $N=40$ is not magic in nuclear structure, nor is it magic for stellar electron-capture rates. Thus the anticipated strong reduction of the capture rate on nuclei will not occur and we expect capture on nuclei to be an important neutronization process probably until neutrino trapping. The magic neutron number $N=50$ is also no barrier as for nuclei like ^{93}Kr ($N=57$) the neutron p-f shell is nearly completely occupied, but due to correlations, protons occupy, for example, the $g_{9/2}$ orbital and thus unblock GT transitions by allowing transformations into $g_{9/2}$,$g_{7/2}$ neutrons. The description of electron capture on nuclei in the collapse simulations needs to be improved.

In the current simulations the inverse reaction rates of the weak processes listed above are derived by detailed balance. Thus an improved description of electron capture will also affect the neutrino absorption on nuclei, although this process is strongly suppressed by Pauli blocking in the final state.

B. Neutrino rates

In the capture process on nuclei, the electron has to overcome the Q values of the nuclei and the internal excitation energy of the GT states in the daughter, so the final neutrino energies are noticeably smaller than for capture on free protons. Typical neutrino spectra for a presupernova model are shown in Fig. 15. In this stage of the collapse the neutrino energies are sufficiently small that they only excite allowed transitions. Conse-

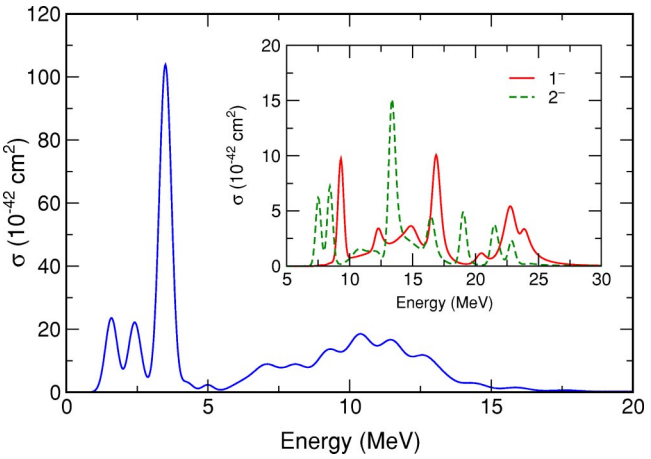

FIG. 16. (Color in online edition) Differential $^{56}\mathrm{Fe}(\nu_e,e^-)^{56}\mathrm{Co}$ cross section for the KARMEN neutrino spectrum, coming from the decay at rest of the muon, as a function of the excitation energy in ^{56}Co. The figure shows the allowed contributions, while the inset gives the contribution of the 1^- and 2^- multipolarities.

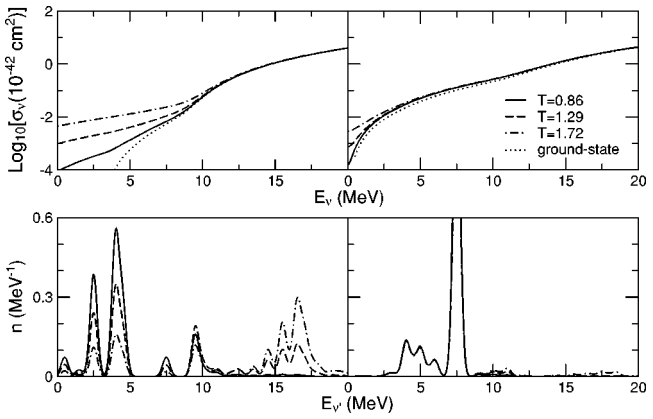

FIG. 17. Inelastic neutrino cross sections for ^{56}Fe (left) and ^{59}Co (right) as a function of initial neutrino energy and for selected temperatures (upper part). Only allowed Gamow-Teller transitions have been considered. Temperatures are in MeV. For $T=0$, the cross section is calculated for the ground state only. At $T>0$, the cross sections have been evaluated for a thermal ensemble of initial states. The corresponding neutrino energy distribution in the final state is shown in the lower part, assuming an initial neutrino energy of $E_\nu=7.5$ MeV. Due to threshold effects a significant portion of the neutrinos are upscattered in energy for even-even nuclei.

quently neutrino-nucleus cross sections for p-f-shell nuclei can be determined on the basis of GT distributions determined in the shell model. In the later stage of the collapse, the increased density also results in higher-energy electrons ($E_e\sim\rho^{1/3}$), which in turn, if captured by protons or nuclei, produce neutrinos with energies larger than 15–20 MeV. For such neutrinos forbidden (mainly $\lambda=1$ dipole and spin-dipole) transitions can significantly contribute to the neutrino-nucleus cross section. Such a situation is shown in Fig. 16, which shows the differential cross section for the process $^{56}\mathrm{Fe}(\nu_e,e^-)^{56}\mathrm{Co}$ computed using the shell model for the Gamow-Teller contribution and the continuum RPA for the forbidden contributions (Kolbe, Langanke, and Martínez-Pinedo, 1999). The calculation adopts a neutrino spectrum corresponding to a muon decaying at rest. The average energy, $\overline{E}_\nu\approx30$ MeV, and momentum transfer, $q\approx50$ MeV, represent the maximum values for ν_e neutrinos expected during the supernova collapse phase, i.e., the maximum contribution expected from forbidden transitions to the total neutrino-nucleus cross sections. In this particular case the 1^+ multipole (Gamow-Teller at the $q=0$ limit) represents 50% of the cross section. The $^{56}\mathrm{Fe}(\nu_e,e^-)^{56}\mathrm{Co}$ cross section for neutrinos from muon decay at rest has been measured by the KARMEN Collaboration. The measured cross section $[2.56\pm1.08(\mathrm{stat})\pm0.43(\mathrm{syst})\times10^{-40}$ cm^2; Zeitnitz, 1994] agrees with the result calculated in the shell model (allowed transitions) plus continuum RPA (forbidden transitions) approach (2.38×10^{-40} cm^2; Kolbe, Langanke, and Martínez-Pinedo, 1999).

Although the most important neutrino reactions during collapse are coherent elastic scattering on nuclei and inelastic scattering off electrons, it has been noted (Haxton, 1988; Bruenn and Haxton, 1991) that neutrino-induced reactions on nuclei can happen as well. Using ^{56}Fe as a representative nucleus, Bruenn and Haxton concluded that charged-current (ν_e,e^-) reactions do not have an appreciable effect on the evolution of the core during infall, due to the high threshold for neutrino absorption. Based on shell-model calculations of the GT strength distributions, Sampaio *et al.* (2001) confirmed this finding for other, more relevant nuclei in the core composition. The same authors showed that finite-temperature effects can increase the (ν_e,e^-) cross sections for low neutrino energies drastically (Sampaio *et al.*, 2001). But this increase is found to be significantly smaller than the reduction of the cross section caused by Pauli blocking of the final phase space, i.e., due to the increasing electron chemical potential. This environmental effect ensures that neutrino absorption on nuclei is unimportant during the collapse compared with inelastic neutrino-electron scattering.

Bruenn and Haxton (1991) observed that inelastic neutrino scattering off nuclei plays the same important role of equilibrating electron neutrinos with matter during infall as neutrino-electron scattering. The influence of finite temperature on inelastic neutrino-nucleus scattering was studied by Fuller and Meyer (1991), using an independent-particle model. While the study of Bruenn and Haxton (1991) was restricted to ^{56}Fe, additional cross sections have been calculated for inelastic scattering of neutrinos on other nuclei based on modern shell-model GT strength distributions (Sampaio *et al.*, 2002). Again, for low neutrino energies the cross sections are enhanced at finite temperatures (Fig. 17). This is caused by the possibility that, at finite temperatures, the initial nucleus can reside in excited states which can be connected with the ground state by sizable GT matrix elements. These states can then be deexcited in inelastic neutrino scattering. Note that in this case the final neutrino energy is larger than the initial (see Fig. 17) so that

the deexcitation occurs additionally with larger phase space. Until neutrino trapping there is little phase-space blocking in inelastic neutrino-nucleus scattering. Toivanen *et al.* (2001) presented the charged- and neutral-current cross sections for neutrino-induced reactions on the iron isotopes $^{52-60}$Fe, using a combination of the shell-model and RPA approaches. Other possible neutrino processes, e.g., nuclear deexcitation by neutrino pair production [Eq. (8k)], have been discussed by Fuller and Meyer (1991), but the estimated rates are probably too small for these processes to be important during the collapse.

Finally we remark that coherent elastic scattering on nuclei scales like $\sim E_\nu^2$ so that neutrinos with low energies are the last to be trapped. In filling this important sink for entropy and energy, processes that affect the production of neutrinos with low energies can be quite relevant for the collapse. Inelastic neutrino scattering on nuclei, including finite-temperature effects, is one such process (Bruenn and Haxton, 1991). The energies of neutrinos generated by electron capture on nuclei are significantly lower than the ones generated by capture on free protons, another reason to implement these processes with appropriate care in collapse simulations.

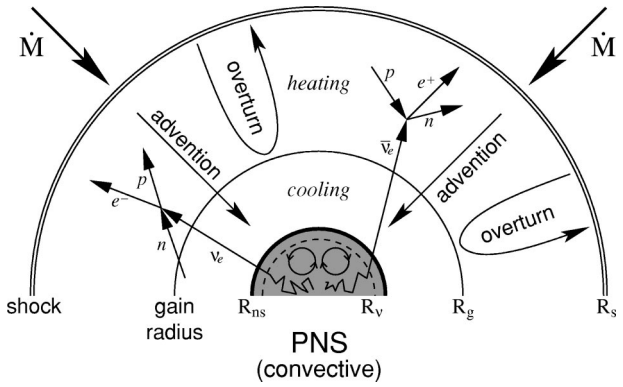

FIG. 18. Sketch of the stellar core during the shock revival phase. R_ν is the neutrinosphere radius, from which neutrinos are expected to stream out freely, R_{ns} is the radius of the protoneutron star (PNS), R_g the gain radius (see text), and R_s the radius at which the shock is stalled. The shock expansion is impeded by mass infall at a rate $\dot{M}$, but supported by convective energy transport from the region of strongest neutrino heating to the stalled shock. Convection inside the protoneutron star as well as correlations in the dense nuclear medium increase the neutrino luminosity. Adapted from Janka *et al.*, 2001.

C. Delayed supernova mechanism

In the delayed supernova mechanism the fate of the explosion is determined by several distinct neutrino processes. When the shock reaches the ν_e neutrinosphere, from which ν_e are expected to stream out freely, electron capture on the shock-heated and shock-dissociated matter increases the ν_e production rate significantly. Additionally neutrinos are produced by the transformation of electron-positron pairs into $\nu\overline{\nu}$ pairs [Eq. (8j)]. This process is strongly temperature dependent (see, for example, Soyeur and Brown, 1979; Itoh *et al.*, 1996) and occurs most effectively in the shock-heated regions of the protoneutron star. Electron-positron pair annihilation and nucleon-nucleon bremsstrahlung [Eq. (8f)] generate pairs of all three neutrino flavors with the same probability and thus are the main mechanisms for the production of ν_μ, ν_τ neutrinos and antineutrinos (Hannestad and Raffelt, 1998; Thompson *et al.*, 2000; Hanhart *et al.*, 2001; Hannestad, 2001; Raffelt, 2001; Thompson and Burrows, 2001; Stoica and Horvath, 2002). The emitted ν_e and $\overline{\nu_e}$ neutrinos, however, can be absorbed again by the free nucleons behind the shock. Due to the temperature and density dependences of the neutrino processes involved, neutrino emission wins over neutrino absorption in a region inside a certain radius (the *gain radius*), while outside the gain radius matter is heated by neutrino interactions that are dominated by absorption of electron neutrinos and antineutrinos on free nucleons which have been previously liberated by dissociation due to the shock (see Fig. 18). As a net effect, neutrinos transport energy across the gain radius to the layers behind the shock. Due to the smaller abundances, neutrino-induced reactions on finite nuclei are expected to contribute only modestly to the shock revival. It has been also suggested that the shock revival is supported by "preheating" (Haxton, 1988). In this scenario the electron neutrinos, which have been trapped during the final collapse phase and are liberated in a very short burst (with luminosities of a few 10^{53} erg s^{-1} lasting for about 10 ms), can partly dissociate the matter (e.g., iron and silicon isotopes) prior to the shock arrival. As reliable neutrino-induced cross sections on nuclei have not been available until recently, the neutrino-nucleus reactions have not been included in collapse and post-bounce simulations.

To describe the important neutrino-nucleon processes, most core-collapse simulations use the same lowest-order cross section for both neutrinos and antineutrinos (Bruenn, 1985; Horowitz, 2002), i.e., they neglect terms of order E_ν/M, where E_ν is the neutrino energy and M the nucleon mass. The most important corrections to the cross section at this order are the nucleon recoil and the weak magnetism related to the form factor F_2 in Eq. (4a) (Horowitz, 2002). The recoil correction is the same for neutrinos and antineutrinos and decreases the cross sections. However, the weak magnetism corrects the cross sections via its parity-violating interference with the dominant axial-vector component. As the interference is constructive for neutrinos and destructive for antineutrinos, inclusion of a weak-magnetism correction increases the neutrino cross section, while it decreases the $\overline{\nu}$-nucleon cross sections. It is then expected that corrections up to order E_ν/M decrease the antineutrino cross section noticeably (by about 25% for 40-MeV antineutrinos), while the ν-nucleon cross sections are only affected by a few percent for $E_\nu \leqslant 100$ MeV (Horowitz, 2002).

Neutral-current processes are sensitive to possible strange-quark contributions in the nucleon which would

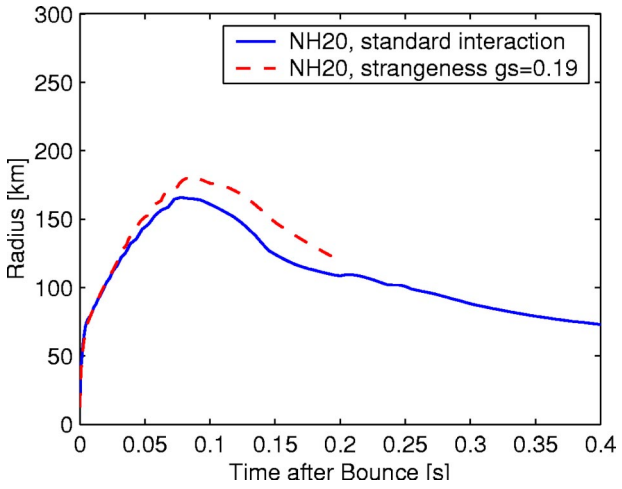

FIG. 19. (Color in online edition) Shock trajectories of a $20M_{\odot}$ star: dashed line, calculated with an isoscalar strange axial form factor in the neutrino-nucleon elastic cross sections; solid line, calculated without such a form factor. Courtesy of M. Liebendörfer.

give rise to an isoscalar piece g_A^s in the axial-vector form factor besides the standard isovector form factor $g_A\boldsymbol{\tau}$ (Jaffe and Manohar, 1990; Beise and MacKeown, 1991). The current knowledge of g_A^s comes from a ν-p elastic-scattering experiment performed at Brookhaven that yielded $g_A^s=-0.15\pm0.08$ (Ahrens *et al.*, 1987), but that is considered rather uncertain (Garvey, Louis, and White, 1993). With $g_A=1.26$ and assuming axial-vector dominance, i.e., the cross section scales like $\sigma\sim|g_A\boldsymbol{\tau}-g_A^s|^2$, a nonvanishing strange axial-vector form factor would reduce the elastic-scattering cross section on neutrons and increase the ν-p elastic cross section (Garvey, Krewald, *et al.*, 1992; Garvey, Kolbe, *et al.*, 1993; Horowitz, 2002). As the matter behind the shock is neutron rich, the net effect will be a reduction of the neutrino-nucleon elastic cross section. This increases the energy transfer to the stalled shock. However, a simulation has shown that this increase is not strong enough for a successful shock revival (Liebendörfer *et al.*, 2002; see Fig. 19).

The physics involved in the attempt to revive the shock by neutrino heating is exhaustively reviewed by Janka *et al.* (2001; see also Burrows and Goshy, 1993). These authors show that the fate of the stalled shock not only depends on neutrino heating above the gain radius, but is also influenced by the energy loss in the cooling region below the gain radius (see also Bethe and Wilson, 1985). Janka (2001) demonstrates the existence of a critical value for the neutrino luminosity from the neutron star needed to revive the shock. This critical luminosity depends on the neutron star's mass and radius and on the mass infall to the shock. One expects that the shock expansion will be eased for high mass-infall rates, which increase the matter pileup on the neutron star and push the shock outwards, and for high ν_e and $\overline{\nu}_e$ luminosities from the neutron star, which lead to an enhancement of neutrino absorption relative to neutrino emission in the gain region.

The explosion depends crucially on the effectiveness with which energy is transported by neutrinos to the region where the shock has stalled. As stressed before, one-dimensional models including sophisticated neutrino transport (e.g., those of Rampp and Janka, 2000 or Liebendörfer *et al.*, 2001) fail to explode. However, the neutrino energy transport is very sensitive to (i) the effect of nucleon-nucleon correlations on the neutrino opacities in dense matter and (ii) convection both in the neutrino-heated region and in the protoneutron star (Janka *et al.*, 2001).

In his pioneering work, Sawyer (1989) calculated the neutrino mean free path, or equivalently the neutrino opacity, in uniform nuclear matter and showed that effects due to the strong interaction between nucleons are important. The same conclusion was reached by Raffelt *et al.* (1996), who demonstrated that the average neutrino-nucleon cross section in the medium is reduced due to spin fluctuations induced by the spin-dependent interaction among nucleons. (For earlier calculations of the neutrino mean free path in uniform nuclear matter, see Sawyer 1975; Friman and Maxwell, 1979; and Iwamoto and Pethick, 1982.) Sawyer (1989) exploited the relation between the equation of state of the matter and the long-wavelength excitations of the system to calculate the weak-interaction rates. However, consistency between the equation of state and the neutrino opacities is more difficult to achieve for large energy (q_0) and momentum (q) transfer of the neutrinos. Here, particle-hole and particle-particle interactions are examples of effects that might influence the equation of state and the neutrino opacities. For the following discussion it is quite illuminating to realize the similarity of neutrino-induced excitations of nuclear matter with the physics of multipole giant resonances in finite nuclei.

For muon and tau neutrinos, neutral-current reactions are the only source of opacities. Here, the energy and momentum transfer is limited by the matter temperature alone. For electron neutrinos the mean free path is dominated by charged-current reactions, for which the energy transfer is typically of the order of the difference between neutron and proton chemical potentials. During the early deleptonization epoch of a proto-neutron star the typical neutron momenta are large ($\sim$100–200 MeV) and the mismatch of proton, neutron, and electron Fermi momenta can be overcome by the neutrino momenta. This is no longer possible in later stages, when the neutrino energies are of order k_bT; then momentum conservation restricts the available phase space for the absorption reaction. Pauli blocking of the lepton in the final state increases the mean free path for charged-current and neutral-current reactions.

We note an important and quite general consequence of the fact that muon and tau neutrinos react with the protoneutron-star matter only by neutral-current reactions: The four neutrino types have similar spectra. Due to universality, ν_μ,ν_τ and $\overline{\nu}_\mu,\overline{\nu}_\tau$ have identical spectra. It is usually even assumed that neutrinos and antineutrinos have the same spectra (one therefore refers to the four neutrino types unifyingly as ν_x neutrinos) exploit-

ing axial-vector dominance in the neutrino cross sections. However, the interference of the axial-vector and the weak-magnetism components makes the $\overline{\nu_x}$ spectra slightly hotter than the ν_x spectra. The ν_x neutrinos decouple deepest in the star, i.e., at a higher temperature than electron neutrinos and antineutrinos, and hence have higher energies. As the matter in the protoneutron star is neutron rich, electron neutrinos, which are absorbed by neutrons, decouple at a larger radius than their antiparticles, which interact with protons by charged-current reactions. As a consequence, decoupled electron neutrinos have, on average, smaller energies than electron antineutrinos. Janka and Hillebrandt (1989) and Yamada *et al.* (1999) have calculated supernova neutrino spectra which yield the average energies of the various supernova neutrinos approximately as $\langle E_{\nu_e}\rangle = 11$ MeV, $\langle E_{\overline{\nu}_e}\rangle = 16$ MeV, and $\langle E_{\nu_x}\rangle = 25$ MeV. Burrows *et al.* (2000) find the same hierarchy, but somewhat smaller average neutrino energies.

For a much deeper and more detailed description of the neutrino mean free paths in dense matter the reader is referred to Reddy *et al.* (1999), Prakash *et al.* (2001), and the earlier work of Burrows and Sawyer (1998, 1999) and Reddy *et al.* (1998). We shall here only briefly summarize the essence of the work presented in these references.

Collapse simulations describe neutrino opacities typically on the mean-field level or even by a nucleon gas. Then an analytical expression can be derived for the vector and axial-vector responses of the medium, which in turn determine the charged- and neutral-current cross sections. Effects due to the strong interaction between nucleons are considered by a medium-dependent effective mass in the dispersion relation. As in finite nuclei, collective excitations in nuclear matter arise due to nucleon-nucleon correlations beyond the mean-field approximation. As it is believed that single-pair excitations dominate over multipair excitations for the kinematics of interest to neutrino scattering and absorption, it appears to be sufficient to determine the vector and axial-vector response, in a first step, within the random-phase approximation (RPA). Assuming that the interaction is short ranged compared to the wavelength of the excitations, it is justified to retain only s-wave components in the interaction, which in turn can be related to Fermi-liquid parameters. It is found that the repulsive nature of the parameter G_0', which is related to the isovector spin-flip or giant Gamow-Teller resonances in nuclei, induces a collective state in the region $\omega/q \sim v_F$ (v_F is the Fermi velocity), while the cross section is reduced at smaller energies. However, these smaller energies are important for the neutrino mean free path at nuclear matter densities (ρ_0) or smaller densities. Assuming a typical neutrino energy $E_\nu \approx 3T$ (corresponding to a Fermi-Dirac distribution with temperature T and zero chemical potential), RPA correlations increase the neutral-current neutrino mean free path (see Fig. 20) at low temperatures and for $\rho = \rho_0$, compared with the mean-field result. An enhancement due to RPA correlations is also found for neutrino absorption mean free

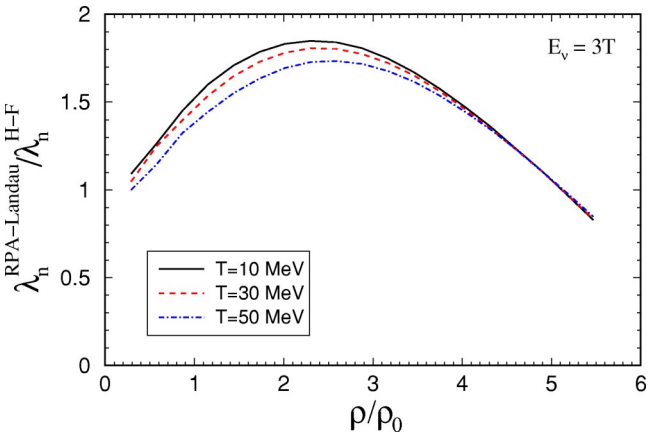

FIG. 20. (Color in online edition) Ratio of neutrino mean free paths in neutron matter calculated in the RPA and Hartree-Fock approaches at various temperatures (Margueron *et al.*, 2002). The interaction is the Gogny force D1P. The neutrino energy is taken as $E_\nu = 3T$.

paths for neutrino-trapped matter. As in the case of neutrino-induced reactions on finite nuclei (see above), finite-temperature effects allow nuclear excitation energy to be transferred to the neutrino in inelastic-scattering processes. This contributes to the cooling of the nuclear matter and increases the neutrino energy in the final state.

Neutrino heating is maximal in the layer just above the gain radius. The energy transport from this region to the shock, which is stalled further out, can be supported by convective overturn and might lead to successful explosions, as has been demonstrated in several simulations with two-dimensional hydrodynamics treatment of the region between the gain radius and the shock (Herant *et al.*, 1994; Burrows *et al.*, 1995; Janka and Müller, 1996). The effect of convection is twofold (Janka *et al.*, 2001). At first, heated matter is transported outwards to cooler regions where the energy loss due to neutrino emission is reduced (the neutrino production rate for electron and positron captures on nucleons depends strongly on temperature). Second, cooler matter is brought down closer to the gain radius, where the neutrino fluxes are larger and hence the heating is more effective. While this picture is certainly appealing, it is not yet clear whether multidimensional simulations will indeed lead to explosions, as the two-dimensional studies did not include state-of-the-art Boltzmann neutrino transport, but treated neutrino transport in an approximate manner. In fact, in a simulation with an improved treatment of neutrino transport the convective overturn was found not to be strong enough to revive the stalled shock (Mezzacappa *et al.*, 1998).

Shock revival can also be supported by convection occurring inside the protoneutron star, where it is mainly driven by the negative lepton gradient established by the rapid loss of leptons in the region around the neutrinosphere (Burrows, 1987; Keil *et al.*, 1996). By this mode, lepton-rich matter will be transported from inside the protoneutron star to the neutrinosphere, which increases the neutrino luminosity and thus is expected to help the

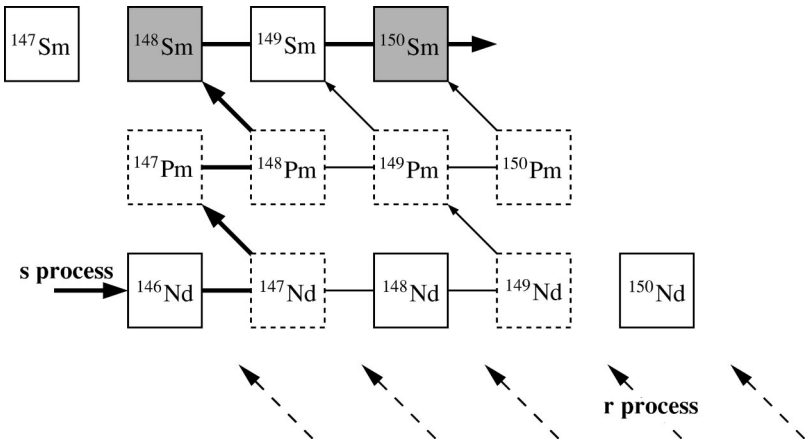

FIG. 21. The s-process reaction path in the Nd-Pm-Sm region with branchings at $A=147$, 148, and 149. Note that ^{148}Sm and ^{150}Sm are shielded against r-process β decays. Adapted from Käppeler, 1999.

explosion. The simulation of protoneutron-star convection is complicated by the fact that neutrinos and matter are strongly coupled. In fact, two-dimensional simulations found that neutrino transport can equilibrate otherwise convective fluid elements (Mezzacappa *et al.*, 1998). Such a damping is possible in regions where neutrinos are still strongly coupled to matter but neutrino opacities are not too high to make neutrino transport insufficient. In the model of Keil *et al.* (1996) the convective mixing occurs very deep inside the core, where the neutrino opacities are high; no damping of the convection by neutrinos is then found.

Wilson and Mayle attempted to simulate convection in their spherical model by introducing neutron fingers and obtained successful explosions (Wilson and Mayle, 1993). This idea is based on the assumption that energy transport (by three neutrino flavors) is more efficient than lepton number transport (only by electron neutrinos). However, this assumption is under debate (Bruenn and Dineva, 1996).

VI. NUCLEOSYNTHESIS BEYOND IRON

While the elements lighter than mass number $A\sim 60$ are made by charged-particle fusion reactions, the heavier nuclei are made by neutron captures, which have to compete with β decays. Very early Burbidge *et al.* (1957) and Cameron (1957) realized that two distinct processes are required to make the heavier elements. This is the slow neutron-capture process (s process), for which the β lifetimes τ_β are shorter than the competing neutron-capture times τ_n. This requirement ensures that the s process runs through nuclei in the valley of stability. The rapid neutron-capture process (r process) requires $\tau_n \ll \tau_\beta$, which is achieved in an extremely neutron-rich environment, as τ_n is inversely proportional to the neutron density of the environment. The r process runs through very neutron-rich, unstable nuclei, which are far-from stability and whose physical properties are often experimentally unknown.

Weak-interaction processes play interesting but different roles in these processes. The half-lives of the β-unstable nuclei along the s-process path are usually known with good precision. However, the nuclear half-life in the stellar environment can change due to the thermal population of excited states in the parent nucleus. This is particularly interesting if the effective lifetime is then comparable to τ_n, leading to branchings in the s-process path, from which the temperature and neutron density of the environment can be determined. Several recent examples are discussed in the next subsection. For the r process, β decays are probably even more crucial. They regulate the flow to larger charge numbers and determine the resulting abundance pattern and duration of the process. Except for a few key nuclei, β decays of r-process nuclei have to be modeled theoretically; we shall briefly summarize the recent progress below. Although a site for the r process is not yet fully determined, it is conceivable that it occurs in the presence of extreme neutrino fluxes. As we shall discuss, neutrino-nucleus reactions can have interesting effects during and after the r process, perhaps allowing for clues that will ultimately identify an r process site.

A. The s process

Analysis of the solar abundances have indicated that two components of the slow neutron-capture process have contributed to the synthesis of elements heavier than $A\sim 60$. The weak component produces the elements with $A\lesssim 90$. Its site is related to the helium-core burning of CNO material in more massive stars (Couch *et al.*, 1974; Käppeler *et al.*, 1994). The main component, which is responsible for the heavier s-process nuclides up to Pb and Bi, is associated with helium flashes occurring during shell burning in low-mass (asymptotic giant branch) stars (Busso *et al.*, 1999). The ^{22}Ne$(\alpha,n)^{25}$Mg and ^{13}C$(\alpha,n)^{16}$O reactions are believed to be the supplier of neutrons for the weak and main components, respectively. The s-process abundances N_s are found to be inversely proportional to the respective (temperature-averaged) neutron-capture cross sections $\langle\sigma\rangle$, as expected for a steady-flow picture (Burbidge *et al.*, 1957), which, however, breaks down for the extemely small cross sections at the magic neutron numbers. As a consequence, the product $N_s\cdot\langle\sigma\rangle$ exhibits almost constant plateaus between the magic neutron numbers, separated by pronounced steps (see, for example, Käppeler, 1999).

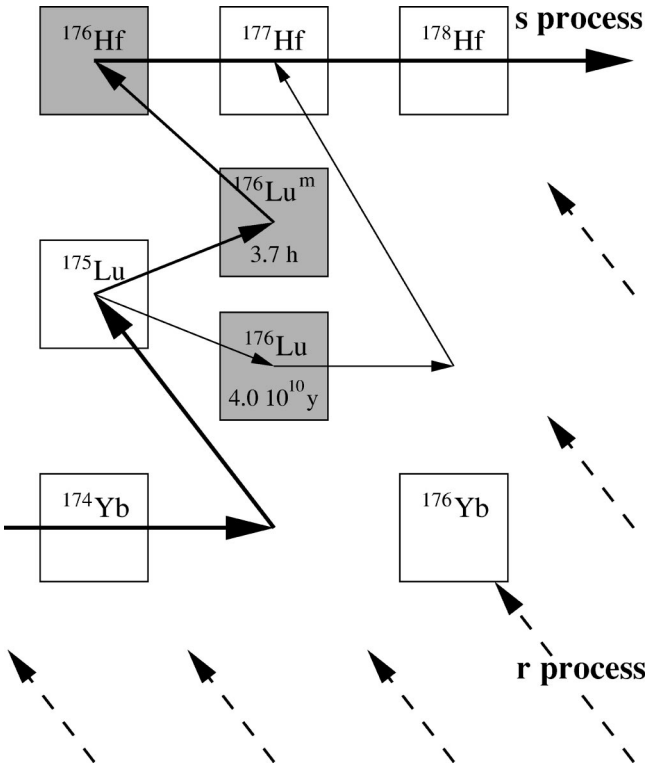

FIG. 22. The s-process neutron-capture path in the Yb-Lu-Hf region (solid lines). For ^{176}Lu the ground state and isomer are shown separately. Note that ^{176}Lu and ^{176}Hf are shielded against r-process β decays Adapted from Doll *et al.*, 1999.

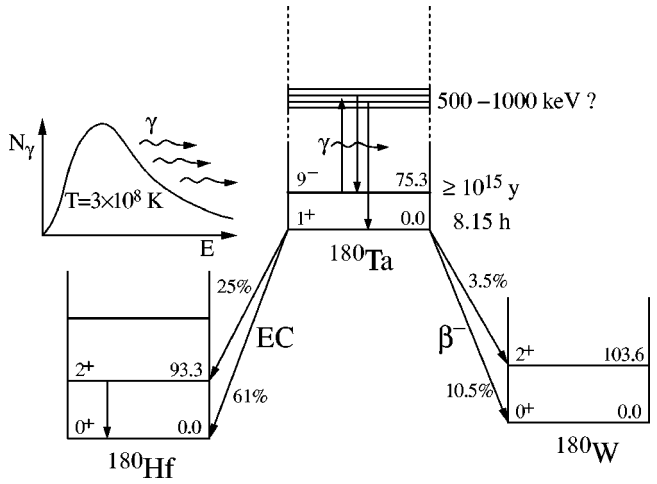

FIG. 23. Schematic energy-level diagram of ^{180}Ta and its daughters, illustrating the possibility of thermally enhanced decay of ^{180}Ta^m in the stellar environment of the s process. The inset shows the photon density at s-process temperature. Adapted from Belic *et al.*, 1999.

The neutron density of the stellar environment during the main s-process component can be determined from branching points occurring, for example, in the $A=147-149$ mass region (see Fig. 21). Here the relative abundances of the two s-process-only isotopes ^{148}Sm and ^{150}Sm ($Z=62$), which are shielded against r-process contributions by the two stable Nd ($Z=60$) isotopes ^{148}Nd and ^{150}Nd, are strongly affected by branchings occurring at ^{147}Nd and, more importantly, at ^{148}Pm and at ^{147}Pm. As the neutron captures on these branching nuclei will bypass ^{148}Sm in the flow pattern, the ^{150}Sm $N_s\langle\sigma\rangle$ value will be larger for this nucleus than for ^{148}Sm. Furthermore, the neutron-capture rate λ_n is proportional to the neutron density N_n. Thus N_n can be determined from the relative ^{150}Sm/^{148}Sm abundances, resulting in $N_n=(4.1\pm0.6)\times10^8$ cm^{-3} (Toukan *et al.*, 1995). A similar analysis for the weak s-process component yields neutron densities of order $(0.5-1.3)\times10^8$ cm^{-3} (Walter *et al.*, 1986a, 1986b). We stress that a 10% determination of the neutron density requires knowledge of the involved neutron-capture cross sections with about 1% accuracy (Käppeler *et al.* 1998), which has not yet been achieved for unstable nuclei. Improvements are expected from new time-of-flight facilities like LANSCE at Los Alamos or NTOF at CERN.

The temperature of the s-process environment can be "measured," if the β half-life of a branching-point nucleus is very sensitive to the thermal population of excited nuclear levels. A prominent example is ^{176}Lu (Beer *et al.*, 1981). For mass number $A=176$, the β decays from the r process terminate at ^{176}Yb ($Z=70$), making ^{176}Hf ($Z=72$) and ^{176}Lu ($Z=71$) s-only nuclides (see Fig. 22). Besides the long-lived ground state [$t_{1/2}=4.00(22)\times10^{10}$ yr], ^{176}Lu has an isomeric state at an excitation energy of 123 keV [$t_{1/2}=3.664(19)$ h]. Both states can be populated by ^{175}Lu(n,γ) with known partial cross sections. At ^{176}Lu, the s-process matter flow is determined by the competition of neutron capture on the ground state and β decay of the isomer. But importantly, the ground and isomeric states couple in the stellar photon bath via the excitation of an intermediate state at 838 keV (Fig. 23 shows a similar process taking place in ^{180}Ta), leading to a matter flow from the isomer to the ground state, which is very temperature dependent. A recent analysis of the ^{176}Lu s-process branching yields an environment temperature of $T=(2.5-3.5)\times10^8$ K (Doll *et al.*, 1999).

Similar finite-temperature effects also play an important role in s-process production of ^{180}Ta. This is the rarest isotope (0.012%) of Nature's rarest element. It exists only in a long-lived isomer ($J^\pi=9^-$) at an excitation energy of 75.3 keV and with a half-life of $t_{1/2}\geqslant1.2\times10^{15}$ yr. The 1^+ ground state decays with a half-life of 8.152(6) h, mainly by electron capture to ^{180}Hf. While potential s-process production paths of the ^{180}Ta isomer have been pointed out, the survival of this state in a finite-temperature environment has long been questionable. While a direct electromagnetic decay to the ground state is strongly suppressed due to angular momentum mismatch, the isomer can decay via thermal population of intermediate states with branchings to the ground state (see Fig. 23). By measuring the relevant electromagnetic coupling strength, Belic *et al.* (1999) determined the temperature-dependent half-life, and thus the ^{180}Ta survival rate, under s-process conditions as $t_{1/2}\lesssim1$ yr, i.e., more than 15 orders of magnitude smaller than the half-life of the isomer! Accompanied by progress in stellar modeling of the convective modes

during the main s-process component (which brings freshly produced ^{180}Ta to cooler zones, where it can survive more easily, on time scales of days) it now appears likely that ^{180}Ta is partly made within s-process nucleosynthesis (Wisshak *et al.*, 2001). The p process[3] (Rayet *et al.*, 1995) and neutrino nucleosynthesis (Woosley *et al.*, 1990) have been proposed as alternative sites for ^{180}Ta production.

The two neighboring isotopes ^{186}Os and ^{187}Os are s-process-only nuclides, shielded against the r process by ^{186}W and ^{187}Rh. The nucleus ^{187}Rh has a half-life of 42 Gyr, which is comparable with the age of the universe. As ^{187}Rh decay has contributed to the observed ^{187}Os abundance, the Os/Rh abundance ratio can serve as a sensitive clock for the age of the universe, once the s-process component is subtracted from the ^{187}Os abundance (Clayton, 1964). To determine the latter, precise measurements of the neutron-capture cross sections on ^{186}Os and ^{187}Os are required, which are in progress at CERN's NTOF facility. A potential complication arises from the fact that ^{187}Os has a low-lying state at 9.8 keV which is populated equally with the ground state at s-process temperatures. The respective neutron-capture cross sections on the excited state can be indirectly determined from (n,n') measurements. Furthermore, one has to consider that the half-life of ^{187}Rh is strongly temperature dependent: If stripped of its electrons, the half-life is reduced by nine orders of magnitude to $t_{1/2}=32.9\pm2$ yr as measured at the GSI storage ring (Bosch *et al.*, 1996). However, the GSI data can be translated into a $\log ft$ value from which the ^{187}Rh half-life can be deduced for every ionization state.

The decay of totally ionized ^{187}Rh is an example of a bound-state β decay. That is, the decay of bare $^{187}Rh^{75+}$ to continuum states of $^{187}Os^{76+}$ is energetically forbidden, but it is possible if the decay electron is captured in the K shell ($Q_\beta=73$ keV) or in the L shell ($Q_\beta=9.1$ keV) (Johnson and Soff, 1985). We note that the decay of neutral ^{187}Rh is energetically allowed for a first-forbidden transition to the ^{187}Os ground state; the long half-life results from the small matrix element and Q_β value related to this transition. Another example of a bound-state β decay with importance for the s process occurs for ^{163}Dy. This nucleus is stable as a neutral atom, but, if fully ionized, can decay to ^{163}Ho with a half-life of 47^{+5}_{-4} d; the measurement of this half-life at the GSI storage ring was the first observation of bound-state β decay (Jung *et al.*, 1992). Consideration of the ^{163}Dy decay at s-process conditions has been found to be essential to explain the abundance of the s-process-only nuclide ^{164}Er, which is produced by neutron capture on ^{163}Ho, the daughter of the bound-state β decay of ^{163}Dy and the subsequent β decay of ^{164}Ho to ^{164}Er.

[3]The p process produces the stable neutron-deficient isotopes of the elements with $Z<34$ by (γ,n) photodisintegration of preexisting more neutron-rich species, possibly followed by cascades of (γ, p) and/or (γ,α) reactions.

B. The r process

Phenomenological parameter studies indicate that the rapid neutron-capture process occurs at temperatures around $T\sim100$ keV and at extreme neutron fluxes (neutron number densities $n>10^{20}$ cm^{-3}; Cowan *et al.*, 1991). It has also been demonstrated that not all r-process nuclides can be made simultaneously under the same astrophysical conditions (constant temperature, neutron density), i.e., the r process is a dynamical process with changing conditions and paths (Kratz *et al.*, 1993). In a good approximation, the neutron captures proceed in $(n,\gamma)\rightleftarrows(\gamma,n)$ equilibrium, fixing the reaction paths at rather low neutron separation energies of $S_n\sim2-3$ MeV (Cowan *et al.*, 1991), implying paths through very neutron-rich nuclei in the nuclear chart, as is shown in Fig. 24. While the general picture of the r process appears to be well accepted, its astrophysical site is still open. The extreme neutron fluxes point to explosive scenarios and, in fact, the neutrino-driven wind above a nascent neutron star in a core-collapse supernova is the currently favored model (Witti *et al.*, 1994a, 1994b; Woosley *et al.*, 1994). But shock-processed helium shells in type-II supernovae (Truran *et al.*, 2001) and neutron-star mergers (Freiburghaus, Rosswog, and Thielmann, 1999; Rosswog *et al.*, 2000) are also being investigated as possible r-process sites. Recent meteoritic clues (Wasserburg *et al.*, 1996; Qian *et al.*, 1998), as well as observations of r-process abundances in low-metallicity stars (Sneden *et al.*, 2000), point to more than one distinct site for the solar r-process nuclides.

In an important astronomical observation, Cayrel *et al.* (2001) have recently detected the r-process nuclides thorium and uranium in an old galactic halo star. As these two nuclei have half-lives comparable to the expected age of the universe, their measured abundance ratio serves as a sensitive clock for determining a lower limit to this age, provided their initial r-process production abundance ratio can be calculated with sufficient accuracy. Cayrel *et al.* (2001) used their observed ^{238}U/^{232}Th abundance ratio from the star CS31082-001 and the r-process model predictions from Cowan *et al.* (1999) and Goriely and Clerbaux (1999) to deduce a value of 12.5 ± 3.3 Gyr for the age of the star. Recently, a refined analysis of the CS31082-001 spectra has led to a significant improvement in the derived abundances, which now provide an age estimate of 14.0 ± 2.4 Gyr (Hill *et al.*, 2002). The effects of different nuclear physics inputs on the r-process production of U and Th have been studied by Goriely and Arnould (2001) and by Schatz *et al.* (2002).

As relevant nuclear input, r-process simulations require neutron separation energies (i.e., masses), half-lives, and neutron-capture cross sections of the very neutron-rich nuclei on the various dynamical r-process paths. Currently only few experimental data are known for r-process nuclei, so these quantities have to be modeled. Traditionally this has been done by global models which fit a certain set of parameters to known experimental data and are then used to predict the properties

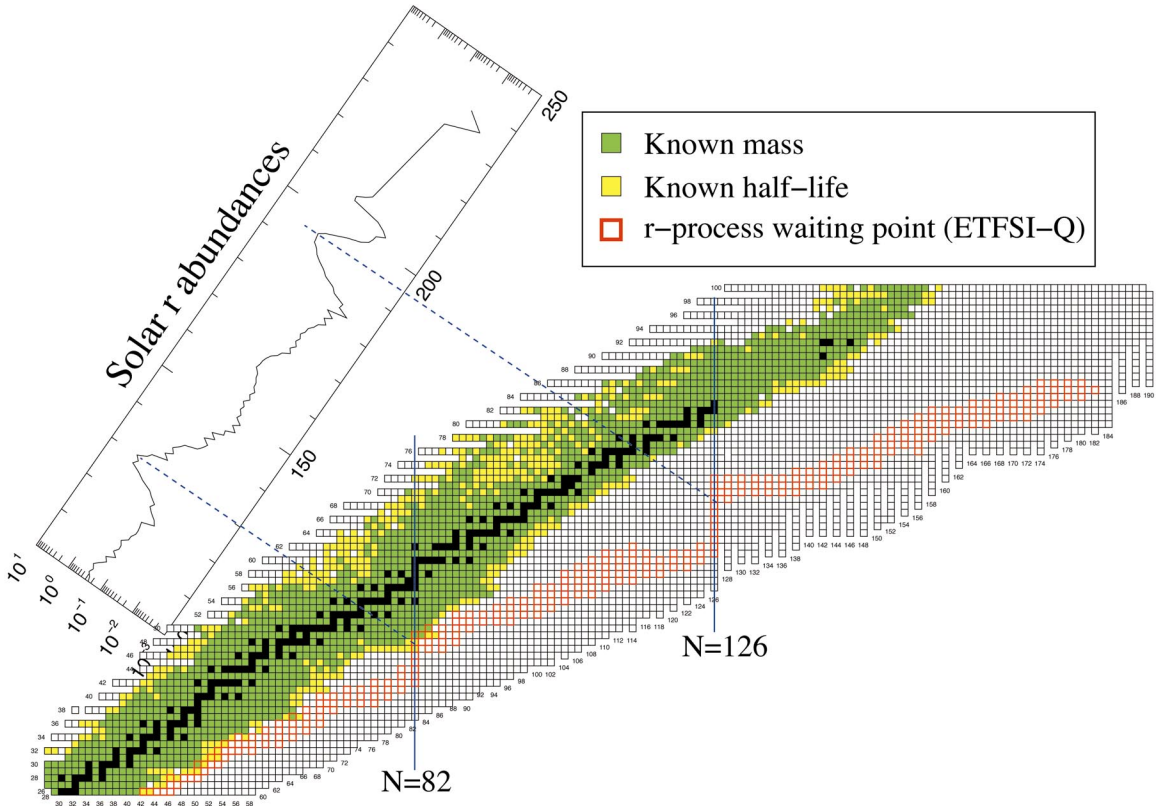

FIG. 24. (Color) A variety of r-process paths occurring under dynamically changing astrophysical conditions, which affect the reaction pathway. The paths are defined by their waiting-point nuclei. After decay to stability the abundances of the r-process progenitors produce the observed solar r-process abundance distribution. The r-process paths generally run through neutron-rich nuclei with experimentally unknown masses and half-lives. In this calculation a mass formula based on the extended Thomas Fermi model with Strutinski integral (ETFSI) and special treatment of shell quenching (see text) has been adopted. Courtesy of Karl-Ludwig Kratz and Hendrik Schatz.

of all nuclei in the nuclear landscape. Arguably the most important input to r-process simulations are neutron separation energies, as they determine, for given temperature and neutron density of the astrophysical environment, the r-process paths. The most commonly used mass tabulations are based on the microscopic-macroscopic finite-range droplet model (FRDM) approach (Möller *et al.*, 1997) or the extended Thomas-Fermi model with Strutinski integral (ETFSI) approach (Aboussir *et al.*, 1995). In more recent developments mass tabulations have been developed adopting parametrizations inspired by shell-model results (Duflo and Zuker, 1995) or calculated on the basis of nuclear many-body theories like the Hartree-Fock model with a BCS treatment of pairing (Goriely *et al.*, 2001). Special attention has also been paid recently to "shell quenching," i.e., the observations made in HFB calculations that the shell gap at magic neutron numbers is less pronounced in very neutron-rich nuclei than in nuclei close to stability (Dobaczewski *et al.*, 1994). Such a vanishing of the shell gap has been experimentally verified for the magic neutron number $N=20$ (Guillemaud-Mueller *et al.*, 1984; Motobayashi *et al.*, 1995). The confirmation of the predicted quenching at the $N=82$ shell closure is the aim of considerable current experimental activities (Kratz *et al.*, 2000). Recent theoretical studies on this topic are reviewed by Sharma and Farhan (2001, 2002). The potential importance of shell quenching for the r process rests on the observation (Chen *et al.*, 1995; Pfeiffer *et al.*, 1997) that it can correct the strong trough just below the peaks in the calculated r-process abundances encountered with conventional mass models. Neutron-capture cross sections become important if the r-process flow drops out of $(n,\gamma)\rightleftarrows(\gamma,n)$ equilibrium, which happens close to freeze-out when the neutron source ceases. They can also be relevant for nuclides with small abundances, for which no flow equilibrium is built up (Surman *et al.*, 1997; Surman and Engel, 2001). Below we summarize recent progress in calculating half-lives for nuclei on the r-process paths.

1. Half-lives

Nuclear half-lives determine the relative r-process abundances. In a simple β-flow equilibrium picture the elemental abundance is proportional to the half-life, with some corrections for β-delayed neutron emission (Kratz *et al.*, 1988). As r-process half-lives are longest for the magic nuclei, these waiting-point nuclei determine the minimal r-process duration time; i.e., the time needed to build up the r-process peak around $A\sim200$

via matter flow from the seed nucleus. We note, however, that this time also depends crucially on the r-process path.

Pioneering experiments to measure half-lives of neutron-rich isotopes near the r-process path succeeded in determining the half-lives of two $N=50$ (^{80}Zn, ^{79}Cu) and two $N=82$ (^{129}Ag, ^{130}Cd) waiting-point nuclei (Gill *et al.*, 1986; Kratz *et al.*, 1986; Pfeiffer *et al.*, 2001). Pfeiffer *et al.* (2001) reviewed the experimental information on r-process nuclei. These data play crucial roles in constraining and testing nuclear models, which are still necessary to predict the bulk of half-lives required in r-process simulations. It is generally assumed that the half-lives are determined by allowed Gamow-Teller (GT) transitions. The calculations of β decays usually require two ingredients: the GT strength distribution in the daughter nucleus and the relative energy scale between parent and daughter, i.e., their mass difference. However, β decays probe only the weak low-energy tail of the GT distributions. Only a few percent of the $3(N-Z)$ Ikeda sum rule (Ikeda *et al.*, 1963) lie within the Q_β window (i.e., at energies accessible in β decay), the rest being located in the region of the Gamow-Teller resonance at higher excitation energies. Due to the strong E^5 energy dependence of the phase space, β decay rates are very sensitive to the correct description of the detailed low-energy GT distribution and its relative energy scale to the parent nucleus. This explains why different calculations of the β-decay half-lives present large deviations among them.

Because of the huge number of nuclei relevant for the r process, the estimates of the half-lives are so far based on a combination of global mass models and the quasiparticle random-phase approximation (QRPA), the latter to calculate the GT matrix elements. Examples of these models are the FRDM/QRPA (Möller *et al.*, 1997) and the ETFSI/QRPA (Borzov and Goriely, 2000). Recently, calculations based on the self-consistent Hartree-Fock-Bogoliubov plus QRPA model became available for r-process waiting-point nuclei with magic neutron numbers $N=50$, 82, and 126 (Engel *et al.*, 1999). The presence of a closed neutron shell has also allowed for the study of these nuclei by shell-model calculations (Martínez-Pinedo and Langanke, 1999; Martínez-Pinedo, 2001), which is the method of choice to determine the β-decay matrix elements. However, an adequate calculation of the nuclear masses for heavy nuclei is still not feasible in the shell model. In Martínez-Pinedo and Langanke (1999), and Martínez-Pinedo, (2001) the masses were adopted from the global model of Duflo and Zuker (1995). Figure 25 compares the half-lives predicted by the different approaches. For $N=82$, the half-lives of ^{131}In, ^{130}Cd, and ^{129}Ag are known experimentally (Kratz *et al.*, 1986; Pfeiffer *et al.*, 2001). Comparison of the predictions of the different models with the few experimental r-process benchmarks reveals some of their insufficiencies. For example, the FRDM/QRPA half-lives show a significant odd-even staggering which is not present in the data, while the ETFSI/QRPA half-lives appear globally too long. The HFB/QRPA and

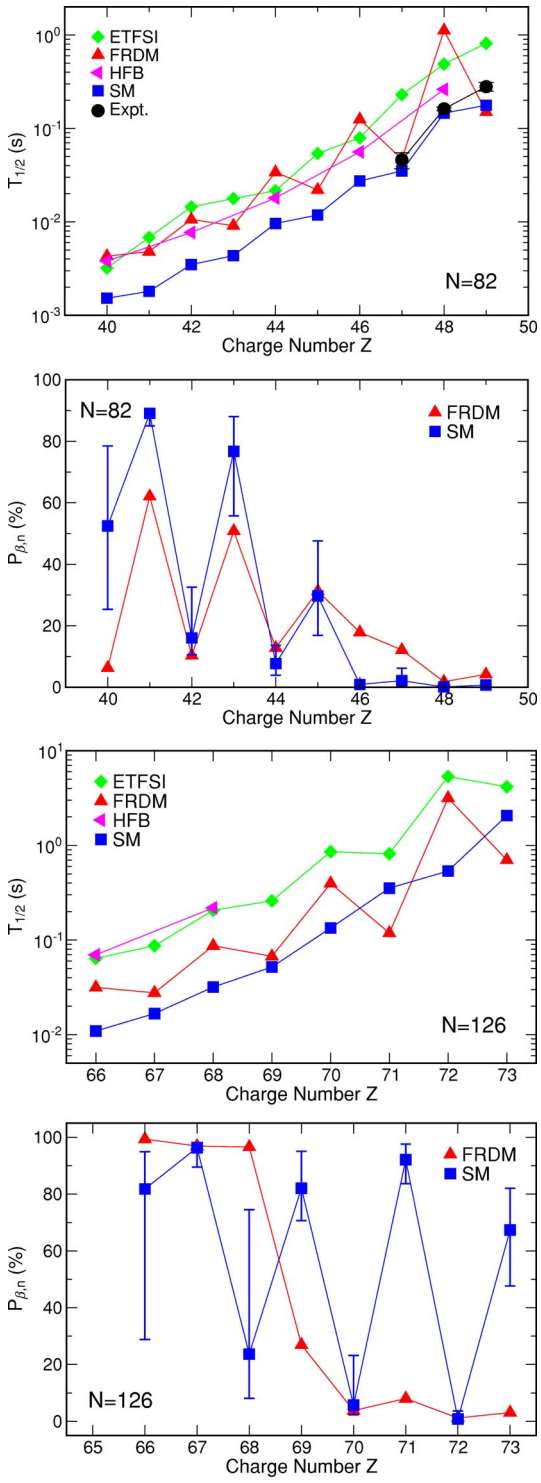

FIG. 25. (Color in online edition) Half-lives and beta-delayed neutron emission probabilities for r-process waiting-point nuclei with neutron numbers $N=82$ (upper panels) and 126 (lower panels), obtained within different theoretical models. In the case of $N=82$ the half-lives of ^{131}In, ^{130}Cd, and ^{129}Ag are experimentally known (Pfeiffer *et al.*, 2001). For the shell-model (SM) probabilities the error bars indicate the sensitivity of the calculations to a change of ± 0.5 MeV in the neutron separation energies.

shell-model approaches obtain half-lives in reasonable agreement with the data and predict shorter half-lives for the unmeasured waiting-point nuclei with $N=82$ than the global FRDM/QRPA and ETFSI/QRPA approaches. For $N=126$ there is no experimental information, so the different models remain untested. While HFB calculations for the half-lives of all the r-process nuclei are conceivable, similar calculations within the shell-model approach are still not feasible due to computer memory limitations.

While the Q_β value for the decay of neutron-rich r-process nuclei is large, the neutron separation energies are small. Hence β decay can lead to final states above neutron threshold and is accompanied by neutron emission. If the r process proceeds by an $(n,\gamma)\rightleftarrows(\gamma,n)$ equilibrium the β-delayed neutron emission probabilities $P_{\beta,n}$ play a role only at the end of the r process when the neutron source has ceased and the produced nuclei decay to stability. The calculated $P_{\beta,n}$ values are very sensitive to both the low-energy Gamow-Teller distribution and the neutron threshold energies. Currently no model describes both quantities simultaneously with sufficient accuracy. Figure 25 compares the $P_{\beta,n}$ computed in the FRDM/QRPA and shell-model approaches for $N=82$ and 126. The predictions of different models can be quite different in mass regions that have not been experimentally determined. For the shell-model approach the error bars indicate the sensitivity of the computed $P_{\beta,n}$ values to a change of ± 0.5 MeV in the neutron separation energies of the daughter nucleus; the effect can be large.

It has been pointed out that first-forbidden transitions might have important contributions in some nuclei close to magic numbers (Blomqvist *et al.*, 1983; Homma *et al.*, 1996; Korgul *et al.*, 2001). A systematic inclusion of first-forbidden transitions in the calculation of r-process beta-decay half-lives in any of the many-body methods used to describe the Gamow-Teller contributions has not been carried out. However, a first attempt towards this goal (Möller *et al.*, 2002) has combined first-forbidden transitions estimated in the gross theory (Takahashi *et al.*, 1973) with Gamow-Teller results taken from QRPA calculations. No significant changes compared to r-process studies, which consider only the GT contributions to the half-lives, have been observed (Kratz, 2002). The influence of first-forbidden transitions in the half-lives of r-process waiting point nuclei with $N=50$, 82, and 126 has recently been studied by Borzov (2003).

The presence of low-lying isomeric states in r-process nuclei might change the effective half-lives in the stellar environment. Currently no estimates of this effect exist except for odd-A nuclei with $N=82$. Here shell-model calculations predict half-lives for the isomeric states very similar to the ground-state half-lives (Martínez-Pinedo and Langanke, 1999). The half-lives of the isomeric state in ^{129}Ag have also been estimated within the QRPA approach and by a second shell-model calculation finding values about a factor of 2 larger than the ^{129}Ag ground-state half-life (Kratz, 2001). This work also reports on the first attempt to measure the half-life of the isomeric state.

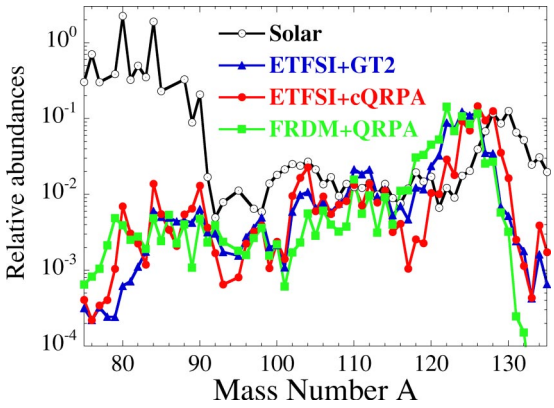

FIG. 26. (Color in online edition) Abundances of r-process nuclides calculated in a dynamical r-process model and for different global sets of β-decay half-lives. In the dynamical r process the matter flow time scale competes with the nuclear time scale, set by the β-decay half-lives. As a consequence the magic neutron numbers (here $N=82$) are reached at different astrophysical conditions and hence at different proton numbers, which is reflected in the shifts of the abundance peaks. From Borzov and Goriely, 2000.

For heavy nuclei ($Z\geqslant 84$) some final states populated by β decay in the daughter nucleus can also decay by fission (Cowan *et al.*, 1991). The relevant beta-delayed fission probabilities depend sensitively on the modeling of the fission barriers (Howard and Möller, 1980; Mamdouh *et al.*, 2001).

Borzov and Goriely have studied the influence of the β half-lives on r-process abundances within two distinct scenarios: the canonical r-process picture with an exposure of the seed nucleus ^{56}Fe to a constant neutron density and temperature for a fixed time (2.4 s) and the neutrino-driven wind model. In the canonical model the location of the r-process abundance peaks depends on the masses, but not on the β half-lives, which act only as bottlenecks for matter flow to more massive nuclei. In the dynamical neutrino-driven wind model the half-lives affect the abundance distribution. This comes about because at later times in this model the environmental conditions shift the r process to more neutron-rich nuclei. Long half-lives then imply that the matter flow reaches the magic neutron numbers later, i.e., for more neutron-rich nuclei. Consequently the abundance peaks are shifted to smaller A values (see Fig. 26, Borzov and Goriely, 2000). Similar studies have been presented by Kratz *et al.* (1998).

2. The possible role of neutrinos in the r process

Among the various possible astrophysical sites for the r process, that proposed by the neutrino-driven wind model (Witti *et al.*, 1994a, 1994b; Woosley *et al.*, 1994) has attracted most attention in recent years. Here it is assumed that the r process occurs in the layers heated by neutrino emission and evaporating from a hot proto-

neutron star after core collapse in a type-II supernova (Thompson *et al.*, 2001). Adopting the parameters of a supernova simulation by Wilson (1985), Woosley and collaborators obtained quite satisfying agreement between an r-process simulation and observation (Woosley *et al.*, 1994). In the classical picture the r-process nuclides are made by successive capture of neutrons, starting from a seed nucleus with mass number $A_{\rm seed}$. Thus to make the third r-process peak around $A\sim 200$ requires a large neutron-to-seed ratio of $n/s\sim 200 - A_{\rm seed}$. In the Wilson supernova models (Wilson, 1985, 2001) this is achieved due to a high entropy found in the neutrino wind at late times (a few seconds after the bounce). However, other models with a different equation of state and treatment of diffusion do not obtain such high entropies; in these models the r process fails to make the $A=200$ peak. To explain the strong sensitivity of r-process nucleosynthesis to the entropy of the environment Qian (1997) noted that the slowest reaction in the nuclear network, which transforms protons, neutrons, and α particles into r-process seed nuclei, is the three-body $\alpha+\alpha+n\rightarrow{}^9$Be reaction. Due to its low binding energy ($E_b=1.57$ MeV), ^{9}Be can be easily destroyed in a hot thermal environment, and thus the matter flow to nuclei heavier than ^{9}Be depends strongly on the entropy of the surroundings. The larger the entropy, the smaller the abundance of surviving ^{9}Be nuclei, which are then transformed into seed nuclei, and the larger the neutron-to-seed ratio. Meyer (1995) pointed out that in a very strong neutrino flux the slow 3-body $\alpha+\alpha+n\rightarrow{}^9$Be reaction can be potentially bypassed by a sequence of two-body reactions started by the neutrino-induced spallation of an α particle; e.g., $^4{\rm He}(\nu,\nu' p)^3{\rm H}(^4{\rm He},\gamma)^7$ Li$(^4{\rm He},\gamma)^{11}$B and $^4{\rm He}(\nu,\nu' n)^3{\rm He}(^4{\rm He},\gamma)^7{\rm Be}(^4{\rm He},\gamma)^{11}$C. This would speed up the mass flow to the seed nuclei and thus reduce the neutron-to-seed ratio.

Systematic studies by Hoffman *et al.* (1997) and Freiburghaus, Rembges, *et al.* (1999) have shown that a successful r process requires either large entropies at the Y_e values currently obtained in supernova models, or smaller values for Y_e.

In the neutrino-driven wind model the extreme flux of ν_e and $\overline{\nu_e}$ neutrinos from a protoneutron star interacts with the free protons and neutrons in the shocked matter by charged-current reactions, setting the proton-to-neutron ratio n/p or equivalently the Y_e value of the r-process matter. As shown by Fuller and Qian one has the simple relation (Qian and Fuller, 1995; Qian, 1997)

$$\frac{n}{p}\approx\frac{L_{\overline{\nu}_e}\langle E_{\overline{\nu}_e}\rangle}{L_{\nu_e}\langle E_{\nu_e}\rangle}. \tag{9}$$

As the neutrino energy luminosities are about equal for all species ($L_\nu\sim 10^{52}$ erg s^{-1}) the n/p ratio is set by the ratio of average energies for the antineutrino and neutrino. As discussed above, their different opacities in the protoneutron star ensure that $\langle E_{\overline{\nu}_e}\rangle>\langle E_{\nu_e}\rangle$ and the matter is neutron rich, as is required for a successful r process. When the matter reaches cooler temperatures, nucleosynthesis starts and the free protons are, in the first step, assemblied into α particles, with some extra neutrons remaining. If these neutrons are still exposed to a large neutrino flux, it will change some of the neutrons into protons, which will then, together with additional neutrons, be bound very quickly into α particles. This so-called α effect (Meyer *et al.*, 1998) would severely reduce the final neutron-to-seed ratio and is therefore very counterproductive to a successful r process. As mentioned above, the neutrino-nucleon cross sections are only considered to lowest order in supernova simulations. The correction introduced by the weak magnetism acts to reduce the neutron-to-proton ratio in a neutrino-driven wind (Horowitz and Li, 1999).

There are possible ways out of this difficulty: One solution is to remove the matter very quickly from the neutron star in order to reduce the neutrino fluxes for the α effect. Such a short dynamical time scale for material in the wind is found in neutrino-driven wind models studied by Kajino and collaborators. These authors also observe that relativistic effects as well as nuclear reaction paths through neutron-rich light elements might be helpful for a successful r process (Otsuki *et al.*, 2000; Terasawa, Sumiyoshi, Kajino, Mathews, *et al.*, 2001; Terasawa, Sumiyoshi, Kajino, Tanihata, *et al.*, 2001; Wanajo *et al.*, 2001). Another intriguing solution is discussed by McLaughlin *et al.* (1999) and Caldwell *et al.* (2000) invoking matter-enhanced active-sterile neutrino oscillations to remove the ν_e from the r-process site.

A simple estimate for the duration of the r process can be made by adding up the half-lives of the waiting-point nuclei, which results in about 1–2 s. However, in the neutrino-driven wind model it appears that the ejected matter passes through the region with the conditions suited for an r process in shorter times ($\sim$0.5 s), implying that there might not be enough time for sufficient matter flow from the seed to nuclides in the $A\sim 200$ mass region. Such a "time problem" is avoided if, as indicated above, the half-lives of the waiting-point nuclei are shorter than conventionally assumed, or if, in a dynamically changing environment, the matter that freezes out to make the $A\sim 200$ r-process peak breaks through the $N=50$ and 82 waiting points closer to the neutron dripline, i.e., through nuclei with shorter half-lives, than the matter that freezes out at these lower magic neutron numbers.

In an environment with large neutrino fluxes the matter flow to heavier nuclei can also be sped up by charged-current (ν_e,e^-) reactions (Nadyozhin and Panov, 1993; Qian *et al.*, 1997) which can compete with β decays. This is particularly important at the waiting-point nuclei associated with $N=50$, 82, and 126. Figure 27 shows the (ν_e,e^-) half-lives (Hektor *et al.*, 2000; Langanke and Kolbe, 2001) for these waiting-point nuclei, considering reasonable supernova neutrino parametrizations and assuming that the ejected matter has reached a radius of 100 km. Due to dependence on L_ν the (ν_e,e^-) half-lives scale with r^2. Indeed, a comparison with the β half-lives (Fig. 27) shows that (ν_e,e^-) reactions can be faster than the longest β decays of the

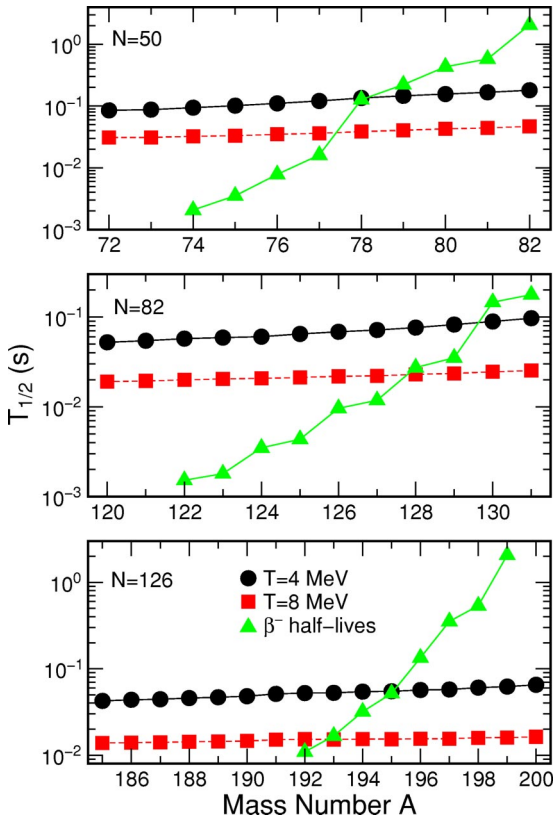

FIG. 27. (Color in online edition) Half-lives of r-process waiting point nuclei vs charged-current (ν_e, e^-) reactions: top panel, $N=50$; middle panel, $N=82$; bottom panel, $N=126$. For the neutrinos a Fermi-Dirac distribution with $T=4$ MeV and zero chemical potential (circles) and a luminosity of $L_\nu \sim 10^{52}$ erg s^{-1} has been adopted. It is assumed that the reactions occur at a radius of 100 km, measured from the center of the neutron star. The half-lives can be significantly shorter if $\nu_e \rightleftarrows \nu_{\mu,\tau}$ oscillations occur. The squares show the half-lives for neutrinos with a Fermi-Dirac distribution with $T=8$ MeV and zero chemical potential, which corresponds to complete $\nu_e \rightleftarrows \nu_{\mu,\tau}$ oscillations.

$N=50, 82,$ and 126 waiting-point nuclei, thus speeding up the breakthrough of matter at the waiting points, if the r process occurs rather close to the surface of the neutron star. This is even further enforced if $\nu_e \rightleftarrows \nu_{\mu,\tau}$ oscillations occur due to the higher energy spectrum of the supernova $\nu_{\mu,\tau}$ neutrinos. However, the presence of charged-current reactions on nuclei in the neutrino-driven wind model also implies neutrino reactions on nucleons strengthening the α effect (Meyer *et al.*, 1998).

Under a strong neutrino flux the weak flow is determined by an effective weak rate given by the addition of the charged-current (ν_e, e^-) and the nuclear beta decay rates (McLaughlin and Fuller, 1997). It has been argued that the solar system r-process abundances provide evidence for the weak steady-flow approximation, which implies that the observed abundances should be proportional to the half-lives of their progenitor nuclei on the r-process path (Kratz *et al.*, 1993, 1988). If this is so, the r-process freeze-out must occur at conditions (i.e., radii) at which β decay dominates over (ν_e, e^-) reactions, at

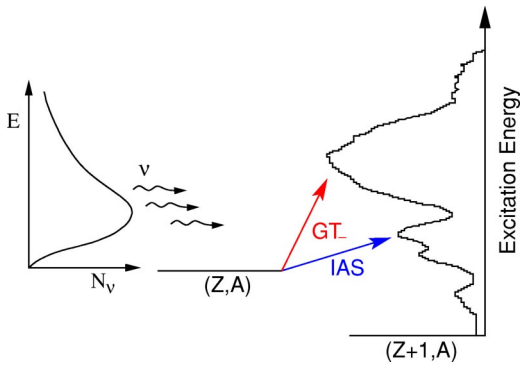

FIG. 28. (Color in online edition) Schematic view of the (ν_e, e^-) reaction on r-process nuclei. Due to the high neutrino energies, the cross sections are dominated by transitions to the Fermi isobaric analog state and Gamow-Teller resonances.

least for late times. The reason is that neutrino capture on magic nuclei with $N=50$, 82, and 126 is not reduced if compared to the neighboring nuclides, as the capture occurs from a reservoir of neutrinos with sufficiently high energies to allow for transitions to the isobaric analog state and GT resonant states (see Fig. 28). Consequently (ν_e, e^-) cross sections scale approximately like the neutron excess $(N-Z)$, reflecting the Fermi and Ikeda sum rules (see Fig. 27). However, the observed solar abundances around the $A=130$ $(N=82)$ and 195 $(N=126)$ peaks do not show such a smooth dependence on A as will be the case if the effective weak rate is dominated by neutrino reactions. If we require that the β-decay half-lives dominate over the (ν_e, e^-) reactions we can put constraints on the neutrino fluence in the neutrino-driven wind scenario, which is particularly strict if neutrino oscillations occur. If, as an illustrative example, we apply the constraint to heavy waiting-point nuclei with $N=126$ (e.g., nuclei with $A \sim 199$) and adopt the neutrino and beta half-lives from Fig. 27, β decay is only faster if the neutrino-nucleus reactions occur at distances larger than ~ 500 km.

As the Q_β values in the very neutron-rich r-process nuclei are large, the isobaric analog state and GT resonant states reside at rather high excitation energies (~ 20–30 MeV) in the daughter nuclei for (ν_e, e^-) reactions. This fact, combined with the small neutron separation energies in these nuclei, ensures that (ν_e, e^-) reactions, as well as neutral-current (ν, ν') reactions, spall neutrons out of the target nuclei (Haxton *et al.*, 1997; Qian *et al.*, 1997), ~ 5–7 neutrons for nuclei in the $A=195$ mass region (Haxton *et al.*, 1997; Hektor *et al.*, 2000). During the r process, i.e., as long as the neutron source is strong enough to establish $(n,\gamma) \rightleftarrows (\gamma,n)$ equilibrium, the neutrons will immediately be recaptured, leading to no effect on the abundance distribution. However, once the neutron source has ceased, e.g., after freeze-out, and if the r-process matter in the neutrino-driven wind model is still subject to strong neutrino fluxes, neutrons liberated during this phase by neutrino-induced reactions will not be recaptured, and this post processing (Haxton *et al.*, 1997; Qian *et al.*, 1997) leads to changes in the r-process abundance distribution. It is

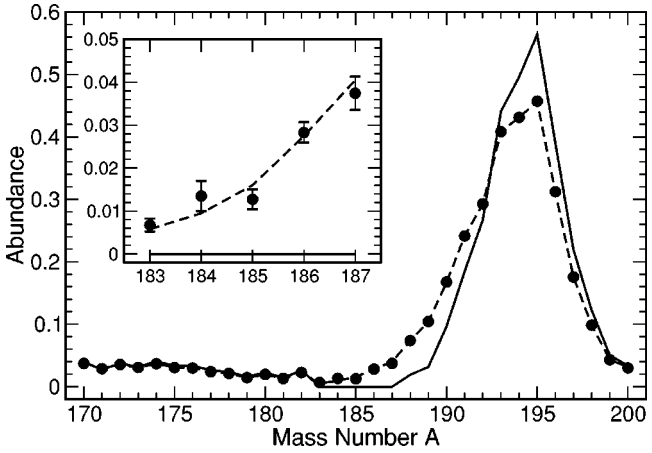

FIG. 29. Effect of post processing by neutrino-induced reactions on the r-process abundance. The unprocessed distribution (solid line) is compared with the distribution after post processing (dashed line). A constant fluence of $\mathcal{F}=0.015$ has been assumed, which provides a best fit to the observed abundances for $A=183-87$ (see inset). The observed abundances are plotted as filled circles with error bars. From Qian *et al.*, 1997.

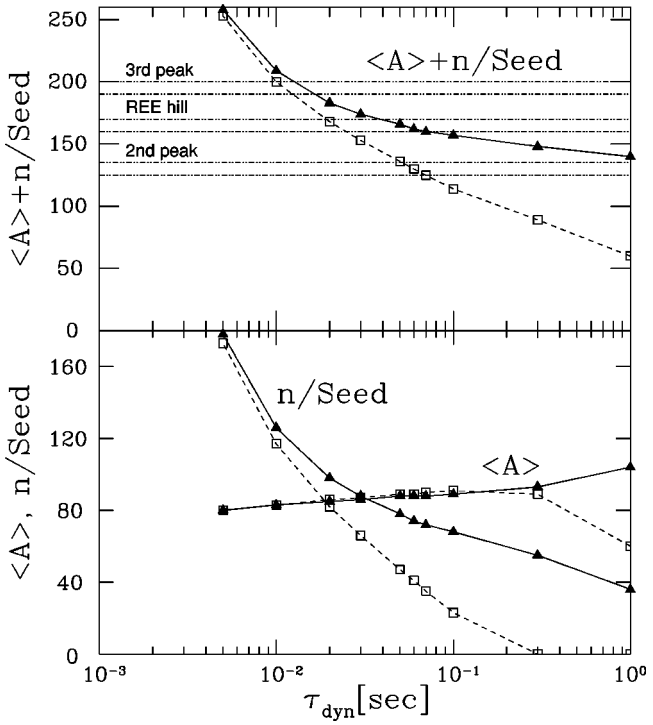

FIG. 30. Production of nuclides by the r process. The lower panel shows the average mass number of heavy seed nuclei $\langle A\rangle$ and the neutron-to-seed ratio (n/Seed) in a neutrino-driven wind simulation with an exponential time dependence of the matter flow, determined by the parameter $\tau_{\rm dyn}$: □, a simulation including neutrino-nucleus reactions; △, a study in which the neutrino-reactions on nuclei have been switched off. The upper panel shows the sum of the mass number of the seed nucleus plus the neutron-to-seed ratio. This quantity shows up to which mass number the r process can produce nuclides. The horizontal lines indicate the second ($A\sim130$) and third ($A\sim200$) r-process peaks as well as the position of the smaller r-process peak related to the deformed nuclei in the rare-earth region (REE hill). From Terasawa, 2002.

argued (Haxton *et al.*, 1997) that due to the smooth dependence of the neutrino cross sections on the mass number, the post processing, in general, shifts abundances from the peaks to the wings at lower A values (Fig. 29). This shift depends on the neutrino exposures and allows constraints to be put on the total neutrino fluence in the neutrino-driven wind model (Haxton *et al.*, 1997; Qian *et al.*, 1997). The limits obtained in this way are compatible with the values predicted by supernova models. Whether β-delayed neutron emission, which was neglected by Haxton *et al.* (1997), might affect the post processing is an open question (Kratz, 2001, 2002).

Attempts to include neutrino-induced reactions in the r-process network within the neutrino-driven wind model have been reported by Fuller and Meyer (1995), McLaughlin and Fuller (1995), Terasawa, Sumiyoshi, Kajino, Mathews, *et al.* (2001), and Terasawa, Sumiyoshi, Kajino, Tanihata, *et al.* (2001). In particular, Meyer *et al.* (1998) studied the competition of the α effect with the possible speedup of the matter flow by charged-current reactions on nuclei. These authors estimated the respective charged-current cross sections for allowed transitions on the basis of the independent-particle model. Improving on this treatment, Borzov and Goriely calculated (ν_e,e^-) cross sections for supernova neutrinos (Fermi-Dirac distribution with $T=4$ MeV) within the ETFSI method, consistently with their most recent estimates for the β half-lives (Borzov and Goriely, 2000). Random-phase approximation-based neutrino-nucleus cross sections for selected nuclei have been reported by Surman and Engel (1998) and Hektor *et al.* (2000). Very recently a tabulation with charged- and neutral-current total and partial neutron spallation cross sections have become available for the neutron-rich r-process nuclei (Langanke and Kolbe, 2001, 2002). This tabulation is based on the RPA and considers allowed and forbidden transitions. Furthermore, the cross sections are tabulated for various supernova neutrino distributions, thus also allowing study of the influence of complete neutrino oscillations on the r process.

Terasawa, Sumiyoshi, Kajino, Mathews, *et al.* (2001) and Terasawa, Sumiyoshi, Kajino, Tanihata, *et al.* (2001) have performed studies similar to the pioneering work of Meyer *et al.* (1998), but combining their neutrino-driven wind model with the complete set of RPA neutrino-nucleus reaction rates (Langanke and Kolbe, 2001, 2002). A typical result is shown in Fig. 30, where the simplifying, but reasonable, assumption of an exponential time dependence of the matter flow, governed by the parameter $\tau_{\rm dyn}$ away from the neutron star, has been assumed. The quantity $\langle A\rangle$ defines the average mass of the heavy seed nuclei present at the beginning of the r process, defined at $T=2.5\times10^9$ K. The neutron-to-seed ratio n/s is very sensitive to the dynamical evolution time. This comes about because the shorter the $\tau_{\rm dyn}$, the less time is available to assemble the seed nuclei from α particles and neutrons. Consequently the abundance of

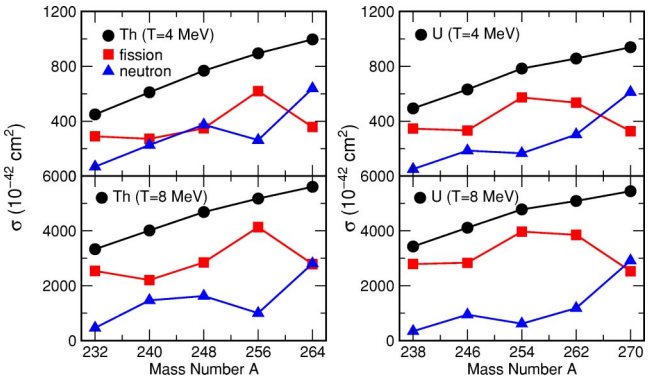

FIG. 31. (Color in online edition) Fission cross sections for selected thorium and uranium isotopes: ●, total (ν_e, e^-) cross sections; ▲, partial $(\nu_e, e^- n)$ cross sections; ■, neutrino-induced cross section. The calculations have been performed for Fermi-Dirac ν_e distributions with temperature $T=4$ and 8 MeV. The first reflects a typical supernova ν_e spectrum, while the latter assumes complete $\nu_{\mu,\tau} \rightarrow \nu_e$ neutrino oscillations.

seed nuclei decreases for shorter $\tau_{\rm dyn}$, increasing the n/s ratio. If the neutrino flux is artificially switched off, matter flow to the third r-process peak at $A \sim 200$ (second r-process peak at $A \sim 130$) is achieved if $\tau_{\rm dyn} \leqslant 0.01$ s ($\tau_{\rm dyn} \leqslant 1$ s). The consistent inclusion of neutrino reactions is counterproductive to a successful r process. This effect becomes more dramatic if the matter flow is slow, as then the α effect strongly suppresses the availability of free neutrons at the beginning of the r process (see also Meyer *et al.*, 1998). No r process, i.e., no production of nuclides in the second r-process peak at $A \sim 130$, is observed if $\tau_{\rm dyn} \gtrsim 0.05$ s.

Recently Qian (2002) has suggested that, within the neutrino-driven wind r-process scenario, charged-current neutrino reactions can induce fission reactions on r-process progenitor nuclei heavier than lead and that the fission products account for the observed r-process abundance in metal-poor stars (Sneden *et al.*, 2000). These observed abundances show a peak around mass number $A \sim 195$, which follows the solar r-process distribution, and enhanced structures at around $A \sim 90$ and ~ 132 which, according to the suggestion of Qian (2002), are fission products that do not follow a solar r-process pattern. First calculations of neutrino-induced fission cross sections have been performed by Kolbe *et al.* (2002) using a combination of the RPA model, to calculate the (ν_e, e^-) excitation function, and a statistical model to determine the final branching probabilities. The neutrino-induced fission cross sections (see Fig. 31) are quite large, as the progenitor nuclei are neutron rich, which increases the Fermi and Gamow-Teller contributions to the total cross sections and places their strengths at energies above the fission barrier in the daughter nucleus. The calculations shown in Fig. 31 use the fission barriers derived by Howard and Möller (1980). More recent evaluations (e.g., those of Mamdouh *et al.*, 2001) predict larger fission barriers which would reduce the fission cross section. The cross sections can be significantly enlarged if $\nu_{\mu,\tau} \rightarrow \nu_e$ neutrino oscillations occur during the neutrino-driven wind r-process scenario.

VII. THE NEUTRINO PROCESS

When the flux of neutrinos generated by the cooling of a neutron star passes through the overlying shells of heavy elements, interesting nuclear transmutations are induced despite the small neutrino-nucleus cross sections. Of particular interest here are neutral-current reactions as they can be induced by ν_μ, ν_τ neutrinos and their antiparticles with the higher energy spectra ($\langle E_\nu \rangle \sim 25$ MeV). These neutrinos are energetic enough to excite the GT resonant state and, more importantly, also the giant dipole resonant states. These states usually reside above particle thresholds and hence decay mainly by proton or neutron emission, generating new nuclides. The neutrino reaction rates are too small to affect the abundances of the parent nuclei, but they can noticeably contribute to the production of the (sometimes much less abundant) daughter nuclei. As a rule of thumb, the neutrino process, i.e., the synthesis of nuclides by neutrino-induced spallation in a supernova, can become a significant production process for the daughter nuclide if one wants to explain abundance ratios of parent-to-daughter which exceed about 10^3 (Woosley, 2001).

The most interesting neutrino nucleosynthesis occurs in the outer burning shells of a massive star, which have not been affected by the fatal core collapse in the center when the neutrinos pass through. However, a little later the shock reaches these shells and the matter will be subjected to rather high temperatures, initiating fast nuclear reactions that involve the nuclides just produced by the neutrino-induced reactions. Hence studies of the neutrino process depend on various neutrino-nucleus reaction rates and on the neutrino spectra and fluxes, especially of the ν_μ, ν_τ neutrinos, and they require a moderate nuclear network to simulate the effects of the reprocessing by the shock. The first investigation of the neutrino process was reported by Woosley *et al.* (1990). A more recent study (Woosley and Weaver, 1995) confirmed the main result that a few specific nuclei (^{7}Li, ^{11}B, ^{19}F) are being made by the neutrino process in significant fractions. For example, ^{11}B and ^{19}F are being made by $(\nu, \nu' p)$ and $(\nu, \nu' n)$ (followed by a β decay) reactions on the abundant ^{12}C and ^{20}Ne, respectively. As noted by Woosley *et al.* (1990), neutrino nucleosynthesis can also contribute to the production of ^{180}Ta (see above) and ^{138}La. First calculations of the relevant total and partial neutrino-induced cross sections have been reported by Heger *et al.* (2002; see also Belic *et al.*, 2002). The nucleus ^{138}La is special, as it is mainly made by the charged-current reaction ^{138}Ba$(\nu_e, e^-)^{138}$La, while the lighter nuclei (^{7}Li, ^{11}B, ^{19}F) and dominantly ^{180}Ta, as well, are being produced by neutral-current reactions induced by ν_μ, ν_τ neutrinos. The neutrino process is therefore sensitive to ν_e and (ν_μ, ν_τ) neutrinos, which are expected to have different spectra in type-II supernovae (see Sec. V.C), and hence it can test this prediction. Moreover, the ^{138}La nucleosynthesis is sensi-

tive to neutrino oscillations, as this nuclide would be significantly overproduced if supernova ν_μ, ν_τ neutrinos had a noticeably larger average energy and if they oscillated into ν_e neutrinos before reaching the ^{138}La production site (helium shell) in massive stars.

Neutrino-induced nucleon spallation on ^{12}C can also knock out a deuteron or a proton-neutron pair, in this way producing ^{10}B. The expected ^{10}B/^{11}B abundance ratio in neutrino nucleosynthesis is $\sim$0.05, which is significantly smaller than the observed abundance ratio, 0.25 (Haxton, 2001). Thus there must be a second process that contributes to the production of ^{10,11}B. These are reactions of energetic protons on ^{12}C in cosmic rays, which yield a ratio ^{10}B/^{11}B of about 0.5, larger than the observed value. A solution might be that the two nuclides are being produced by both mechanisms, neutrino nucleosynthesis and cosmic-ray spallation. It is interesting to note that the first process, being associated with supernovae, is a primary process, while the latter is a secondary process, as it requires the existence of protons and ^{12}C in the interstellar medium. As a consequence the ^{10}B/^{11}B abundance ratio should have changed during the history of the galaxy. This can be tested once observers are able to distinguish between the abundances of the two different boron nuclides in stellar spectra (Haxton, 2001).

VIII. BINARY SYSTEMS

Weak processes can also play interesting roles in the evolution and nucleosynthesis processes in close binary systems where one component is a compact object (white dwarf or neutron star) and the other a massive star. If the latter expands during helium-core burning, mass flow from the hydrogen envelopment of the star onto the surface of the compact object sets in. If the respective mass accretion rate is rather low (10^{-8} $-10^{-10} M_\odot$ yr^{-1}), the hydrogen, accreted on the surface of the compact object, burns explosively under degenerate conditions, leading to a nova (if the compact object is a white dwarf) or an x-ray burst (neutron star). This means that the energy released by the nuclear reactions is used to heat the matter rather than for expansion. The rise in temperature increases the nuclear reaction rates, triggering a thermonuclear runaway until degeneracy is finally lifted and an outer layer of matter is ejected. In a type-Ia supernova the faster mass accretion rate onto the surface of a white dwarf (likely a carbon-oxygen white dwarf with sub-Chandrasekhar mass $\sim 0.7 M_\odot$) leads to steady hydrogen and subsequently helium burning. If the growing mass of the white dwarf exceeds the Chandrasekhar mass, contraction sets in and the carbon in the center ignites by fusion reactions with screening enhancement. As the environment is highly degenerate, a thermonuclear runaway is triggered which eventually will explode the entire star.

A. Novae

The main energy source of a nova is the CNO cycle, with additional burning from proton reactions on nuclei between neon and sulfur, if the white dwarf also contained some ^{20}Ne (Truran, 1982). A nova expels matter that is enriched in β-unstable ^{14,15}O for carbon-oxygen white dwarfs (leading to the production of stable ^{14,15}N nuclides) or can contain nuclides up to the sulfur mass region for neon-oxygen novae (José and Hernanz, 1998; Starrfield *et al.*, 1998, 2000). The most important role of weak-interaction processes in novae is their limitation of the energy generation during the thermonuclear runaway. An interesting branching occurs at $T \sim 8 \times 10^7$ K. For lower temperatures the β decay of ^{13}N with a half-life of $\sim$10 m dominates over the ^{13}N(p,γ) reaction and sets the time scale for the nuclear burning. As charged-particle fusion reactions are sensitively dependent on temperature, their reaction rates strongly increase with rising temperature, and for $T \geqslant 8 \times 10^7$ K and densities of order 10^4 g cm^{-3} the proton capture on ^{13}N is faster than the β decay. The CNO cycle turns into the *hot* CNO cycle, and now the positron decay of ^{15}O with a half-life of 122 s is the slowest reaction occurring in the CNO nova network. It turns out that, once the degeneracy is lifted, the dynamical expansion time scale is faster than the one for nuclear energy generation, set by the ^{15}O half-life. As a consequence the runaway is quenched (Truran, 1982). We mention that determination of the dominant resonant contribution to the ^{13}N$(p,\gamma)^{14}$O rate was the first successful application of the Coulomb dissociation technique in nuclear astrophysics (Motobayashi *et al.*, 1991).

Weak-interaction rates relevant for nova studies can be derived from either experimental data or shell-model calculations.

B. X-ray bursts

An x-ray burst is explained as a thermonuclear runaway in the hydrogen-rich envelope of an accreting neutron star (Lewin *et al.*, 1993; Taam *et al.*, 1993). Due to the higher gravitational potential of a neutron star, the accreted matter on the surface reaches larger densities than in a nova (up to a few 10^6 g cm^{-3}) and the temperature during the runaway can rise up to 2×10^9 K (Schatz *et al.*, 1998). Under these conditions hydrogen burning is explosively fast. The trigger reactions of the runaway are the triple-alpha reactions and the breakout from the hot CNO cycle, mainly by α capture on ^{15}O and ^{18}Ne. We note that these two reaction rates are yet insufficiently known due to uncertain resonant contribution at low energies (Görres *et al.*, 1995; Mao *et al.*, 1996). The thermonuclear runaway is driven first by the αp process, a sequence of (α,p) and (p,γ) reactions which shifts the ashes of the hot CNO cycle to the Ar and Ca mass region, and then by the rp process (short for rapid proton-capture process). The rp process represents proton-capture reactions along the proton dripline and subsequent β decays of dripline nuclei processing

the material from the Ar-Ca region up to ^{56}Ni (Schatz *et al.*, 1998). The β half-lives on the rp-process path up to ^{56}Ni are fairly well known.

The runaway freezes out in thermal equilibrium at peak temperatures of $(2-3)\times10^9$ K with an abundance distribution rich in ^{56}Ni, forming Ni oceans on the surface of the neutron star. Further matter flow at these temperatures is suppressed due to the low proton separation energy of ^{57}Cu and the long half-life of ^{56}Ni. Reignition of the rp process then takes place during the cooling phase, starting with proton capture on ^{56}Ni and potentially shifting matter up to the ^{100}Sn region, where the rp process ends in a cycle in the Sn-Te-I range (Schatz *et al.*, 2001). A matter flow to even heavier nuclei is possible, if the rp process operates in a repetitive manner; i.e., a new rp process is ignited after the ashes of the previous process have decayed to stability and before these nuclei have sunk too deep into the crust of the neutron star (see below). Such repetitive rp-process models, abbreviated as $(\mathrm{rp})^2$-process models, have been studied by Boyd *et al.* (2002).

The reaction path beyond ^{56}Ni runs through the even-even $N=Z$ nuclei which, due to their known long half-lives [^{64}Ge has a half-life of 63.7(25) s], represent a strong impedance to the matter flow. This cannot always be overcome by proton captures, as for some of the α-like nuclei the resulting odd-A nucleus is proton unbound and exists only as a resonance. Such situations occur, for example, for the $^{68}\mathrm{Se}(p,\gamma)^{69}\mathrm{Br}$ and $^{72}\mathrm{Kr}(p,\gamma)^{73}\mathrm{Rb}$ reactions. It has been suggested (Görres *et al.*, 1995) that the gap in the reaction path can be bridged by two-proton captures, with the resonance serving as an intermediate state (as in the triple-α reaction). The reaction rate for such a two-step process depends crucially on the resonance energy, with some appropriate screening corrections.

Most half-lives along the rp-process path up to the ^{80}Zr region are known experimentally. This region of the nuclear mass chart is known for strong ground-state deformations, caused by coupling of the p-f-shell orbitals to the $g_{9/2}$ and $d_{5/2}$ levels. The strong deformation makes theoretical half-life predictions quite inaccurate, mainly due to uncertainties in the Q values stemming from insufficiently well-known mass differences. We note that the effective half-life of a nucleus along the rp-process path could be affected by the feeding of isomeric states in the proton captures or by the thermal population of excited states in general. Again, deformation plays a major role, as then even in α-like nuclei excited states are at rather low energies (e.g., the first 2^+ state in ^{80}Zr is at 290 keV). Clearly measurement of the half-lives is indispensable for rp-process studies beyond $A=80$. An important step has recently been taken with the measurement of the half-life of ^{80}Zr at the Holifield Facility in Oak Ridge (Ressler *et al.*, 2000). The experimental value of $4.1^{+0.8}_{-0.6}$ s reduces the previous (theoretical) uncertainty considerably and, in fact, it is shorter than the value adopted previously in x-ray burst simulations. Fast proton captures on the daughter products ^{80}Y and ^{80}Sr allow matter flow to heavier nuclei, with the α nucleus ^{84}Mo ($N=Z=42$) being the next bottleneck. Experiments to measure this important half-life are in progress.

Nucleosynthesis during the cooling phase in an x-ray burst alters considerably the abundance distribution in the atmosphere, ocean, and crust of the neutron star. For example, the rp process may be a possible contributor to the presently unexplained relatively high observed abundance of light p nuclei like ^{92}Mo and ^{96}Ru (Schatz *et al.*, 1998). This assumes that the matter produced in the x-ray burst gets expelled out of the large gravitational potential of the neutron star, which is still questionable. Due to continuing accretion the rp-process ashes are pressed into the ocean and crust of the neutron star, there replacing the neutron star's original material. When the ashes sink into the crust, they reach regions of higher densities and, accordingly, larger electron chemical potentials. Thus consecutive electron captures will become energetically favored and make the ashes more neutron rich. At densities beyond neutron drip [$\rho\sim(4-6)\times10^{11}$ g cm^{-3}] neutron emissions become possible, and at even higher densities pycnonuclear reactions can set in (Bisnovatyi-Kogan and Checketkin, 1979; Sato, 1979; Haensel and Zdunik, 1990). Importantly, these processes (electron capture, pycnonuclear reactions) generate energies that can be locally stored in the neutron star's ocean and crust and that will affect their thermal properties (Brown and Bildsten, 1998). Earlier studies of these processes in accreting neutron stars have assumed that iron is the end product of nuclear burning and the sole nucleus reaching the crust of the neutron star (see, for example, Hanesel and Zdunik, 1990). But clearly the rp process produces a wide mixture of heavy elements (Schatz *et al.*, 1999), in which abundance distribution depends on the accretion rate.

The ashes consist mainly of even-even $N=Z$ nuclei, for which electron capture at neutron star conditions always occur in steps of two. At first, the capture on the even-even nucleus sets in once sufficiently high-energy electrons are available to effectively overcome the Q_{EC} value to the odd-odd daughter nucleus. Due to nuclear pairing, which favors even-even nuclei, the Q_{EC} value for the produced daughter nucleus is noticeably lower, so that electron capture on the daughter readily follows at the same conditions. The energy gain of the double-electron capture is of order the difference of the two Q_{EC} values; this gain is split between the emitted neutrino and local heating. Considering a blob of accreted matter initially consisting solely of ^{56}Ni and assuming temperature $T=0$, the evolution of this blob was followed on the neutron star surface until neutron-drip densities and beyond (Haensel and Zdunik, 1990). The rp-process simulations, however, indicate a finite temperature of the ashes of a few 10^8 K, allowing electron capture even from the high-energy tail of the electron distribution and significantly reducing the required densities.

C. Type-Ia supernovae

Type-Ia supernovae at high redshifts serve currently as the standard candles for the largest distances in the

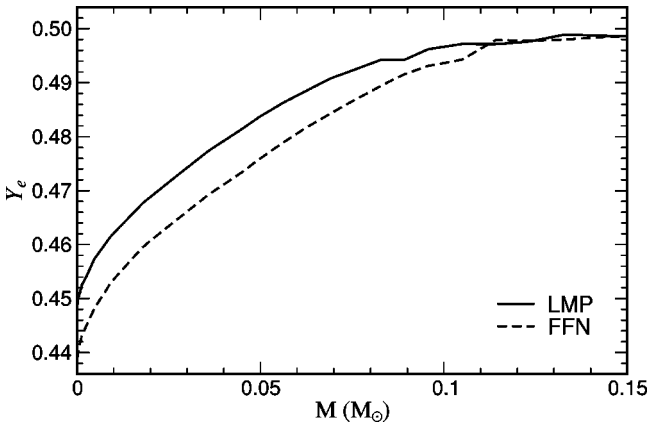

FIG. 32. Y_e profile as a function of radial mass for the standard type-Ia supernova model WS15 (Nomoto *et al.*, 1984) using the FFN and the shell-model weak-interaction rates of Langanke and Martínez-Pinedo (LMP). Courtesy of F. Brachwitz.

universe. Importantly, recent surveys of such distant supernovae provide evidence for an accelerating expansion of the universe over the last several 10^9 years (Riess *et al.*, 1998; Perlmutter *et al.*, 1999).

Type-Ia supernovae have been identified as thermonuclear explosions of accreting white dwarfs with high accretion rates in a close binary system. While the general explosion mechanism is probably understood, several issues are still open, like the masses of the stars in the binary or the carbon/oxygen ratio and distribution in the white dwarf. Probably the most important problem remaining is the modeling of the matter transport during the explosion and the velocity of the burning front, both requiring multidimensional simulations (see, for example, Reinecke *et al.*, 1999; Hillebrandt and Niemeyer, 2000; Woosley, 2001).

Type-Ia supernovae contribute about half the abundance of Fe-group nuclides in galactic evolution. Thus one can expect that type-Ia supernovae should not overproduce abundances of nuclides in the iron group, such as ^{54}Cr or ^{50}Ti, relative to ^{56}Fe by more than a factor of 2 compared with the relative solar abundances. This requirement puts stringent constraints on models, in particular, on the central density of the progenitor white dwarf and the flame speed (Iwamoto *et al.*, 1999). When the flame travels outwards, it heats the matter to temperatures of a few 10^9 K and brings its composition close to nuclear statistical equilibrium. As the original matter (^{16}O, ^{12}C) had an electron-to-baryon ratio of $Y_e=0.5$, the nuclear statistical equilibrium composition is dominated by ^{56}Ni, which after being expelled decays to ^{56}Fe. However, behind the flame front, which travels with a few percent of the local sound speed (Niemeyer and Hillebrandt, 1995), electron captures occur, which lower Y_e and drive the matter composition to become more neutron rich. This effect is larger the greater the central density of the white dwarf (which increases the electron-capture rates) and the slower the flame speed (which allows more time for electron captures). Figure 32 shows the Y_e profile obtained in a standard type-Ia model WS15 (Nomoto *et al.*, 1984), with slow deflagration flame speed (1.5% of sound velocity), central ignition density $\rho=2.1\times10^9$ g cm^{-3}, and a transition from deflagration to detonation at density $\rho=2.1\times10^7$ g cm^{-3}. The calculations were performed by Brachwitz (2001) with the FFN (Fuller *et al.*, 1982b) and shell-model (Langanke and Martínez-Pinedo, 2001) weak-interaction rate sets. The differences are quite significant, even if one considers that about 60% of the captures occur on free protons, which are unaffected by the differences in these rate sets. Under otherwise identical conditions the slower shell-model rates yield a central Y_e value of 0.45, which is about 0.01 larger than that given by the FFN rates. Consequently very neutron-rich nuclei with $Y_e\leqslant0.45$ are significantly suppressed (see Fig. 33). In fact, no nuclide is significantly overproduced

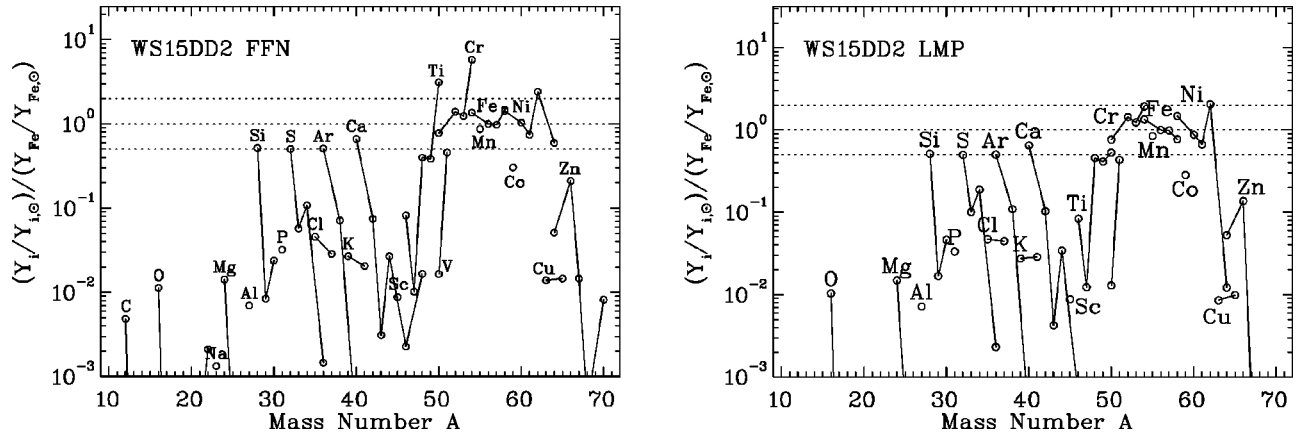

FIG. 33. Ratio of calculated to solar abundances predicted by the WS15 model (Nomoto *et al.*, 1984) using the FFN and the shell-model rates (LMP). The ordinate is normalized to ^{56}Fe. Intermediate-mass elements exist but are underproduced by a factor of 2–3 for SNe Ia models in comparison to Fe group elements. When the FFN rates are used, the Fe group does not show a composition close to solar. ^{50}Ti and ^{54}Cr especially are strongly overproduced by more than a factor of 3. The change from FFN rates (left) to LMP (right) reduces the overproduction over solar close to the acceptable limit of a factor of 2. Courtesy of F. Brachwitz.

in this model compared to the solar abundance. The net effect of the new rates is that, for an otherwise unchanged model, it increases the central density by about a factor of 1.3 (Brachwitz *et al.*, 2000; Woosley, 2001). This can have quite interesting consequences if one wants to use the nucleosynthesis constraint to distinguish between two quite distinct type-Ia models. On the basis of recent models it has been concluded that the majority of type-Ia progenitors grow towards the Chandrasekhar mass through steady hydrogen and helium burning (Hachisu *et al.*, 1999). Such systems would lead to rather low central densities $\rho \leqslant 2\times10^9$ g cm^{-3}. In these models, only a small fraction of progenitors would deviate from steady hydrogen burning, at the end of the accretion history experiencing weak hydrogen flashes; such cases correspond to the WS15-model discussed above, yielding higher central densities. We stress, however, that changes in the nucleosynthesis caused by differences in the central densities in the models can be counterbalanced by changes in the flame speed.

IX. CONCLUSIONS AND FUTURE PERSPECTIVES

It has long been recognized that nuclear weak-interaction processes play essential roles in many astrophysical scenarios. In a few cases these are specific reactions, which are particularly important, and these reactions have been studied with increasingly refined models. Examples are the various weak-interaction processes in the solar hydrogen-burning chains, including the initial $p+p$ fusion reaction (Kamionkowski and Bahcall, 1994; Park *et al.*, 1998, 2001a; Kong and Ravndal, 2001) or the very challenging ^{3}He$+p$ reaction (Marcucci *et al.*, 2000, 2001; Park *et al.*, 2001b), which generates the highest-energy neutrinos in the sun. Another typical example is the solar electron-capture rate on ^{7}Be, for which the nuclear matrix element can be determined from the experimental lifetime of atomic ^{7}Be, while the proper description of the solar plasma effects on the capture rate with the desired accuracy has been quite demanding.

However, most astrophysical applications require the knowledge of weak-interaction rates for a huge body of nuclei. If, as for s-process nucleosynthesis, the nuclei involved are close to the valley of stability and hence quite long lived, the needed rates (usually half-lives) have been determined experimentally in decades-long efforts. For the s process the challenge now focuses on the branching-point nuclei, where the reaction flow branches into two (or more) paths and where, in some cases, the observed relative abundances of nuclides along the different paths depend on the stellar conditions (temperature, neutron density) and hence allow determination of these quantities inside the star. Again, the approach is to measure the necessary data, e.g., half-lives of excited nuclear states.

Other astrophysical scenarios involve nuclei far from stability, often under extreme conditions (high density, neutron flux, temperature). These scenarios include core-collapse (type-II) and thermonuclear (type-Ia) supernovae, r-process nucleosynthesis, and explosive hydrogen burning; and the interest in all of these has been enhanced recently by novel observations and data (supernova 1987A, high-redshift supernova survey, Hubble Space Telescope, . . .). A direct experimental determination of the corresponding stellar weak-interaction rates has been possible in a few cases, like the half-lives of r-process and rp-process waiting-point nuclei. However, in nearly all cases so far the weak-interaction processes had to be theoretically modeled—a very demanding job if one considers that often results for many hundreds of nuclei for a large range of stellar conditions are needed. These data were then derived globally, based on parametrized nuclear structure arguments, as an appropriate treatment of the involved nuclear structure problem was prohibited by both the available computational capabilities and the lack of experimental guidance. Although evaluation of rate sets for astrophysical purposes often appears to be a theoretical problem, the second point—experimental guidance—is crucial and often overlooked. It is Fowler's strategy and legacy that nuclear models used to derive nuclear ingredients in astrophysical applications should be consistent, but more importantly they should be accurate and, as a consequence, experimental data are to be used whenever available. Therefore the role of experimental data in nuclear astrophysics is twofold: If possible, they supply the needed information directly, or equally important, they constitute constraints and guidance for the nuclear models from which the needed information is obtained. Thus the renaissance of nuclear structure study, which we have witnessed in recent years, has two consequences in nuclear astrophysics. The recent development of new facilities, techniques, and devices brought a large flood of new experimental information, in particular for the proton- and neutron-rich nuclei away from stability. These data indicate that the nuclear structure models adopted to derive the global data and rate sets were usually too simple and improvements were warranted. The experimental renaissance went hand-in-hand with decisive progress in nuclear structure theory, made possible by the development of new models and better computer hardware and software. Due to both experimental and theoretical advances, it is now possible to calculate nuclear data sets for astrophysical applications on the basis of realistic models rather than on crude and often oversimplified parametrizations. This review presents a summary of recent theoretical calculations.

The advances in nuclear structure modeling have also led to progress in astrophysically important nuclear input other than weak-interaction processes. Typical examples are the equation of state, derived on the basis of the relativistic mean-field model guided by the relativistic Brückner-Hartree-Fock theory (Shen *et al.*, 1998a, 1998b), which serves as an alternative to the standard Lattimer-Swesty equation of state (Lattimer and Swesty, 1991), or the nuclear mass table and level-density parametrizations determined within the framework of the Hartree-Fock model with BCS pairing (Demetriou and Goriely, 2001; Goriely *et al.*, 2001). Such mass tables, or

equivalently neutron separation energies, play an essential role in r-process nucleosynthesis and are conventionally derived by parametrizations constrained to known masses.

Other astrophysical areas, loosely or indirectly related to the topic of this review, have also benefited from the progress in modeling nuclear weak-interaction processes. A field with rapidly growing importance is gamma-ray astronomy with beta-unstable nuclei. Due to γ-ray observatories in space it has been possible in recent years to search the sky for sources of known γ rays which can then be associated with recent nucleosynthesis activities. A highlight has been the observation of the 1.157 MeV γ line, produced in the β-decay scheme of ^{44}Ti, in the Cassiopeia supernova remnant (Iyudin *et al.*, 1994). Knowing the date of the supernova, the ^{44}Ti half-life, the distance to the source, and the measured intensity of the γ line allows determination of how much ^{44}Ti has been ejected into the interstellar medium by the supernova event. Furthermore, as γ rays, in contrast to optical wavelengths, can escape from the galactic bulk, γ-ray observation allows us to detect historical supernovae which have not been observed optically (Iyudin *et al.*, 1998); the same could be said of x-ray observations, for example, those by Aschenbach (1998). Such searches for historical supernovae and an improved determination of the supernova frequency in our galaxy will be one of the main missions of future γ-ray observatories in space, like INTEGRAL.[4] A longer-lived radioactive nuclide produced in supernovae is ^{60}Fe. Investigations of rock samples taken from the ocean floor, by precision accelerator mass spectroscopy, found a significant increase of ^{60}Fe abundance compared to other iron isotopes, pointing to a close-by supernova about 5 million years ago (Knie *et al.*, 1999).

Weak processes on nuclei and electrons are the means to observe solar and supernova neutrinos (Balantekin and Haxton, 1999). Solar neutrinos have rather low energies ($E_\nu \leq 14$ MeV) and hence induce specific low-lying transitions, which are theoretically modeled best by shell-model calculations. Applications have been performed, for example, for ^{37}Cl (Aufderheide, Bloom, *et al.*, 1994), ^{40}Ar (Ormand *et al.*, 1995) and ^{71}Ga (Haxton, 1998), the detector material in the Homestake observatory (Cleveland *et al.*, 1998), ICARUS,[5] and GALLEX/SAGE/GNO detectors (Abdurashitov *et al.*, 1999; Hampel *et al.*, 1999; Altmann *et al.*, 2000), respectively. Supernova neutrinos have higher energies; in particular, the energies of μ,τ neutrinos and antineutrinos are expected to be high enough to excite the giant dipole resonances in nuclei. Studies for detector materials like Na, Fe, and Pb have been performed in hybrid approaches combining shell-model calculations for allowed transitions, with the RPA model for forbidden transitions or treating the forbidden transitions on the basis of the Goldhaber-Teller model (Fuller *et al.*, 1999; Kolbe and Langanke, 2001).

Despite experimental and theoretical progress, lack of knowledge of relevant or accurate weak-interaction data still constitutes a major obstacle in the simulation of some astrophysical scenarios today. This refers mainly to type-II supernovae and r-process nucleosynthesis.

Core-collapse supernovae, as the breeding places of carbon and oxygen, and hence life in the universe, currently attract significant attention, and the quest to definitely identify the explosion mechanism is on the agenda of several international and interdisciplinary collaborations. While most of the efforts concentrate on computational developments towards a multidimensional treatment of the hydrodynamics and the neutrino transport, some relevant and potentially important nuclear problems remain.

The improved description of weak-interaction rates in the iron mass range has led to significant changes in the presupernova models. Evaluation of electron-capture rates for heavier nuclei will be available in the near future. First results imply that capture on heavy nuclei, usually ignored in collapse simulations, can compete with capture on free protons. Whether the inclusion of this process then leads to changes in the collapse trajectory has yet to be seen.

Further, finite-temperature neutrino-nucleus rates will also soon be available. This will then test whether inelastic neutrino scattering on nuclei, not yet modeled in the simulations, influences the collapse dynamics or supports the revival of the shock wave by preheating of infalling matter after the bounce.

The largest nuclear uncertainty in collapse simulations is likely associated with the description of nuclear matter at high density, extreme isospin, and finite temperature. In particular, a reliable description of the neutrino opacity in nuclear matter might very well be what is needed for successful explosion simulations. Nucleon-nucleon correlations have been identified as strongly influencing the neutrino opacities, and nuclear models like the RPA are quite useful in guiding the way.

Ultimately one would like to see the many-body Monte Carlo techniques, which have been so successfully applied to few-body systems or the nuclear shell model, extended to the nuclear matter problem. First steps along these lines have been reported by Schmidt and Fantoni (1999) and Fantoni *et al.* (2001), who proposed a novel constrained-path diffusion Monte Carlo model to study nuclear matter at temperature $T=0$. The shell-model Monte Carlo model, formulated in momentum space and naturally at finite temperature, constitutes an alternative approach. First attempts in this direction have been taken by the Caltech group (Zheng, 1996) and by Rombouts (1998). Whether the notorious sign problem in the SMMC approach can also be circumvented for nuclear matter has still to be demonstrated. Müller *et al.* (2000) have investigated whether nuclear matter can be formulated on a spatial lattice with nearest-neighbor interactions, similar to the Hub-

[4]http://astro.estec.esa.nl/SA-general/Projects/Integral/integral.html

[5]http://www.aquila.infn.it/icarus

bard model for high-T_c superconductors. Besides these theoretical efforts it is equally important to improve our understanding of the nuclear interaction in extremely neutron-rich nuclei (matter).

Despite four decades of intense research, an astrophysical site of r-process nucleosynthesis has not yet been identified. Recent astronomical and meteoric evidence points now to more than one source for the solar r-process nuclides, and it is clearly a major goal in the astrophysics community to solve this cosmic riddle. However, the puzzle will not be definitely solved if the nuclear uncertainties involved are not removed. This is even more necessary as recent research shows that the r process is a dynamical process under changing astrophysical conditions. This implies dynamically changing r-process paths. To determine the paths one needs to know the masses of nuclei far from stability accurately, besides the condition of the astrophysical environment. In a dynamical r process, the astrophysical time scale will compete with the nuclear time scale, i.e., with the time needed for matter flow from the seed nuclei to the heavier r-process nuclides. This nuclear time scale is set by the half-lives of the nuclei along the paths, in particular by those of the longer-lived waiting-point nuclei associated with the magic neutron numbers. The half-lives of waiting-point nuclei are a very illustrative example of the need for reliable experimental data: Modern global theoretical models predict half-lives at the waiting points with a spread of nearly one order of magnitude, and only data can decide. For the $N=50$ and $N=82$ waiting points such data exist for a few key nuclides (Pfieffer *et al.*, 2001), but not for the $N=126$ nuclei.

r-process nucleosynthesis as well as other astrophysical processes will tremendously benefit from future experimental developments in nuclear physics. Worldwide radioactive ion-beam facilities, with important and dedicated programs in nuclear astrophysics, have just started operation, are under construction or are in the proposal stage. These new facilities will increase our knowledge about nuclei far from stability, and they will determine astrophysically relevant nuclear input directly (e.g., masses and half-lives for the r process, half-lives and cross sections for the rp process, etc.). But equally important, the radioactive ion-beam facilities will guide and constrain the nuclear models, in this way indirectly contributing to the reduction of the nuclear inaccuracies in astrophysical models. Ultimately nuclear physics can and will provide a stringent test and guidance for astrophysical theories and ideas.

ACKNOWLEDGMENTS

We should like to thank many colleagues and friends for helpful collaborations and discussions: D. Arnett, S. M. Austin, J. N. Bahcall, R. N. Boyd, F. Brachwitz, R. Canal, E. Caurier, J. Christensen-Dalsgaard, J. J. Cowan, D. J. Dean, R. Diehl, J. Dobaczewski, J. L. Fisker, G. M. Fuller, E. García-Berro, S. Goriely, J. Görres, W. C. Haxton, A. Heger, M. Hernanz, W. Hillebrandt, R. Hix, J. Isern, H.-Th. Janka, J. José, T. Kajino, F. Käppeler, E. Kolbe, S. E. Koonin, K.-L. Kratz, M. Liebendörfer, A. Martínez-Andreu, G. J. Mathews, A. Mezzacappa, Y. Mochizuki, E. Müller, W. Nazarewicz, F. Nowacki, I. Panov, B. Pfeiffer, A. Poves, Y.-Z. Qian, G. Raffelt, R. Reiferth, A. Richter, C. E. Rolfs, J. M. Sampaio, H. Schatz, M. Terasawa, F.-K. Thielemann, J. W. Truran, P. Vogel, M. Wiescher, S. E. Woosley, and A. P. Zuker. Our work has been supported by the Danish Research Council and the Schweizerische Nationalfonds. Computational resources were provided by the Center for Advanced Computational Research at Caltech, by the Danish Center for Scientific Computing, and by the Center for Computational Sciences at Oak Ridge National Laboratory.

REFERENCES

Abdurashitov, J. N., E. L. Faizov, V. N. Gavrin, A. O. Gusev, A. V. Kalikhov, T. V. Knodel, I. I. Knyushenko, V. N. Kornoukhov, I. N. Mirmov, A. M. Pshukov, A. M. Shalagin, A. A. Shikhin, *et al.* (SAGE Collaboration), 1994, Phys. Lett. B **328**, 234.

Abdurashitov, J. N., V. N. Gavrin, S. V. Girin, V. V. Gorbachev, T. V. Ibragimova, A. V. Kalikhov, N. G. Khairnasov, T. V. Knodel, I. N. Mirmov, A. A. Shikhin, E. P. Veretenkin, V. M. Vermul, *et al.* (SAGE Collaboration), 1999, Phys. Rev. C **60**, 055801.

Aboussir, Y., J. M. Pearson, A. K. Dutta, and F. Tondeur, 1995, At. Data Nucl. Data Tables **61**, 1.

Adelberger, E. G., S. M. Austin, J. N. Bahcall, A. B. Balantekin, G. Bogaert, L. S. Brown, L. Buchmann, F. E. Cecil, A. E. Champagne, L. de Braeckeleer, C. A. Duba, S. R. Elliott, *et al.*, 1998, Rev. Mod. Phys. **70**, 1265.

Ahmad, Q. R., R. C. Allen, T. C. Andersen, J. D. Anglin, J. C. Barton, E. W. Beier, M. Bercovitch, J. Bigu, S. Biller, R. A. Black, I. Blevis, R. J. Boardman, *et al.* (SNO Collaboration), 2002a, Phys. Rev. Lett. **89**, 011301.

Ahmad, Q. R., R. C. Allen, T. C. Andersen, J. D. Anglin, J. C. Barton, E. W. Beier, M. Bercovitch, J. Bigu, S. Biller, R. A. Black, I. Blevis, R. J. Boardman, *et al.* (SNO Collaboration), 2002b, Phys. Rev. Lett. **89**, 011302.

Ahmad, Q. R., R. C. Allen, T. C. Andersen, J. D. Anglin, G. Bühler, J. C. Barton, E. W. Beier, M. Bercovitch, J. Bigu, S. Biller, R. A. Black, I. Blevis, *et al.* (SNO Collaboration), 2001, Phys. Rev. Lett. **87**, 071301.

Ahrens, L. H., S. H. Aronson, P. L. Connolly, B. G. Gibbard, M. J. Murtagh, S. J. Murtagh, S. Terada, D. H. White, J. L. Callas, D. Cutts, J. S. Hoftun, M. Diwan, *et al.*, 1987, Phys. Rev. D **35**, 785.

Alford, W. P., B. A. Brown, S. Burzynski, A. Celler, D. Frekers, R. Helmer, R. Henderson, K. P. Jackson, K. Lee, A. Rahav, A. Trudel, and M. C. Vetterli, 1993, Phys. Rev. C **48**, 2818.

Alford, W. P., R. L. Helmer, R. Abegg, A. Celler, D. Frekers, P. Green, O. Haeusser, K. Henderson, K. Hicks, K. P. Jackson, R. Jeppesen, C. A. Miller, *et al.*, 1990, Nucl. Phys. A **514**, 49.

Altmann, M., M. Balata, P. Belli, E. Bellotti, R. Bernabei, E. Burkert, C. Cattadori, G. Cerichelli, M. Chiarini, M. Cribier, S. d'Angelo, G. Del Re, *et al.* (GNO Collaboration), 2000, Phys. Lett. B **490**, 16.

Álvarez, L. W., 1949, Report UCRL-328, University of California Radiation Laboratory.

Anderson, B. D., T. Chittrakarn, A. R. Baldwin, C. Lebo, R. Madey, P. C. Tandy, J. W. Watson, B. A. Brown, and C. C. Foster, 1985, Phys. Rev. C **31**, 1161.
Anderson, B. D., C. Lebo, A. R. Baldwin, T. Chittrakarn, R. Madey, and J. W. Watson, 1990, Phys. Rev. C **41**, 1474.
Angulo, C., and P. Descouvemont, 2001, Nucl. Phys. A **690**, 755.
Anselmann, P., W. Hampel, G. Heusser, J. Kiko, T. Kirsten, E. Pernicka, R. Plaga, U. Ronn, M. Sann, C. Schlosser, R. Wink, M. Wojcik, *et al.* (GALLEX Collaboration), 1992, Phys. Lett. B **285**, 376.
Armbruster, B., I. Blair, B. A. Bodmann, N. E. Booth, G. Drexlin, V. Eberhard, J. A. Edgington, C. Eichner, K. Eitel, E. Finckh, H. Gemmeke, J. Hößl, *et al.*, 1998a, Phys. Rev. C **57**, 3414.
Armbruster, B., I. M. Blair, B. A. Bodmann, N. E. Booth, G. Drexlin, V. Eberhard, J. A. Edgington, C. Eichner, K. Eitel, E. Finckh, H. Gemmeke, J. Hößl, *et al.*, 1998b, Phys. Rev. Lett. **81**, 520.
Arnett, D., 1996, *Supernova and Nucleosynthesis* (Princeton University, Princeton, NJ).
Arnould, M., and K. Takahashi, 1999, Rep. Prog. Phys. **62**, 395.
Aschenbach, B., 1998, Nature (London) **396**, 141.
Athanassopoulos, C., L. B. Auerbach, R. L. Burman, D. O. Caldwell, E. D. Church, I. Cohen, J. B. Donahue, A. Fazely, F. J. Federspiel, G. T. Garvey, R. M. Gunasingha, R. Imlay, *et al.* (LSND Collaboration), 1998, Phys. Rev. Lett. **81**, 1774.
Athanassopoulos, C., L. B. Auerbach, R. L. Burman, I. Cohen, D. O. Caldwell, B. D. Dieterle, J. B. Donahue, A. M. Eisner, A. Fazely, F. J. Federspiel, G. T. Garvey, M. Gray, *et al.* (LSND Collaboration), 1996, Phys. Rev. Lett. **77**, 3082.
Aufderheide, M. B., 1991, Nucl. Phys. A **526**, 161.
Aufderheide, M. B., S. D. Bloom, G. J. Mathews, and D. A. Resler, 1996, Phys. Rev. C **53**, 3139.
Aufderheide, M. B., S. D. Bloom, D. A. Resler, and C. D. Goodman, 1994, Phys. Rev. C **49**, 678.
Aufderheide, M. B., S. D. Bloom, D. A. Ressler, and G. J. Mathews, 1993a, Phys. Rev. C **47**, 2961.
Aufderheide, M. B., S. D. Bloom, D. A. Ressler, and G. J. Mathews, 1993b, Phys. Rev. C **48**, 1677.
Aufderheide, M. B., I. Fushiki, G. M. Fuller, and T. A. Weaver, 1994, Astrophys. J. **424**, 257.
Aufderheide, M. B., I. Fushiki, S. E. Woosley, and D. H. Hartmann, 1994, Astrophys. J. **91**, 389.
Ref. in figure 3 is how J. N. Bahcall, calls his latest solar model published in the ref Bahcall *et al.* 2001.
Bahcall, J. N., 1997, Phys. Rev. C **56**, 3391.
Bahcall, J. N., N. A. Bahcall, and G. Shaviv, 1968, Phys. Rev. Lett. **20**, 1209.
Bahcall, J. N., C. M. González-García, and C. Peña-Garay, 2002, J. High Energy Phys. **07**, 054.
Bahcall, J. N., M. H. Pinsonneault, and S. Basu, 2001, Astrophys. J. **555**, 990.
Balantekin, A. B., and W. C. Haxton, 1999, in *Frontiers in Nuclear Physics: Proceedings of the Eleventh Physics Summer School,* edited by S. Kuyucak (World Scientific, Singapore).
Baleisis, A., and D. Arnett, 2001, Nucl. Phys. A **688**, 185c.
Bambynek, W., H. Behrens, M. H. Chen, B. Crasemann, M. L. Fitzpatrick, K. W. D. Ledingham, H. Genz, M. Mutterer, and R. L. Intermann, 1977, Rev. Mod. Phys. **49**, 77; **49**, 961(E).
Beane, S. R., P. F. Bedaque, W. C. Haxton, D. R. Phillips, and M. J. Savage, 2001, in *At the Frontier of Particle Physics: Handbook of QCD*, edited by M. Shifman (World Scientific, Singapore).
Beer, H., F. Käppeler, K. Wisshak, and R. A. Ward, 1981, Astrophys. J., Suppl. Ser. **46**, 295.
Behrens, H., and W. Bühring, 1971, Nucl. Phys. A **162**, 111.
Behrens, H., and W. Bühring, 1982, *Electron Radial Wave Functions and Nuclear Beta-decay* (Clarendon, Oxford).
Beise, E. J., and R. D. McKeown, 1991, Comments Nucl. Part. Phys. **20**, 105.
Belic, D., C. Arlandini, J. Besserer, J. de Boer, J. J. Carroll, J. Enders, T. Hartmann, F. Käppeler, H. Kaiser, U. Kneissl, E. Kolbe, K. Langanke, *et al.*, 2002, Phys. Rev. C **65**, 035801.
Belic, D., C. Arlandini, J. Besserer, J. de Boer, J. J. Carroll, J. Enders, T. Hartmann, F. Käppeler, H. Kaiser, U. Kneissl, M. Loewe, H. J. Maier, *et al.*, 1999, Phys. Rev. Lett. **83**, 5242.
Bethe, H. A., 1990, Rev. Mod. Phys. **62**, 801.
Bethe, H. A., G. E. Brown, J. Applegate, and J. M. Lattimer, 1979, Nucl. Phys. A **324**, 487.
Bethe, H. A., and J. R. Wilson, 1985, Astrophys. J. **295**, 14.
Bisnovatyi-Kogan, G. S., and V. M. Chechetkin, 1979, Sov. Phys. Usp. **22**, 89.
Blomqvist, J., A. Kerek, and B. Fogelberg, 1983, Z. Phys. A **314**, 199.
Boger, J., R. L. Hahn, J. K. Rowley, A. L. Carter, B. Hollebone, D. Kessler, I. Blevis, F. Dalnoki-Veress, A. DeKok, J. Farine, D. R. Grant, C. K. Hargrove, *et al.* (SNO Collaboration), 2000, Nucl. Instrum. Methods Phys. Res. A **449**, 172.
Bonetti, R., C. Broggini, L. Campajola, P. Corvisiero, A. D'Alessandro, M. Dessalvi, A. D'Onofrio, A. Fubini, G. Gervino, L. Gialanella, U. Greife, A. Guglielmetti, *et al.* (LUNA Group), 1999, Phys. Rev. Lett. **82**, 5205.
Borzov, I., and S. Goriely, 2000, Phys. Rev. C **62**, 035501. See also URL http://www-astro.ulb.ac.be/Html/bd.html
Borzov, I.N., 2003, Phys. Rev. C **67**, 025802.
Bosch, F., T. Faestermann, J. Friese, F. Heine, P. Kienle, E. Wefers, K. Zeitelhack, K. Beckert, B. Franzke, O. Klepper, C. Kozhuharov, G. Menzel, *et al.*, 1996, Phys. Rev. Lett. **77**, 5190.
Boyd, R., M. Hencheck, and B. Meyer, 2002, unpublished.
Boyd, R. N., 2000, in *Heavy Elements and Related New Phenomena,* edited by R. K. Gupta and W. Greiner (Word Scientific, Singapore), Vol. 2, pp. 893–975.
Brachwitz, F., 2001, Ph.D. thesis (Universität Basel).
Brachwitz, F., D. J. Dean, W. R. Hix, K. Iwamoto, K. Langanke, G. Martínez-Pinedo, K. Nomoto, M. R. Strayer, F. Thielemann, and H. Umeda, 2000, Astrophys. J. **536**, 934.
Brown, B. A., and B. H. Wildenthal, 1988, Annu. Rev. Nucl. Part. Sci. **38**, 29.
Brown, E. F., and L. Bildsten, 1998, Astrophys. J. **496**, 915.
Bruenn, S. W., 1985, Astrophys. J., Suppl. Ser. **58**, 771.
Bruenn, S. W., and T. Dineva, 1996, Astrophys. J. Lett. **458**, L71.
Bruenn, S. W., and W. C. Haxton, 1991, Astrophys. J. **376**, 678.
Buballa, M., S. Drożdż, S. Krewald, and J. Speth, 1991, Ann. Phys. (N.Y.) **208**, 346.
Burbidge, E. M., G. R. Burbidge, W. A. Fowler, and F. Hoyle, 1957, Rev. Mod. Phys. **29**, 547.
Burrows, A., 1987, Astrophys. J. Lett. Ed. **318**, L57.
Burrows, A., 2000, Nature (London) **403**, 727.
Burrows, A., 2001, Prog. Part. Nucl. Phys. **46**, 59.
Burrows, A., and J. Goshy, 1993, Astrophys. J. Lett. **416**, L75.
Burrows, A., J. Hayes, and B. A. Fryxell, 1995, Astrophys. J. **450**, 830.
Burrows, A., and R. F. Sawyer, 1998, Phys. Rev. C **58**, 554.
Burrows, A., and R. F. Sawyer, 1999, Phys. Rev. C **59**, 510.

Burrows, A., T. Young, P. Pinto, R. Eastman, and T. Thompson, 2000, Astrophys. J. **539**, 865.
Busso, M., R. Gallino, and G. J. Wasserburg, 1999, Annu. Rev. Astron. Astrophys. **37**, 239.
Caldwell, D. O., G. M. Fuller, and Y. Qian, 2000, Phys. Rev. D **61**, 123005.
Cameron, A. G. W., 1957, "Stellar Evolution, Nuclear Astrophysics, and Nucleogenesis," Report CRL-41, Chalk River, Ontario.
Cameron, A. G. W., 1958, Annu. Rev. Nucl. Sci. **8**, 299.
Carlson, J., and R. Schiavilla, 1998, Rev. Mod. Phys. **70**, 743.
Caurier, E., 2002, private communication.
Caurier, E., K. Langanke, G. Martínez-Pinedo, and F. Nowacki, 1999, Nucl. Phys. A **653**, 439.
Caurier, E., P. Navrátil, W. E. Ormand, and J. P. Vary, 2001, Phys. Rev. C **64**, 051301(R).
Caurier, E., A. P. Zuker, A. Poves, and G. Martínez-Pinedo, 1994, Phys. Rev. C **50**, 225.
Cayrel, R., V. Hill, T. C. Beers, B. Barbuy, M. Spite, F. Spite, B. Plez, J. Andersen, P. Bonifacio, P. François, P. Molaro, B. Nordström, *et al.*, 2001, Nature (London) **409**, 691.
Chen, B., J. Dobaczewski, K.-L. Kratz, K. Langanke, B. Pfeiffer, F.-K. Thielemann, and P. Vogel, 1995, Phys. Lett. B **355**, 37.
Christensen-Dalsgaard, J., 2002, Rev. Mod. Phys. **74**, 1073.
Christensen-Dalsgaard, J., W. Dappen, S. V. Ajukov, E. R. Anderson, H. M. Antia, S. Basu, V. A. Baturin, G. Berthomieu, B. Chaboyer, S. M. Chitre, A. N. Cox, P. Demarque, *et al.*, 1996, Science **272**, 1286.
Clayton, D. D., 1964, Astrophys. J. **139**, 637.
Clayton, D. D., 1968, *Principles of Stellar Evolution and Nucleosynthesis* (McGraw-Hill, New York).
Cleveland, B. T., T. Daily, R. Davis, J. R. Distel, K. Lande, C. K. Lee, P. S. Wildenhain, and J. Ullman, 1998, Astrophys. J. **496**, 505.
Cohen, S., and D. Kurath, 1965, Nucl. Phys. **73**, 1.
Cooperstein, J., and J. Wambach, 1984, Nucl. Phys. A **420**, 591.
Corsico, A. H., O. G. Benvenuto, L. G. Althaus, J. Isern, and E. Garcia-Berro, 2001, New Astron. **6**, 197.
Couch, R. G., A. B. Schmiedekamp, and W. D. Arnett, 1974, Astrophys. J. **190**, 95.
Cowan, J. J., B. Pfeiffer, K.-L. Kratz, F.-K. Thielemann, C. Sneden, S. Burles, D. Tytler, and T. C. Beers, 1999, Astrophys. J. **521**, 194.
Cowan, J. J., F.-K. Thielemann, and J. W. Truran, 1991, Phys. Rep. **208**, 267.
Davids, B., D. W. Anthony, T. Aumann, S. M. Austin, T. Baumann, D. Bazin, R. R. C. Clement, C. N. Davids, H. Esbensen, P. A. Lofy, T. Nakamura, B. M. Sherrill, *et al.*, 2001, Phys. Rev. Lett. **86**, 2750.
Davis, R., Jr., 1955, Phys. Rev. **97**, 766.
Davis, R., Jr., D. S. Harmer, and K. C. Hoffman, 1968, Phys. Rev. Lett. **20**, 1205.
Demetriou, P., and S. Goriely, 2001, Nucl. Phys. A **695**, 95.
Dobaczewski, J., I. Hamamoto, W. Nazarewicz, and J. A. Sheikh, 1994, Phys. Rev. Lett. **72**, 981.
Doll, C., H. G. Börner, S. Jaag, F. Käppeler, and W. Andrejtscheff, 1999, Phys. Rev. C **59**, 492.
Dominguez, I., O. Straniero, and J. Isern, 1999, Mon. Not. R. Astron. Soc. **306**, L1.
Donnelly, T. W., and W. C. Haxton, 1979, At. Data Nucl. Data Tables **23**, 103.
Donnelly, T. W., and W. C. Haxton, 1980, At. Data Nucl. Data Tables **25**, 1.
Donnelly, T. W., and R. P. Peccei, 1979, Phys. Rep. **50**, 1.
Drożdż, S., S. Nishizaki, J. Speth, and J. Wambach, 1990, Phys. Rep. **197**, 1.
Duflo, J., and A. P. Zuker, 1995, Phys. Rev. C **52**, R23.
Dzitko, H., S. Turck-Chieze, P. Delbourgo-Salvador, and C. Lagrange, 1995, Astrophys. J. **447**, 428.
Edmonds, A. R., 1960, *Angular Momentum in Quantum Mechanics* (Princeton University Press, Princeton, NJ).
El-Kateb, S., K. P. Jackson, W. P. Alford, R. Abegg, R. E. Azuma, B. A. Brown, A. Celler, D. Frekers, O. Haeusser, R. Helmer, R. S. Henderson, K. H. Hicks, *et al.*, 1994, Phys. Rev. C **49**, 3128.
Engel, J., M. Bender, J. Dobaczewski, W. Nazarewicz, and R. Surman, 1999, Phys. Rev. C **60**, 014302.
Engel, J., E. Kolbe, K. Langanke, and P. Vogel, 1996, Phys. Rev. C **54**, 2740.
Fantoni, S., A. Sarsa, and K. E. Schmidt, 2001, Phys. Rev. Lett. **87**, 181101.
Fermi, E., 1934, Z. Phys. **88**, 161.
Feynman, R. P., and M. Gell-Mann, 1958, Phys. Rev. **109**, 193.
Fowler, W. A., 1958, Astrophys. J. **127**, 551.
Freedman, D. Z., 1974, Phys. Rev. D **9**, 1389.
Freiburghaus, C., J.-F. Rembges, T. Rauscher, E. Kolbe, F.-K. Thielemann, K.-L. Kratz, B. Pfeiffer, and J. J. Cowan, 1999, Astrophys. J. **516**, 381.
Freiburghaus, C., S. Rosswog, and F.-K. Thielemann, 1999, Astrophys. J. Lett. **525**, L121.
Friman, B., and O. Maxwell, 1979, Astrophys. J. **232**, 541.
Fujita, Y., H. Akimune, I. Daito, M. Fujiwara, M. N. Harakeh, T. Inomata, J. Jänecke, K. Katori, H. Nakada, S. Nakayama, A. Tamii, M. Tanaka, *et al.*, 1996, Phys. Lett. B **365**, 29.
Fukuda, S., Y. Fukuda, M. Ishitsuka, Y. Itow, T. Kajita, J. Kameda, K. Kaneyuki, K. Kobayashi, Y. Koshio, M. Miura, S. Moriyama, M. Nakahata, *et al.* (Super-Kamiokande Group), 2001, Phys. Rev. Lett. **86**, 5656.
Fukuda, Y., T. Hayakawa, E. Ichihara, K. Inoue, K. Ishihara, H. Ishino, Y. Itow, T. Kajita, J. Kameda, S. Kasuga, K. Kobayashi, Y. Kobayashi, *et al.* (Super-Kamiokande Group), 1998a, Phys. Rev. Lett. **81**, 1562.
Fukuda, Y., T. Hayakawa, E. Ichihara, K. Inoue, K. Ishihara, H. Ishino, Y. Itow, T. Kajita, J. Kameda, S. Kasuga, K. Kobayashi, Y. Kobayashi, *et al.* (Super-Kamiokande Group), 1998b, Phys. Rev. Lett. **81**, 1158.
Fukuda, Y., T. Hayakawa, E. Ichihara, K. Inoue, K. Ishihara, H. Ishino, Y. Itow, T. Kajita, J. Kameda, S. Kasuga, K. Kobayashi, Y. Kobayashi, *et al.* (Super-Kamiokande Group), 1999, Phys. Rev. Lett. **82**, 2644.
Fuller, G. M., 1982, Astrophys. J. **252**, 741.
Fuller, G. M., W. A. Fowler, and M. J. Newman, 1980, Astrophys. J., Suppl. **42**, 447.
Fuller, G. M., W. A. Fowler, and M. J. Newman, 1982a, Astrophys. J. **252**, 715.
Fuller, G. M., W. A. Fowler, and M. J. Newman, 1982b, Astrophys. J., Suppl. Ser. **48**, 279.
Fuller, G. M., W. A. Fowler, and M. J. Newman, 1985, Astrophys. J. **293**, 1.
Fuller, G. M., W. C. Haxton, and G. C. McLaughlin, 1999, Phys. Rev. D **59**, 085005.
Fuller, G. M., and B. S. Meyer, 1991, Astrophys. J. **376**, 701.
Fuller, G. M., and B. S. Meyer, 1995, Astrophys. J. **453**, 792.
Gamow, G., 1941, Phys. Rev. **59**, 617.

Gamow, G., and M. Schoenberg, 1940, Phys. Rev. **58**, 1117.
Gamow, G., and M. Schoenberg, 1941, Phys. Rev. **59**, 539.
Garvey, G. T., E. Kolbe, S. Krewald, and K. Langanke, 1993, Phys. Rev. C **48**, 1919.
Garvey, G. T., S. Krewald, E. Kolbe, and K. Langanke, 1992, Phys. Lett. B **289**, 249.
Garvey, G. T., W. C. Louis, and D. H. White, 1993, Phys. Rev. C **48**, 761.
Gill, R. L., R. F. Casten, D. D. Warner, A. Piotrowski, H. Mach, J. C. Hill, F. K. Wohn, J. A. Winger, and R. Moreh, 1986, Phys. Rev. Lett. **56**, 1874.
Glashow, S. L., J. Iliopoulos, and L. Maiani, 1970, Phys. Rev. D **2**, 1285.
Goodman, C. D., C. A. Goulding, M. B. Greenfield, J. Rapaport, D. E. Bainum, C. C. Foster, W. G. Love, and F. Petrovich, 1980, Phys. Rev. Lett. **44**, 1755.
Goriely, S., and M. Arnould, 2001, Astron. Astrophys. **379**, 1113.
Goriely, S., and B. Clerbaux, 1999, Astron. Astrophys. **346**, 804.
Goriely, S., F. Tondeur, and J. M. Pearson, 2001, At. Data Nucl. Data Tables **77**, 311.
Görres, J., M. Wiescher, and F.-K. Thielemann, 1995, Phys. Rev. C **51**, 392.
Groom, D. E., M. Aguilar-Benitez, C. Amsler, R. M. Barnett, P. R. Burchat, C. D. Carone, C. Caso, G. Conforto, O. Dahl, M. Doser, S. Eidelman, J. L. Feng, *et al.* (Particle Data Group), 2000, Eur. Phys. J. C **15**, 1. See also URL http://pdg.lbl.gov
Grotz, K., and H. V. Klapdor, 1990, *The Weak Interaction in Nuclear, Particle and Astrophysics* (Hilger, Bristol).
Gruzinov, A. V., and J. N. Bahcall, 1998, Astrophys. J. **504**, 996.
Guillemaud-Mueller, D., C. Detraz, M. Langevin, F. Naulin, M. Desaintsimon, C. Thibault, F. Touchard, and M. Epherre, 1984, Nucl. Phys. A **426**, 37.
Hachisu, I., M. Kato, and K. Nomoto, 1999, Astrophys. J. **522**, 487.
Haensel, P., and J. L. Zdunik, 1990, Astron. Astrophys. **227**, 431.
Hampel, W., J. Handt, G. Heusser, J. Kiko, T. Kirsten, M. Laubenstein, E. Pernicka, W. Rau, M. Wojcik, Y. Zakharov, R. V. Ammon, K. H. Ebert, *et al.* (GALLEX Collaboration), 1999, Phys. Lett. B **447**, 127.
Hanhart, C., D. R. Phillips, and S. Reddy, 2001, Phys. Lett. B **499**, 9.
Hannestad, S., 2001, Nucl. Phys. A **688**, 373c.
Hannestad, S., and G. Raffelt, 1998, Astrophys. J. **507**, 339.
Hansen, C. J., 1966, Ph.D. thesis (Yale University).
Hansen, C. J., 1968, Astrophys. Space Sci. **1**, 499.
Haxton, W. C., 1988, Phys. Rev. Lett. **60**, 1999.
Haxton, W. C., 1998, Phys. Lett. B **431**, 110.
Haxton, W. C., 2001, in *Proceedings of the Carolina Symposium on Neutrino Physics,* March, 2000, edited by J. Bahcall, W. Haxton, K. Kubodera, and C. Poole (World Scientific, Singapore/London), p. 21.
Haxton, W. C., K. Langanke, Y. Z. Qian, and P. Vogel, 1997, Phys. Rev. Lett. **78**, 2694.
Hayes, A. C., and I. S. Towner, 2000, Phys. Rev. C **61**, 044603.
Heeger, K. M., and R. G. H. Robertson, 1996, Phys. Rev. Lett. **77**, 3720.
Heger, A., E. Kolbe, W. Haxton, K. Langanke, G. Martínez-Pinedo, and S. E. Woosley, 2002, unpublished.
Heger, A., K. Langanke, G. Martínez-Pinedo, and S. E. Woosley, 2001, Phys. Rev. Lett. **86**, 1678.
Heger, A., and S. E. Woosley, 2001, private communication.
Heger, A., S. E. Woosley, G. Martínez-Pinedo, and K. Langanke, 2001, Astrophys. J. **560**, 307.
Hektor, A., E. Kolbe, K. Langanke, and J. Toivanen, 2000, Phys. Rev. C **61**, 055803.
Herant, M., W. Benz, W. R. Hix, C. L. Fryer, and S. A. Colgate, 1994, Astrophys. J. **435**, 339.
Heyde, K. L. G., 1994, *The Nuclear Shell Model* (Springer-Verlag, Berlin).
Hill, V., B. Plez, R. Cayrel, T. C. Beers, B. Nordström, J. Andersen, M. Spite, F. Spite, B. Barbuy, P. Bonifacio, E. Depagne, P. François, *et al.*, 2002, Astron. Astrophys. **387**, 560.
Hillebrandt, W., and J. C. Niemeyer, 2000, Annu. Rev. Astron. Astrophys. **38**, 191.
Hjorth-Jensen, M., T. T. S. Kuo, and E. Osnes, 1995, Phys. Rep. **261**, 126.
Hoffman, R. D., S. E. Woosley, and Y.-Z. Qian, 1997, Astrophys. J. **482**, 951.
Holmgren, H. P., and R. Johnston, 1958, Bull. Am. Phys. Soc. **3**, 26.
Homma, H., E. Bender, M. Hirsch, K. Muto, H. V. Klapdor-Kleingrothaus, and T. Oda, 1996, Phys. Rev. C **54**, 2972.
Honma, M., T. Mizusaki, and T. Otsuka, 1995, Phys. Rev. Lett. **75**, 1284.
Horowitz, C. J., 2002, Phys. Rev. D **65**, 043001.
Horowitz, C. J., and G. Li, 1999, Phys. Rev. Lett. **82**, 5198.
Howard, W. M., and P. Möller, 1980, At. Data Nucl. Data Tables **25**, 219.
Ikeda, K. I., S. Fujii, and J. I. Fujita, 1963, Phys. Lett. **3**, 271.
Itoh, N., H. Hayashi, A. Nishikawa, and Y. Kohyama, 1996, Astrophys. J., Suppl. Ser. **102**, 411.
Itoh, N., N. Tomizawa, M. Tamamura, S. Wanajo, and S. Nozawa, 2002, Astrophys. J. **579** 380.
Iwamoto, K., F. Brachwitz, K. Nomoto, N. Kishimoto, H. Umeda, W. R. Hix, and F.-K. Thielemann, 1999, Astrophys. J., Suppl. Ser. **125**, 439.
Iwamoto, N., and C. Pethick, 1982, Phys. Rev. D **25**, 313.
Iyudin, A. F., R. Diehl, H. Bloemen, W. Hermsen, G. G. Lichti, D. Morris, J. Ryan, V. Schönfelder, H. Steinle, M. Varendorff, C. de Vries, and C. Winkler, 1994, Astron. Astrophys. **284**, L1.
Iyudin, A. F., V. Schönfelder, K. Bennett, H. Bloemen, R. Diehl, W. Hermsen, G. G. Lichti, R. D. van der Meulen, J. Ryan, and C. Winkler, 1998, Nature (London) **396**, 142.
Jaffe, R. L., and A. Manohar, 1990, Nucl. Phys. B **337**, 509.
Janka, H.-T., 2001, Astron. Astrophys. **368**, 527.
Janka, H.-T., and W. Hillebrandt, 1989, Astron. Astrophys. **224**, 49.
Janka, H.-T., K. Kifonidis, and M. Rampp, 2001, in *Physics of Neutron Star Interiors*, edited by D. Blaschke, N. K. Glendenning, and A. Sedrakian, Lecture Notes in Physics No. 578 (Springer-Verlag, Berlin), p. 333.
Janka, H.-T., and E. Müller, 1996, Astron. Astrophys. **306**, 167.
Johnson, C. W., E. Kolbe, S. E. Koonin, and K. Langanke, 1992, Astrophys. J. **392**, 320.
Johnson, C. W., S. E. Koonin, G. H. Lang, and W. E. Ormand, 1992, Phys. Rev. Lett. **69**, 3157.
Johnson, W. R., and G. Soff, 1985, At. Data Nucl. Data Tables **33**, 405.
José, J., and M. Hernanz, 1998, Astrophys. J. **494**, 680.

Jung, M., F. Bosch, K. Beckert, H. Eickhoff, H. Folger, B. Franzke, A. Gruber, P. Kienle, O. Klepper, W. Koenig, C. Kozhuharov, R. Mann, *et al.*, 1992, Phys. Rev. Lett. **69**, 2164.
Junghans, A. R., E. C. Mohrmann, K. A. Snover, T. D. Steiger, E. G. Adelberger, J. M. Casandjian, H. E. Swanson, L. Buchmann, S. H. Park, and A. Zyuzin, 2001, Phys. Rev. Lett. **88**, 041101.
Junghans, A. R., and K. Snover, 2002, private communication.
Kamionkowski, M., and J. N. Bahcall, 1994, Astrophys. J. **420**, 884.
Käppeler, F., 1999, Prog. Part. Nucl. Phys. **43**, 419.
Käppeler, F., F.-K. Thielemann, and M. Wiescher, 1998, Annu. Rev. Nucl. Part. Sci. **48**, 175.
Käppeler, F., M. Wiescher, U. Giesen, J. Görres, I. Baraffe, M. El Eid, C. M. Raiteri, M. Busso, R. Gallino, M. Limongi, and A. Chieffi, 1994, Astrophys. J. **437**, 396.
Kar, K., A. Ray, and S. Sarkar, 1994, Astrophys. J. **434**, 662.
Kavanagh, R. W., 1960, Nucl. Phys. **15**, 411.
Keil, W., H.-T. Janka, and E. Müller, 1996, Astrophys. J. Lett. **473**, L111.
Kifonidis, K., T. Plewa, H.-T. Janka, and E. Müller, 2000, Astrophys. J. Lett. **531**, L123.
Kirsten, T. A., 1999, Rev. Mod. Phys. **71**, 1213.
Knie, K., G. Korschinek, T. Faestermann, C. Wallner, J. Scholten, and W. Hillebrandt, 1999, Phys. Rev. Lett. **83**, 18.
Kolbe, E., G. M. Fuller, and K. Langanke, 2002, unpublished.
Kolbe, E., and K. Langanke, 2001, Phys. Rev. C **63**, 025802.
Kolbe, E., K. Langanke, and G. Martínez-Pinedo, 1999, Phys. Rev. C **60**, 052801.
Kolbe, E., K. Langanke, and P. Vogel, 1994, Phys. Rev. C **50**, 2576.
Kolbe, E., K. Langanke, and P. Vogel, 1999, Nucl. Phys. A **652**, 91.
Kolbe, E., K. Langanke, and P. Vogel, 2000, Phys. Rev. C **62**, 055502.
Kong, X., and F. Ravndal, 2001, Phys. Rev. C **64**, 044002.
Koonin, S. E., D. J. Dean, and K. Langanke, 1997, Phys. Rep. **278**, 2.
Korgul, A., H. Mach, B. Fogelberg, W. Urban, W. Kurcewicz, and V. I. Isakov, 2001, Phys. Rev. C **64**, 021302(R).
Krastev, P. I., and A. Y. Smirnov, 2002, Phys. Rev. D **65**, 073022.
Kratz, K.-L., J. Bitouzet, F.-K. Thielemann, P. Moeller, and B. Pfeiffer, 1993, Astrophys. J. **403**, 216.
Kratz, K.-L., 2001, Nucl. Phys. A **688**, 308c.
Kratz, K.-L., 2002, private communication.
Kratz, K.-L., H. Gabelmann, W. Hillebrandt, B. Pfeiffer, K. Schlosser, and F.-K. Thielemann, 1986, Z. Phys. A **325**, 489.
Kratz, K.-L., P. Möller, B. Pfeiffer, and W. B. Walters, 2000, in *Capture Gamma-Rays and Related Studies*, edited by S. Wender, AIP Conf. Proc. No. 529 (AIP, Melville, NY), p. 295.
Kratz, K.-L., B. Pfeiffer, and F.-K. Thielemann, 1998, Nucl. Phys. A **630**, 352.
Kratz, K.-L., F.-K. Thielemann, W. Hillebrandt, P. Möller, V. Harms, A. Wohr, and J. W. Truran, 1988, J. Phys. G **14**, S331.
Krumlinde, J., and P. Möller, 1984, Nucl. Phys. A **417**, 419.
Kunz, R., M. Jaeger, A. Mayer, J. W. Hammer, G. Staudt, S. Harissopoulos, and T. Paradellis, 2001, Phys. Rev. Lett. **86**, 3244.
Kuramoto, T., M. Fukugita, Y. Kohyama, and K. Kubodera, 1990, Nucl. Phys. A **512**, 711.
Kurylov, A., M. J. Ramsey-Musolf, and P. Vogel, 2002, Phys. Rev. C **65**, 055501.
Langanke, K., and E. Kolbe, 2001, At. Data Nucl. Data Tables **79**, 293.
Langanke, K., and E. Kolbe, 2002, At. Data Nucl. Data Tables **82**, 191.
Langanke, K., E. Kolbe, and D. J. Dean, 2001, Phys. Rev. C **63**, 032801.
Langanke, K., and G. Martínez-Pinedo, 2000, Nucl. Phys. A **673**, 481.
Langanke, K., and G. Martínez-Pinedo, 2001, At. Data Nucl. Data Tables **79**, 1.
Langanke, K., G. Martínez-Pinedo, and J. M. Sampaio, 2001, Phys. Rev. C **64**, 055801.
Langanke, K., and A. Poves, 2000, Nucl. Phys. News **10** (3), 16.
Langanke, K., and M. Wiescher, 2001, Rep. Prog. Phys. **64**, 1657.
Lattimer, J. M., and F. D. Swesty, 1991, Nucl. Phys. A **535**, 331.
Leising, M. D., 2001, Astrophys. J. **563**, 185.
Lewin, W. H. G., J. van Paradijs, and R. Taam, 1993, Space Sci. Rev. **62**, 233.
Liebendörfer, M., 2002, private communication.
Liebendörfer, M., O. E. B. Messer, A. Mezzacappa, R. W. Hix, F.-K. Thielemann, and K. Langanke, 2002, in *Proceedings of the 11th Workshop on "Nuclear Astrophysics*," Ringberg Castle, Tegernsee, Germany, edited by W. Hillebrandt and E. Müller (Max-Planck-Institut für Astrophysik, Garching).
Liebendörfer, M., A. Mezzacappa, F.-K. Thielemann, O. E. Bronson Messer, W. Raphael Hix, and S. W. Bruenn, 2001, Phys. Rev. D **63**, 103004.
Mamdouh, A., J. Pearson, M. Rayet, and F. Tondeur, 2001, Nucl. Phys. A **679**, 337.
Mao, Z. Q., H. T. Fortune, and A. G. Lacaze, 1996, Phys. Rev. C **53**, 1197.
Marcucci, L. E., R. Schiavilla, M. Viviani, A. Kievsky, and S. Rosati, 2000, Phys. Rev. Lett. **84**, 5959.
Marcucci, L. E., R. Schiavilla, M. Viviani, A. Kievsky, S. Rosati, and J. F. Beacom, 2001, Phys. Rev. C **63**, 015801.
Margueron, J., J. Navarro, N. van Giai, and W. Jiang, 2002, in *The Nuclear Many-Body Problem 2001,* Proceedings of the NATO Advanced Research Workshop, edited by W. Nazarewicz and D. Vretenar, NATO Science Series II, No. 53 (Kluwer Academic, Dordrecht), p. 329.
Martínez-Pinedo, G., 2001, Nucl. Phys. A **688**, 357c.
Martínez-Pinedo, G., and K. Langanke, 1999, Phys. Rev. Lett. **83**, 4502.
Martínez-Pinedo, G., K. Langanke, and D. J. Dean, 2000, Astrophys. J., Suppl. Ser. **126**, 493.
Martínez-Pinedo, G., A. Poves, E. Caurier, and A. P. Zuker, 1997, Phys. Rev. C **55**, 187.
Mazurek, T., 1973, Ph.D. thesis (Yeshiva University).
Mazurek, T. J., 1975, Astrophys. Space Sci. **35**, 117.
Mazurek, T. J., J. W. Truran, and A. G. W. Cameron, 1974, Astrophys. Space Sci. **27**, 161.
Mazzocchi, C., Z. Janas, J. Döring, M. Axiotis, L. Batist, R. Borcea, D. Cano-Ott, E. Caurier, G. de Angelis, E. Farnea, A. Faßbender, A. Gadea, *et al.*, 2001, Eur. Phys. J. A **12**, 269.
McLaughlin, G. C., J. M. Fetter, A. B. Balantekin, and G. M. Fuller, 1999, Phys. Rev. C **59**, 2873.
McLaughlin, G. C., and G. M. Fuller, 1995, Astrophys. J. **455**, 202.
McLaughlin, G. C., and G. M. Fuller, 1997, Astrophys. J. **489**, 766.
Messer, O. E. B., *et al.*, 2002, unpublished.
Meyer, B. S., 1995, Astrophys. J. Lett. **449**, L55.

Meyer, B. S., G. C. McLaughlin, and G. M. Fuller, 1998, Phys. Rev. C **58**, 3696.
Mezzacappa, A., 2001, private communication.
Mezzacappa, A., and S. W. Bruenn, 1993a, Astrophys. J. **405**, 637.
Mezzacappa, A., and S. W. Bruenn, 1993b, Astrophys. J. **410**, 740.
Mezzacappa, A., A. C. Calder, S. W. Bruenn, J. M. Blondin, M. W. Guidry, M. R. Strayer, and A. S. Umar, 1998, Astrophys. J. **495**, 911.
Mezzacappa, A., M. Liebendörfer, O. E. B. Messer, W. Raphael Hix, F.-K. Thielemann, and S. W. Bruenn, 2001, Phys. Rev. Lett. **86**, 1935.
Mikheyev, S. P., and A. Y. Smirnov, 1986, Sov. J. Nucl. Phys. **42**, 913.
Möller, P., J. R. Nix, and K.-L. Kratz, 1997, At. Data Nucl. Data Tables **66**, 131.
Möller, P., B. Pfeiffer, and K.-L. Kratz, 2002, "New calculations of gross beta-decay properties for astrophysical applications: Speeding up the classical r process," LANL report LA-UR-02-2919. See also http://t16web.lanl.gov/Moller/publications/rspeed2002.html
Möller, P., and J. Randrup, 1990, Nucl. Phys. A **514**, 1.
Motobayashi, T., Y. Ikeda, Y. Ando, K. Ieki, M. Inoue, N. Iwasa, T. Kikuchi, M. Kurokawa, S. Moriya, S. Ogawa, H. Murakami, S. Shimoura, *et al.*, 1995, Phys. Lett. B **346**, 9.
Motobayashi, T., T. Takei, S. Kox, C. Perrin, F. Merchez, D. Rebreyend, K. Ieki, H. Murakami, Y. Ando, N. Iwasa, M. Kurokawa, S. Shirato, *et al.*, 1991, Phys. Lett. B **264**, 259.
Müller, H.-M., S. Koonin, R. Seki, and U. van Kolck, 2000, Phys. Rev. C **61**, 044320.
Musolf, M. J., and T. W. Donnelly, 1992, Nucl. Phys. A **546**, 509.
Nabi, J.-U., and H. V. Klapdor-Kleingrothaus, 1999a, Eur. Phys. J. A **5**, 337.
Nabi, J.-U., and H. V. Klapdor-Kleingrothaus, 1999b, At. Data Nucl. Data Tables **71**, 149.
Nadyozhin, D. K., and I. V. Panov, 1993, in *Proceedings of the Third International Symposium on Weak and Electromagnetic Interaction in Nuclei (WEIN-92)*, edited by Tc. Vylov (World Scientific, Singapore), p. 479.
Navrátil, P., J. P. Vary, and B. R. Barrett, 2000, Phys. Rev. C **62**, 054311.
Niemeyer, J. C., and W. Hillebrandt, 1995, Astrophys. J. **452**, 769.
Nomoto, K., F.-K. Thielemann, and K. Yokoi, 1984, Astrophys. J. **286**, 644.
Oda, T., M. Hino, K. Muto, M. Takahara, and K. Sato, 1994, At. Data Nucl. Data Tables **56**, 231.
Ormand, W. E., P. M. Pizzochero, P. F. Bortignon, and R. A. Broglia, 1995, Phys. Lett. B **345**, 343.
Ortiz, C. E., A. García, R. A. Waltz, M. Bhattacharya, and A. K. Komives, 2000, Phys. Rev. Lett. **85**, 2909.
Osterfeld, F., 1992, Rev. Mod. Phys. **64**, 491.
Otsuka, T., M. Honma, T. Mizusaki, N. Shimizu, and Y. Utsuno, 2001, Prog. Part. Nucl. Phys. **47**, 319.
Otsuki, K., H. Tagoshi, T. Kajino, and S. Wanajo, 2000, Astrophys. J. **533**, 424.
Park, T.-S., K. Kubodera, D.-P. Min, and M. Rho, 1998, Astrophys. J. **507**, 443.
Park, T.-S., L. E. Marcucci, R. Schiavilla, M. Viviani, A. Kievsky, S. Rosati, K. Kubodera, D.-P. Min, and M. Rho, 2001a, e-print nucl-th/0106025.
Park, T.-S., L. E. Marcucci, R. Schiavilla, M. Viviani, A. Kievsky, S. Rosati, K. Kubodera, D.-P. Min, and M. Rho, 2001b, e-print nucl-th/0107012.
Perlmutter, S., G. Aldering, G. Goldhaber, R. A. Knop, P. Nugent, P. G. Castro, S. Deustua, S. Fabbro, A. Goobar, D. E. Groom, I. M. Hook, A. G. Kim, *et al.* (The Supernova Cosmology Project), 1999, Astrophys. J. **517**, 565.
Pfeiffer, B., K.-L. Kratz, and F.-K. Thielemann, 1997, Z. Phys. A **357**, 235.
Pfeiffer, B., K.-L. Kratz, F.-K. Thielemann, and W. B. Walters, 2001, Nucl. Phys. A **693**, 282.
Pieper, S.-C., 2002, in *The Nuclear Many-Body Problem 2001*, Proceedings of the NATO Advanced Research Workshop, edited by W. Nazarewicz and D. Vretenar, NATO Science Series II, No. 53 (Kluwer Academic, Dordrecht), p. 11.
Pontecorvo, B., 1946, "Inverse Beta Process," Report PD-205, Chalk River, Ontario.
Pontecorvo, B., 1959, Sov. Phys. JETP **9**, 1148.
Pontecorvo, B., 1968, Sov. Phys. JETP **26**, 984.
Pontecorvo, B., 1991, Cambridge Monogr. Part. Phys., Nucl. Phys., Cosmol. **1**, 25.
Poves, A., and F. Nowacki, 2001, in *An Advanced Course in Modern Nuclear Physics*, edited by J. M. Arias and M. Lozano, Lecture Notes in Physics, No. 581 (Springer-Verlag, Berlin), p. 70.
Prakash, M., J. M. Lattimer, R. F. Sawyer, and R. R. Volkas, 2001, Annu. Rev. Nucl. Part. Sci. **51**, 295.
Qian, Y.-Z., 1997, Nucl. Phys. A **621**, 363c.
Qian, Y.-Z., 2002, Astrophys. J. Lett. **569**, L103.
Qian, Y.-Z., and G. M. Fuller, 1995, Phys. Rev. D **52**, 656.
Qian, Y. Z., W. C. Haxton, K. Langanke, and P. Vogel, 1997, Phys. Rev. C **55**, 1532.
Qian, Y.-Z., P. Vogel, and G. J. Wasserburg, 1998, Astrophys. J. **494**, 285.
Raffelt, G. G., 1996, *Stars as Laboratories for Fundamental Physics* (The University of Chicago Press, Chicago).
Raffelt, G. G., 1999, Annu. Rev. Nucl. Part. Sci. **49**, 163.
Raffelt, G. G., 2000, Phys. Rep. **333**, 593.
Raffelt, G. G., 2001, Astrophys. J. **561**, 890.
Raffelt, G. G., D. Seckel, and G. Sigl, 1996, Phys. Rev. D **54**, 2784.
Rampp, M., and H.-T. Janka, 2000, Astrophys. J. Lett. **539**, L33.
Rampp, M., and H.-T. Janka, 2002, Astron. Astrophys. **396**, 361.
Rapaport, J., T. Taddeucci, T. P. Welch, C. Gaarde, J. Larsen, D. J. Horen, E. Sugarbaker, P. Koncz, C. C. Foster, C. D. Goodman, C. A. Goulding, and T. Masterson, 1983, Nucl. Phys. A **410**, 371.
Rayet, M., M. Arnould, M. Hashimoto, N. Prantzos, and K. Nomoto, 1995, Astron. Astrophys. **298**, 517.
Reddy, S., M. Prakash, and J. M. Lattimer, 1998, Phys. Rev. D **58**, 013009.
Reddy, S., M. Prakash, J. M. Lattimer, and J. A. Pons, 1999, Phys. Rev. C **59**, 2888.
Reinecke, M., W. Hillebrandt, and J. C. Niemeyer, 1999, Astron. Astrophys. **347**, 724.
Ressler, J. J., A. Piechaczek, W. B. Walters, A. Aprahamian, M. Wiescher, J. C. Batchelder, C. R. Bingham, D. S. Brenner, T. N. Ginter, C. J. Gross, R. Grzywacz, D. Kulp, *et al.*, 2000, Phys. Rev. Lett. **84**, 2104.

Riess, A. G., A. V. Filippenko, P. Challis, A. Clocchiatti, A. Diercks, P. M. Garnavich, R. L. Gilliland, C. J. Hogan, S. Jha, R. P. Kirshner, B. Leibundgut, M. M. Phillips, *et al.*, 1998, Astron. J. **116**, 1009.
Rombouts, S., 1998, unpublished.
Rönnqvist, T., H. Condé, N. Olsson, E. Ramström, R. Zorro, J. Blomgren, A. Håkansson, A. Ringbom, G. Tibell, O. Jonsson, L. Nilsson, P. U. Renberg, *et al.*, 1993, Nucl. Phys. A **563**, 225.
Rosswog, S., M. B. Davies, F.-K. Thielemann, and T. Piran, 2000, Astron. Astrophys. **360**, 171.
Rowe, D., 1968, Rev. Mod. Phys. **40**, 153.
Salam, A., 1968, in *Elementary Particle Physics*, edited by N. Svartholm (Almqvist and Wiksell, Stockholm), p. 367.
Sampaio, J. M., K. Langanke, and G. Martínez-Pinedo, 2001, Phys. Lett. B **511**, 11.
Sampaio, J. M., K. Langanke, G. Martínez-Pinedo, D. J. Dean, and E. Kolbe, 2002, e-print nucl-th/0209057.
Sampaio, J. M., K. Langanke, G. Martínez-Pinedo, and D. J. Dean, 2002, Phys. Lett. B **529**, 19.
Sato, K., 1975, Prog. Theor. Phys. **54**, 1325.
Sato, K., 1979, Prog. Theor. Phys. **62**, 957.
Sato, K., and H. Sato, 1975, Prog. Theor. Phys. **54**, 1564.
Sawyer, R. F., 1975, Phys. Rev. D **11**, 2740.
Sawyer, R. F., 1989, Phys. Rev. C **40**, 865.
Schatz, H., A. Aprahamian, V. Barnard, L. Bildsten, A. Cumming, M. Ouellette, T. Rauscher, F.-K. Thielemann, and M. Wiescher, 2001, Phys. Rev. Lett. **86**, 3471.
Schatz, H., A. Aprahamian, J. Görres, M. Wiescher, T. Rauscher, J. F. Rembges, F.-K. Thielemann, B. Pfeiffer, P. Möller, K.-L. Kratz, H. Herndl, B. A. Brown, *et al.*, 1998, Phys. Rep. **294**, 167.
Schatz, H., L. Bildsten, A. Cumming, and M. Wiescher, 1999, Astrophys. J. **524**, 1014.
Schatz, H., R. Toenjes, B. Pfeiffer, T. C. Beers, J. J. Cowan, V. Hill, and K.-L. Kratz, 2002, Astrophys. J. **579,** 626. See also URL http://groups.nscl.msu.edu/nero/Web/materials.html
Schiavilla, R., and R. B. Wiringa, 2002, Phys. Rev. C **65**, 054302.
Schmid, K. W., 2001, Prog. Part. Nucl. Phys. **46**, 145.
Schmid, K. W., F. Grümmer, and A. Faessler, 1987, Ann. Phys. (N.Y.) **180**, 1.
Schmid, K. W., R. R. Zheng, F. Grümmer, and A. Faessler, 1989, Nucl. Phys. A **499**, 63.
Schmidt, K. E., and S. Fantoni, 1999, Phys. Lett. B **446**, 99.
Schopper, H. W., 1966, *Weak Interactions and Nuclear Beta Decay* (North-Holland, Amsterdam).
Sharma, M. M., and A. R. Farhan, 2001, Nucl. Phys. A **688**, 353c.
Sharma, M. M., and A. R. Farhan, 2002, Phys. Rev. C **65**, 044301.
Shen, H., H. Toki, K. Oyamatsu, and K. Sumiyoshi, 1998a, Nucl. Phys. A **637**, 435.
Shen, H., H. Toki, K. Oyamatsu, and K. Sumiyoshi, 1998b, Prog. Theor. Phys. **100**, 1013.
Smith, M., and R. Rehm, 2001, Annu. Rev. Nucl. Sci. **51**, 91.
Sneden, C., J. J. Cowan, I. I. Ivans, G. M. Fuller, S. Burles, T. C. Beers, and J. E. Lawler, 2000, Astrophys. J. Lett. **533**, L139.
Soyeur, M., and G. E. Brown, 1979, Nucl. Phys. A **324**, 464.
Starrfield, S., W. Sparks, J. Truran, and M. Wiescher, 2000, Astrophys. J., Suppl. Ser. **127**, 485.
Starrfield, S., J. Truran, M. Wiescher, and W. M. Sparks, 1998, Mon. Not. R. Astron. Soc. **296**, 502.
Stoica, S., and J. E. Horvath, 2002, Phys. Rev. C **65**, 028801.
Surman, R., and J. Engel, 1998, Phys. Rev. C **58**, 2526.
Surman, R., and J. Engel, 2001, Phys. Rev. C **64**, 035801.
Surman, R., J. Engel, J. R. Bennett, and B. S. Meyer, 1997, Phys. Rev. Lett. **79**, 1809.
Sutaria, F. K., and A. Ray, 1995, Phys. Rev. C **52**, 3460.
Taam, R., S. E. Woosley, T. Weaver, and D. Lamb, 1993, Astrophys. J. **413**, 324.
Takahashi, K., M. Yamada, and T. Kondoh, 1973, At. Data Nucl. Data Tables **12**, 101.
Talmi, I., 1993, *Simple Models of Complex Nuclei* (Harwood Academic, Chur, Switzerland).
Terasawa, M., 2002, Ph.D. thesis (University of Tokyo).
Terasawa, M., K. Sumiyoshi, T. Kajino, G. J. Mathews, and I. Tanihata, 2001, Astrophys. J. **562**, 470.
Terasawa, M., K. Sumiyoshi, T. Kajino, I. Tanihata, G. J. Mathews, and K. Langanke, 2001, Nucl. Phys. A **688**, 581c.
Thompson, T. A., and A. Burrows, 2001, Nucl. Phys. A **688**, 377c.
Thompson, T. A., A. Burrows, and J. E. Horvath, 2000, Phys. Rev. C **62**, 035802.
Thompson, T. A., A. Burrows, and B. S. Meyer, 2001, Astrophys. J. **562**, 887.
Toivanen, J., E. Kolbe, K. Langanke, G. Martínez-Pinedo, and P. Vogel, 2001, Nucl. Phys. A **694**, 395.
Toukan, K. A., K. Debus, F. Käppeler, and G. Reffo, 1995, Phys. Rev. C **51**, 1540.
Truran, J. W., 1982, in *Essays in Nuclear Astrophysics*, edited by C. A. Barnes, D. D. Clayton, and D. N. Schramm (Cambridge University Press, Cambridge, England), p. 467.
Truran, J. W., J. J. Cowan, and B. D. Fields, 2001, Nucl. Phys. A **688**, 330c.
Tubbs, D. L., and D. N. Schramm, 1975, Astrophys. J. **201**, 467.
van Kolck, U., 1999, Prog. Part. Nucl. Phys. **43**, 337.
Vetterli, M. C., O. Haeusser, R. Abegg, W. P. Alford, A. Celler, D. Frekers, R. Helmer, R. Henderson, K. H. Hicks, K. P. Jackson, R. G. Jeppesen, C. A. Miller, *et al.*, 1990, Phys. Rev. C **40**, 559.
Volpe, C., N. Auerbach, G. Colò, T. Suzuki, and N. van Giai, 2000, Phys. Rev. C **62**, 015501.
Walecka, J. D., 1975, in *Muon Physics*, edited by V. W. Hughes and C. S. Wu (Academic, New York), Vol. II, Sec. V, 4, p. 113.
Walecka, J. D., 1995, *Theoretical Nuclear and Subnuclear Physics* (Oxford University Press, New York).
Wallerstein, G., I. Iben, P. Parker, A. M. Boesgaard, G. M. Hale, A. E. Champagne, C. A. Barnes, F. Käppeler, V. V. Smith, R. D. Hoffman, F. X. Timmes, C. Sneden, *et al.*, 1997, Rev. Mod. Phys. **69**, 995.
Walter, G., H. Beer, F. Käppeler, and R.-D. Penzhorn, 1986a, Astron. Astrophys. **155**, 247.
Walter, G., H. Beer, F. Käppeler, G. Reffo, and F. Fabbri, 1986b, Astron. Astrophys. **167**, 186.
Wanajo, S., T. Kajino, G. J. Mathews, and K. Otsuki, 2001, Astrophys. J. **554**, 578.
Warburton, E., and B. Brown, 1992, Phys. Rev. C **46**, 923.
Wasserburg, G. J., M. Busso, and R. Gallino, 1996, Astrophys. J. Lett. **466**, L109.
Weaver, T. A., and S. E. Woosley, 1993, Phys. Rep. **227**, 65.
Weinberg, S., 1967, Phys. Rev. Lett. **19**, 1264.
Whitehead, R. R., 1980, in *Moment Methods in Many Fermion Systems*, edited by B. J. Dalton, S. M. Grimes, J. D. Vary, and S. A. Williams (Plenum, New York), p. 235.

Wilkinson, J. H., 1965, *The Algebraic Eigenvalue Problem* (Clarendon, Oxford).
Williams, A. L., W. P. Alford, E. Brash, B. A. Brown, S. Burzynski, H. T. Fortune, O. Haeusser, R. Helmer, R. Henderson, P. P. Hui, K. P. Jackson, B. Larson, *et al.*, 1995, Phys. Rev. C **51**, 1144.
Wilson, J. R., 1985, in *Relativistic Astrophysics*, edited by J. Centrella, J. LeBlanc, and R. Bowers (Jones and Bartlett, Boston), p. 422.
Wilson, J. R., 2001, invited talk at "Fermi and Astrophysics," Pescara, Italy, unpublished.
Wilson, J. R., and R. W. Mayle, 1993, Phys. Rep. **227**, 97.
Wiringa, R. B., S. C. Pieper, J. Carlson, and V. R. Pandharipande, 2000, Phys. Rev. C **62**, 014001.
Wisshak, K., F. Voss, C. Arlandini, F. Bečvář, O. Straniero, R. Gallino, M. Heil, F. Käppeler, M. Krtička, S. Masera, R. Reifarth, and C. Travaglio, 2001, Phys. Rev. Lett. **87**, 251102.
Witti, J., H.-T. Janka, and K. Takahashi, 1994a, Astron. Astrophys. **286**, 841.
Witti, J., H.-T. Janka, and K. Takahashi, 1994b, Astron. Astrophys. **286**, 857.
Wolfenstein, L., 1978, Phys. Rev. D **17**, 2369.
Woosley, S. E., 1986, in *Nucleosynthesis and Chemical Evolution*, edited by B. Hauck, A. Maeder, and G. Meynet, Geneva Observatory Saas-Fee Advanced Course No. 16, p. 1.
Woosley, S. E., 2001, private communication.
Woosley, S. E., D. H. Hartmann, R. D. Hoffman, and W. C. Haxton, 1990, Astrophys. J. **356**, 272.
Woosley, S. E., A. Heger, and T. A. Weaver, 2002, Rev. Mod. Phys. **74**, 1015.
Woosley, S. E., and T. A. Weaver, 1995, Astrophys. J., Suppl. Ser. **101**, 181.
Woosley, S. E., J. R. Wilson, G. J. Mathews, R. D. Hoffman, and B. S. Meyer, 1994, Astrophys. J. **433**, 229.
Wörtche, H. J. (EUROSUPERNOVA Collaboration), 2001, Nucl. Phys. A **687**, 321c.
Yamada, S., H.-T. Janka, and H. Suzuki, 1999, Astron. Astrophys. **344**, 533.
Zeitnitz, B., 1994, Prog. Part. Nucl. Phys. **32**, 351.
Zheng, D., 1996, unpublished.